SEISMIC BEHAVIOR OF HYBRID COUPLED SHEAR WALLS USING ECCENTRIC STEEL BRACING SYSTEM

By

Yahia Walid Istanbouli

Supervisor

Dr. Nazzal S. Armouti

This thesis was submitted in partial fulfillment of the requirements for the Masters Degree of Science in Civil Engineering

Faculty of Graduate Studies

The University of Jordan

December, 2011

Committee Decision

This thesis (Seismic Behavior of Hybrid Coupled Shear Walls Using Eccentric Steel Bracing System) was successfully defended and approved on Nov. 28, 2011

Examination Committee	**Signature**
Dr. Nazzal S. Armouti, Chairman Associate Professor of Civil Engineering	------------------------
Dr. Abdelqader S. Najmi, Member Professor of Civil Engineering	------------------------
Dr. Samih S. Qaqish, Member Professor of Civil Engineering	------------------------
Dr. Nasim Shatarat, Member Associate Professor of Civil Engineering (The Hashemite University)	------------------------

DEDICATION

To my family, friends and all who have supported me to make this real...

To the precious lives lost to earthquake worldwide...

ACKNOWLEDGMENT

I gratefully acknowledge the help and support received from my supervisor, Dr. Nazzal Armouti. It has been a great privilege to work under his guidance.

The valuable reviews of the committee members, Prof. Abdelqader Najmi, Prof. Samih Qaqish and Dr. Naseem Shatarat are greatly acknowledged.

Table of Contents

3. MODELS DESCRIPTION AND RESULTS DISCUSSION

4. SUMMARY AND CONCLUSIONS

List of Tables

List of Figures

List of Photos

Notations

A	Area
CP	Control Parameter
D	Wall in-plane depth
E	Modulus if elasticity
E_{sec}	Secant modulus of elasticity
F	Force
F_e	Elastic Force
F_y	Yield Force
H	Structure height
M	Bending moment
M_A, M_B	End moments
M_b	Base moment
M_y	Yield bending moment
M_P	Plastic bending moment
M_u	Ultimate bending moment
M_0, M_1, M_2	Overturning moments
N	Axial Force
N_P	Plastic axial force
P	Force
P_g	Gravity Force
R	Force reduction factor
S	Elastic section modulus
S_a	Pseudo acceleration
T	Axial force
T	Period

V	Shear forces
V_p	Plastic shear forces
Z	Plastic section modulus
a	Distance between face of the wall to the inflection point
b_f	Flange width
b_{st}	Width of stiffener
d	Section depth
e	Length of link
e_0	Maximum length of shear link
f_c	Compressive stress
f'_c	Specified compressive strength of concrete
f'_{cc}	Strength of confined concrete in compression
f_u	Ultimate stress
f_y	Yield stress
h	Section height
k	Stiffness
l	Lever arm length
l_e	Required embedment length
l_p	Plastic hinge length
s	Stiffeners spacing
t	Time
t_f	Flange thickness
t_{st}	Thickness of stiffener
t_w	Web thickness
t_{wall}	Wall thickness
β	Coupling ratio
β1	Ratio of average concrete compressive strength to maximum stress

γ	Link rotation angle
Δ	Displacement
Δ_e	Maximum elastic displacement
Δ_m	Maximum displacement
Δ_P	Plastic displacement
Δ_u	Ultimate displacement
Δ_y	Yield displacement
ε	Strain
ε_c	Concrete compressive strain
ε_{cc}	Compressive strain in confined concrete at maximum stresses
ε_{cu}	Ultimate concrete compressive strain
ε_h	Hardening strain
ε_y	Yield strain
$\acute{\varepsilon}$	Strain rate
θ	Rotation
θy	Yield rotation
θP	Plastic rotation
κ	Curvature
κe	Elastic curvature
κh	Hardening curvature
κu	Ultimate curvature
κm	Maximum curvature
κy	Yield curvature
$\mu \varepsilon$	Strain ductility, material ductility
$\mu\ \theta$	Rotation ductility, member ductility
$\mu\ \Delta$	Displacement ductility, structure ductility
$\mu\ \kappa$	Curvature ductility, cross section ductility

μc	Capacity ductility, available ductility
μd	Demand ductility, required ductility
μh	Hysteric ductility
ρy	Yield ratio
σ	Normal stress
σy	Yield stress
τ	Shear stress
τy	Yield shear stress

SEISMIC BEHAVIOR OF HYBRID COUPLED SHEAR WALLS USING ECCENTRIC STEEL BRACING SYSTEM

By

Yahia Walid Istanbouli

Supervisor

Dr. Nazzal S. Armouti

ABSTRACT

This research aims to investigate the behavior of hybrid coupled shear walls using eccentric steel bracing system.

The proposed system was modeled using ADINA finite element environment. The proposed specimen consists of two shear walls; each wall was 15.0 m height and 4.0 m width. The shear walls were coupled using eccentric steel bracing system. The proposed system was compared with two traditional systems: cantilever shear walls and hybrid beam-coupled walls. All of the three models were subjected to pushover analysis (i.e. monotonic static loading with inelastic response) and the mechanical response was measured in terms of stiffness, strength and ductility capacity.

The modeled specimen, of the new proposed system, proved efficient comparing to the traditional systems studied, in terms of the mechanical response of the system, such as elastic stiffness, story drift control, top story deflection control and kinematics properties expressed by ductility capacity.

The proposed system experienced two phases of plastic hinge formation over the entire height of the system. The first plastic hinge formation was in the short links of the eccentric bracing system and the later was at the ends of the coupling beams.

In order to investigate the ability of the system to dissipate the absorbed energy, the new proposed system was subjected to cyclic lateral loading. Analysis results showed that the system employed the desired fat hysterical loops, proved the ability to form plastic hinges in predetermined locations and showed the potency to dissipate energy over the entire height of the system.

CHAPTER ONE
INTRODUCTION

1.1 Foreword

The world's fifth-largest, 9.0 magnitude quake has occurred on March 11^{th}, 2011, This severe earthquake associated with tsunami waves had struck the island of Japan, moving the island further toward east and shifting the planet's axis. Sadly, death toll has passed 9,000 civilian, while moreover than 14,000 are still missing according to official records (New York Times Newspaper).

. In addition to this tragedy, the jeopardy of high nuclear alert is facing the Japanese nation.

Current earthquake events are providing a continuous proof to the need for considering these excitations in structural configurations extensively and improving the inelastic response of the structural systems in order to prevent sudden collapse under severe seismic events.

Beside the life safety, the cost matter is controlling the seismic design of structures. This research aims to provide a general background on the response of various lateral resisting systems and to sustain the field with a proposed alternative system, in order to help in saving lives and considering cost consequently.

Shear wall structures are considered in the field of resisting lateral forces. However, in many practical situations shear walls are connected by a group of lateral members. These lateral members are generally constructed due to the existence of an arrangement of openings (e.g. windows and doors).

The behavior of these coupled shear walls under various seismic events is a hot issue to deal with it, and many researches have focused on it (El-Tawil, 2002a) and (El-Tawil, 2002a).

The following pages show some before/after photos from March 11th, 2011 earthquake that struck Japan. All pictures are courtesy of New York Times newspaper.



Photo 1.1: Fukushima Daiichi Nuclear Plant, before and after

(New York Times Newspaper)



Photo 1.2: Sendai, before and after

(New York Times Newspaper)



Photo 1.3: Iwaki, before and after

(New York Times Newspaper)

1.2 Research Objective

This research aims to provide a general background on the structural systems used in coupling shear walls in seismic areas, to advance an alternative hybrid coupling system for study, and to compare it with other traditional systems.

The implication of this study is that the connecting beams are essentially weaker than the walls. The walls which behave basically as cantilevers, can then impose sufficient rotations on these connecting beams to make them yield before walls do. If suitably detailed, the beams are capable of dissipating energy over the entire height of the wall, in addition to plastic hinge formation at the base.

In the case where coupled shear walls are relatively remote from each other, the coupling beam will be subjected to flexural yielding (long link behavior) which, unfortunately, provides lower levels of ductility (Naiem, 2001). According to seismic provisions for structural steel buildings of the American Institute for Steel Construction (AISC seismic provisions, 2005), the shear yielding (short link) in the plastic hinge is good in energy dissipation and provides larger degrees of flexibility without failure.

This research is intended to study enhancing such coupling beams with diagonal bracing. so that to transform the normal long steel coupling beam behavior into an Eccentric Steel Bracing System coupling the remote shear walls, with a short, easy-replaceable, link: "*FUSE*" to control drift and rotation angle.

1.3 Thesis Layout

As previously stated, this research aims to provide a background on the seismic behavior of the coupled shear walls, and to introduce an alternative system for study and comparison.

Chapter two is partitioned into two parts; the first part discusses the response of structural elements of concrete and structural steel, independently, under seismic excitation, at the level of material, section, member and global structure. While the

second part of chapter two discusses the seismic behavior of various seismic resistant systems, such as shear walls and modern coupling systems of wall. Finally, chapter two will bring forward a proposal of eccentrically braced frames as a preference for coupling shear walls.

Chapter three covers the results obtained from the Finite Element (F.E.) models adopted in this research, and will present comparison between these results. Results mainly concern with structural response of systems; such as story drift, ductility capacity, energy dissipation and plastic hinge location.

1.4 Analysis Methodology

Finite element (FE) analysis has been carried out for decades. Many programs are currently available in the market with trustworthy results, to provide the needed analysis; such as SAP2000 (Armouti, 2004) and ADINA (Khatri and Anderson, 1995).

Between the true behavior and the approximated one, these programs stand. But the intricacy of the true behavior is an arising problem, due to cost and complexity of the analysis which leads to undesirable time consuming.

The ultimate strength design (USD) methodology carried out for seismic excitations considers the composite action of reinforcing steel with concrete. Reinforcement takes tension stresses and concrete takes compression stresses. But, this composite action is not considered in the analysis stage for the most FE programs. For example, a reinforced concrete wall is modeled with elastic shell elements using a linear modulus of elasticity E_c, and with an effective moment of inertia represents cracking in the section, while the steel reinforcement is not considered in the analysis. As a result

of this elastic analysis, the effect of stiffness degradation in reinforced concrete section is not modeled by conventional FE methods.

ADINA finite element computer program suite is considered in this research for structural modeling because it is powered to represent the composite behavior previously discussed. ADINA is used worldwide in engineering practice and research in applications involving static and dynamic nonlinear analysis of solids and structures (Khatri and Anderson, 1995). ADINA program has been frequently selected both by individuals and organizations, as the analysis tool of choice because the prescribed solution methods are known to be reliable and effective. For example, after the 1989 Loma Prieta and 1994 Northridge earthquakes, the ADINA program was chosen by the California Department of Transportation for the re-analysis of seven existing highway bridges, including the San Francisco Bay Bridge (Khatri and Anderson, 1995).

In this research, ADINA program was adopted for the previous mentioned reasons. In order to clarify how ADINA works throughout this research, and since ADINA program is widely recognized, but not known locally, any information relating to the program will be presented respectively to help follower researchers in this field.

1.5 Review of Literature

In the last few decades, many researches have been carried out to focus on the behavior of coupled walls. Nevertheless, few studies were oriented to study the hybrid systems of coupling walls.

El-Tawil et al. (2002a) and (2002b) have discussed the behavior of hybrid coupled walls (HCW) under pushover forcing function. In their work the researchers concluded

that the coupling ratio is an influential parameter whose effect on behavior must be thoroughly understood before a successful design can be achieved. However, their research was controlled by a system response which is dominated by first mode of behavior (due to pushover analysis), and where coupling beams are designed to yield in shear.

In their study, the researchers showed that when magnified by the seismic deflection amplification factor, the proposed design method overestimates inelastic deformations and therefore provides conservative estimates of seismic drift demands. The procedure adopted in their work was found to provide an accurate estimate of force demands because it satisfies compatibility and equilibrium principles.

Another study was carried by Sharooz et al. (2006) on seismic performance of hybrid corewall buildings, and has focused on providing an overview of design issue for (a) steel or hybrid coupling beams and their connections to corewalls, and (b) connections between outrigger beams and corewalls. The researchers concluded that inelastic deformation can be concentrated in replaceable fuses while ensuring elastic response of the coupling beams. This assumption carried out by Shahrooz et al. is to be put into the use of this current research. However, it is also known as *Capacity Design* and will be clarified subsequently.

In their work, an accurate design model for outrigger beam-core wall connections has been developed. This model predicts the connection capacity and its expected mode of failure. Using the proposed model, a capacity design approach may be followed to prevent brittle failure modes (i.e. stud pullout failure or stud fracture) by dissipating energy through ductile yielding and eventual fracture of the shear tab connecting the outrigger beam to the embedded stud plate.

The famous studies of Tom Paulay are well recognized worldwide in the area of coupling shear walls using reinforced concrete coupling beams. In his paper; the displacement capacity of reinforced concrete coupled walls, Paulay (2002) has brought out some interesting formulas for deformation calculations of such coupling beams, and also stated that to satisfy the intents of performance-based seismic structural design, the importance of more realistic predictions of target displacement capacities should be more widely recognized, and has concluded that coupled wall structures offer distinct advantages such as: (i) very good displacement control, (ii) a strong coupling systems allow the use of slender walls without jeopardizing drift limits, (iii) displacement limits during ductile response are not affected by higher mode dynamic effects, (iv) with appropriate detailing of the reinforcement, they can be expected to deliver large hysteretic damping than any other conventionally constructed reinforced concrete systems.

Finally, a coordinated analytical and experimental research program at the University of Cincinnati, by Gong and Shahrooz (2001) has focused on cyclic response of steel/composite coupling beams, their connections to reinforced concrete walls and overall behavior of composite coupled wall systems. The researchers have found that nominal encasement around steel coupling beams provides an effective means of preventing web buckling. Hence, web stiffeners can be eliminated. However, this encasement can also increase the stiffness of the encased coupling beam by positive means.

CHAPTER TWO
HYBRID COUPLED SHEAR WALLS

2.1 Introduction

For decades, the structural behavior of buildings under seismic excitations has been under concerns of engineers. Improving such behavior is a continuous challenging matter that faces researchers.

The objective of modern building codes is to have structures capable of achieving the following performance levels:

- to resist minor earthquakes without significant damage.
- to resist moderate earthquakes with repairable damage.
- to resist major earthquakes without collapse.

In this chapter, the structural elements response under seismic excitations will be discussed firstly and then the overall structural response of the proposed seismic resistant systems will be brought forward.

2.2 Seismic Performance: A Background

2.2.1 Seismic Performance

2.2.1.1 Methods of Analysis

The response of a system (stresses and strains) due to seismic excitations can be evaluated by means of different methods which provide different degrees of accuracy.

Depending on the nature of the considered variables, these methods of analysis can be classified into two types: deterministic and probabilistic.

The deterministic methods of analysis are divided into two main categories; linear elastic analysis and inelastic analysis as explained below:

1. Linear Elastic Methods

a. Equivalent lateral force analysis

This method is the oldest and simplest analysis procedure and is used mostly for current building design (Gioncu and Mazzolani, 2002). The method is solely based on the assumption that the structural response is dominantly controlled by the fundamental period of vibration and the corresponding modal shape. The stress analysis is usually conservative for low to medium high buildings with a regular configuration.

Figure 2.1 shows the linear distribution of forces on a system, and the elastic spectrum which is used for the equivalent lateral forces analysis to obtain pseudo acceleration using the natural period of the system.

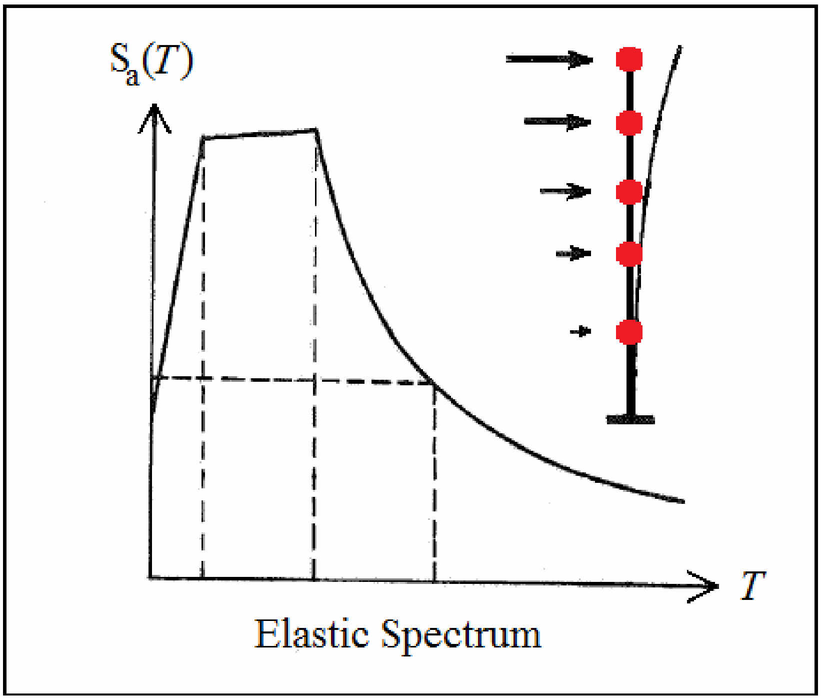


Figure 2.1: Equivalent lateral force

b. Modal superposition method

This method is well known to be a powerful tool for determining the dynamic linear response of elastic damped structural systems (Gioncu and Mazzolani, 2002). The superposition of modal response is expressing the response of multi-degree-of-freedom systems (MDOF).

Figure 2.2 shows sample of mode superposition for a system; fundamental, second, N^{th} mode and their resultant.

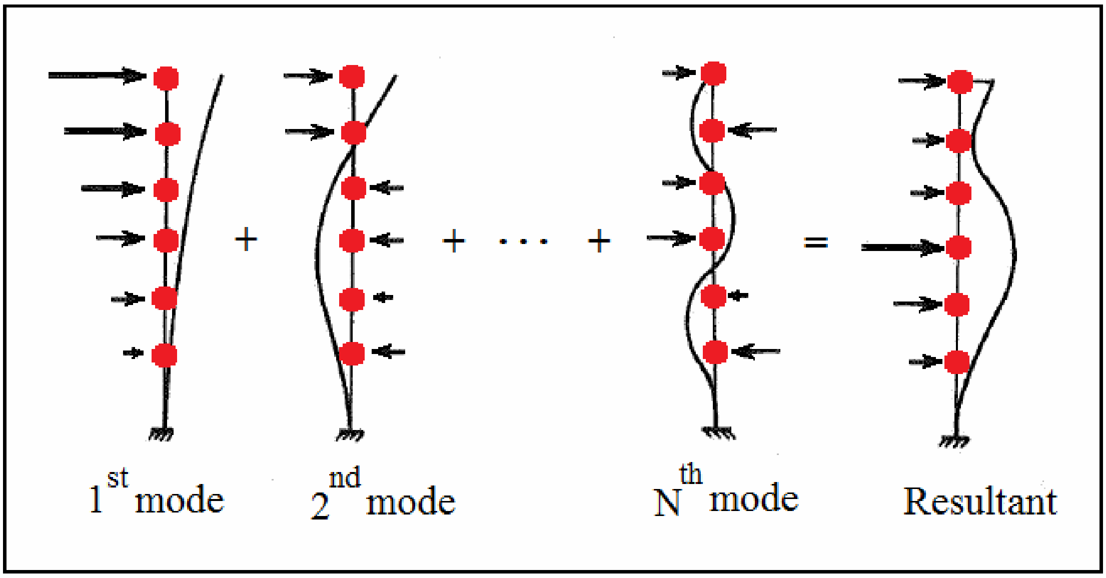


Figure 2.2: Mode superposition

c. Elastic time-history analysis

This method accounts for linear elastic dynamic response analysis to a base excitation employed by direct integration in time of the equations of motion (Gioncu and Mazzolani, 2002). Figure 2.3 shows forces transmitted to a system and internal forces developed accordingly.

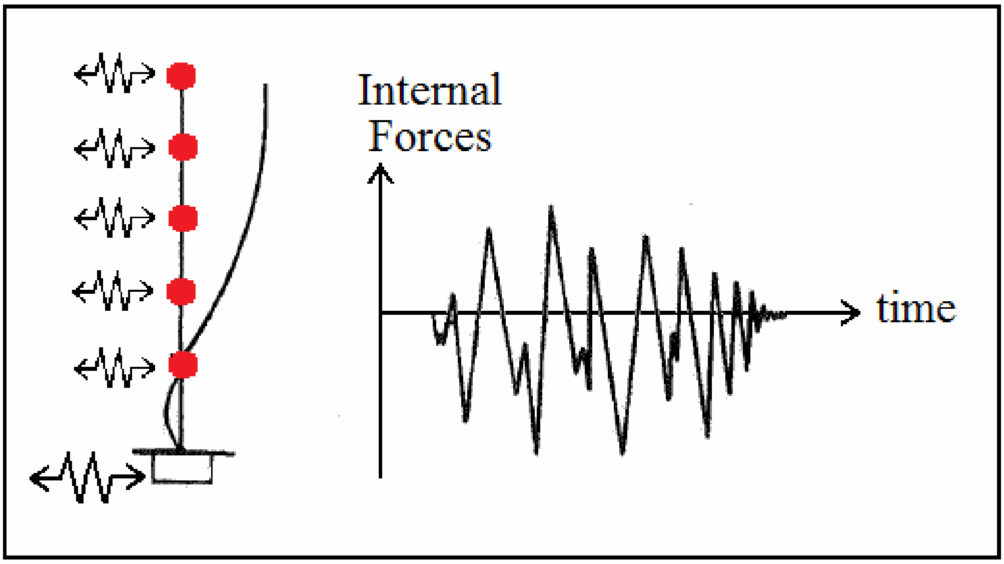


Figure 2.3: Elastic time history analysis

2. Inelastic Methods

a. Plastic analysis

Plastic analysis is used to establish a collapse mechanism in a structure subjected to a loading pattern of seismic actions. This procedure was initially developed for the analysis of steel-frame structures to account for the redistribution of stresses in the inelastic stages. Figure 2.4 shows a collapse mechanism of a structure utilizing plastic analysis.

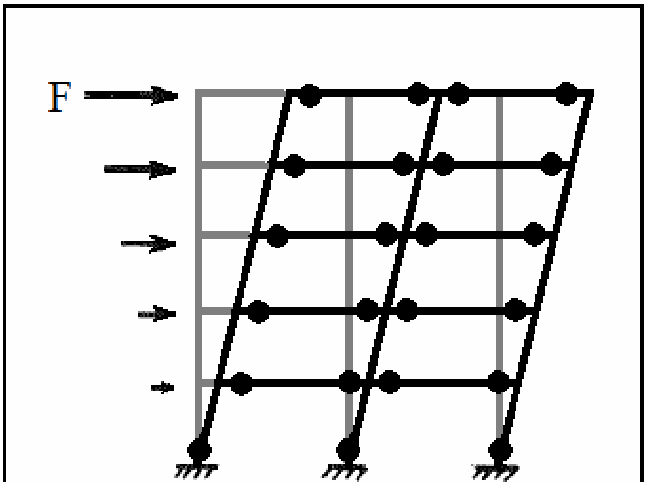


Figure 2.4: Mechanism case of plastic analysis

b. Pushover analysis

Under this method of analysis, the structure will be subjected to static incremental (monotonic) lateral loads. Figure 2.5 shows the pushover analysis curve adopted by Federal Emergency Management Agency (FEMA, 2002) and a structure subjected to such analysis.

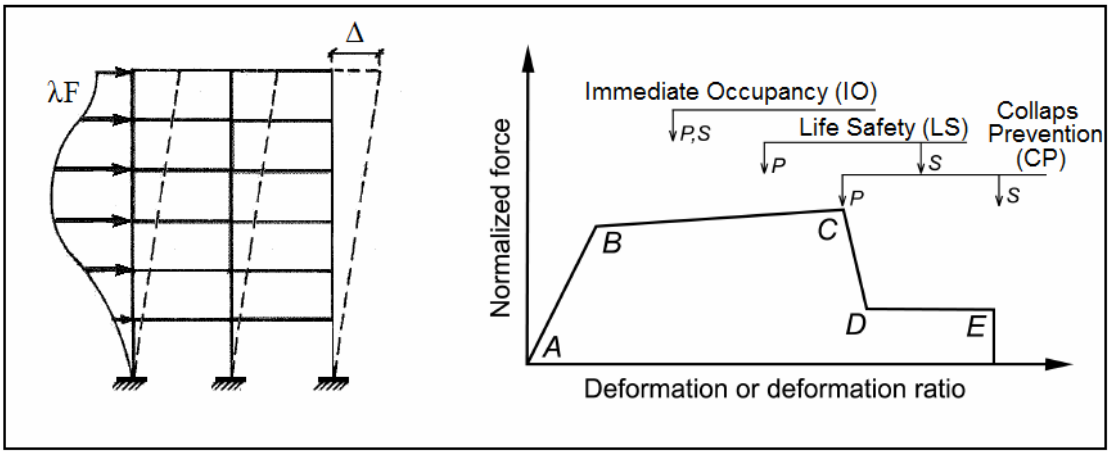


Figure 2.5: Pushover analysis

A non-linear inelastic static analysis procedure is performed, and an inelastic load-deflection response curve is obtained by controlling the displacement at the top of the structure. The implementation of such method is relatively simple, and provides reasonable information on the strength and ductility of the structure and the distribution of demands (FEMA, 2002). This method provides a sight into the critical members likely to possess inelastic response during seismic events, for which attention should be given during the design and detailing process.

The nonlinear static procedure is generally a more reliable approach to characterize the performance of a structure than are linear procedures. However, it is not exact, and cannot accurately account for changes in dynamic response as the structure degrades in stiffness or account for higher mode effects (FEMA, 2002).

c. Inelastic time-history analysis

This method applies a direct numerical integration of the equations of motion. In this aim, different algorithms can be adopted, in which inelastic deformation of the structure elements must be considered. The analysis may be performed using real or simulated ground motions. The variation of displacements at different levels of a frame is presented in Figure 2.6.

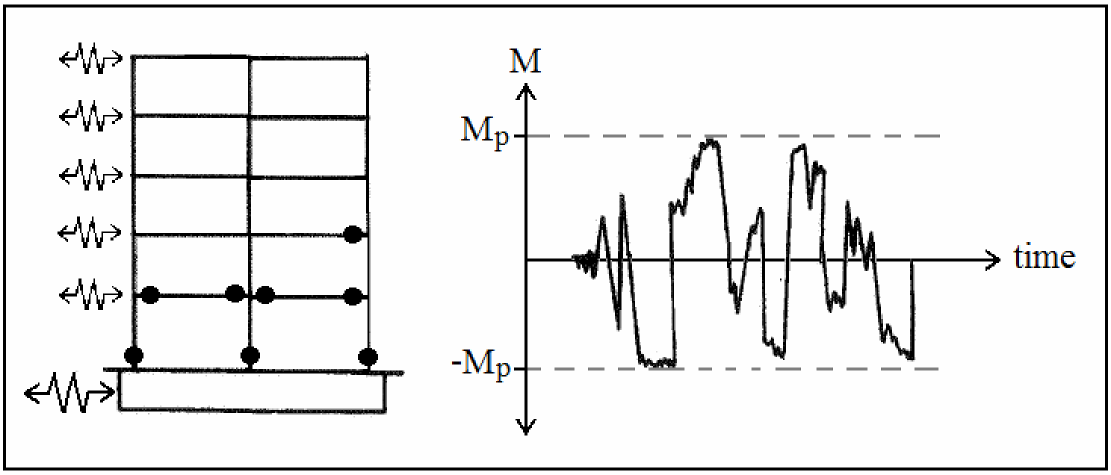


Figure 2.6: Inelastic time history

This method has the ability to describe the actual behavior of a structure during an earthquake. But many challenges face this method: (1) the choice of a proper acceleration time history record and (2) the use of proper mathematical models for structural elements and the modeling of the hysteretic load-deformation behavior of them.

However, modeling complexity and time consuming is the major obstacles facing this method during implementation.

2.2.1.2 Limit States for Seismic Design: Performance Levels

Systems are generally designed for two demands: strength and stiffness, in the traditional practice for non-seismic loads. However, in the presence of seismic

excitations, the ductility demand must be considered also. Refer to Figure 2.7 where each performance level is associated with significant structural demand and specified type of analysis.

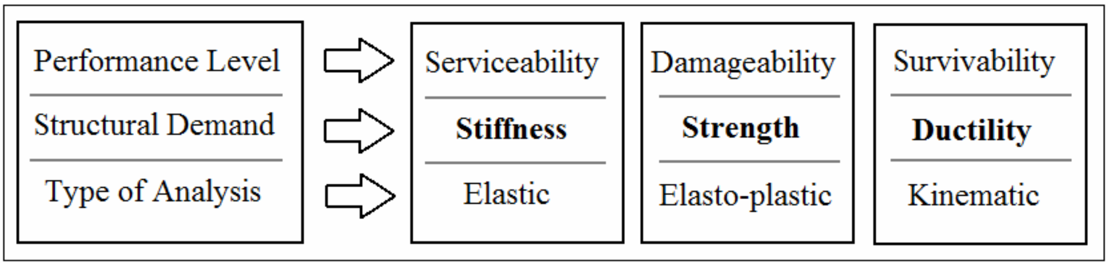


Figure 2.7: Performance levels (Gioncu and Mazzolani, 2002)

1. Serviceability limit state

   This limit state is represented by stiffness demand.

   Stiffness check which corresponds to the serviceability limit state is associated with the control of the structural displacements during minor earthquakes (story drift, sway control), and to ensure that all deformations under the loading action are reliably quantified and resisted purely in elastic manner (Gioncu and Mazzolani, 2002).

2. Ultimate (Damageability) limit state

   This limit state is represented by strength demand.

   Strength check, including stability, which corresponds to the ultimate limit state, focuses on the ability of protecting the structure against damage, and to assure that the overall system is functioning in a desired elastic manner, or with limited plastic deformations in predetermined locations (Gioncu and Mazzolani, 2002).

3. Survivability limit state

   This limit state is represented by ductility demand.

Survivability limit state is represented by the ability of the system to undergo large deformations beyond the elastic limit, and to dissipate absorbed energy through plastic deformations (Gioncu and Mazzolani, 2002).

Ductility demand check focuses on minimizing and localizing major damage and to ensure survival of a building. Although achieving this limit is somehow considered to be "failure", remarkable additional inelastic deformations may still be possible without structural collapse. Thus, the building remains functional for the purposes of civil evacuation and life safety.

It is important to mention that modern codes consider two levels of performance; serviceability and ultimate limit states. Serviceability limit state covers stiffness and strength demands to ensure the capability of the structure to respond in elastic manner with partial plasticization, however, in the ultimate limit state demand of strength checks the elasto-plastic analysis and ductility demand covers the kinematic analysis.

2.2.1.3 Capacity Design

The strength of an element under ductility demands is considerably less than that corresponding to elastic response. The capacity design procedure ensures that energy dissipation can be maintained during severe events (Paulay and Priestley, 1992). The following features shall characterize the procedure (Paulay and Priestley, 1992):

1. Potential plastic hinge regions within the structure are previously defined. These regions are carefully detailed to ensure that estimated ductility demands in these regions can be achieved.
2. Undesirable modes of inelastic deformation, such as shear deformations or anchorage failures and instability, within plastic hinge regions, are prohibited.

3. Potentially brittle regions must be protected by ensuring that their strength exceeds the demands resulting from the overstrength of the plastic hinges.

2.2.2 Ductility Definition

2.2.2.1 Introduction

Ductility can be defined as the ability of a structure to undergo inelastic deformations beyond its initial yield, without any significant reduction in ultimate strength. Ductility is generally expressed by ductility ratio; this ratio relates the maximum inelastic deformation under consideration to the actual yield deformation. The importance of ductility calculations is to predict the ultimate deformation capacity of the structure under investigation.

2.2.2.2 Ductility Types

The following is a discussion on types of ductility:

- Material ductility (also named deformation ductility, strain ductility and kinematic ductility), which characterizes the plastic deformations in the materials for various types of loading. Figure 2.8 shows a stress-strain curve that describes the material ductility

$$\mu_\varepsilon = \frac{\varepsilon}{\varepsilon_y} \quad \text{(Eq. 2.1)}$$

Where the stress is

$$\sigma = \frac{P}{A} \quad \text{(Eq. 2.2)}$$

While strain is

$$\varepsilon = \frac{\Delta}{l}$$

(Eq. 2.3)

Where

A = Area

P = Force

Δ = Displacement

□ = Strain

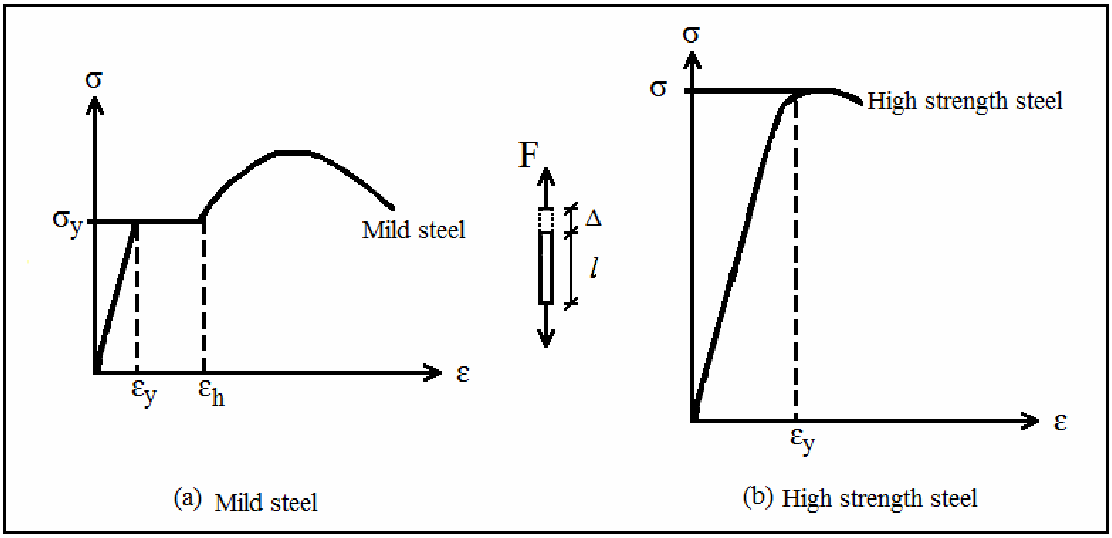


Figure 2.8: Material ductility

○ Cross section ductility (curvature ductility). Curvature ductility corresponds directly to the cross-sectional plastic deformations. Figure 2.9 shows curvature ductility of a section.

$$\mu_{\kappa} = \frac{\kappa}{\kappa_y}$$

(Eq. 2.4)

Where

κ = Curvature

κy = Yield curvature

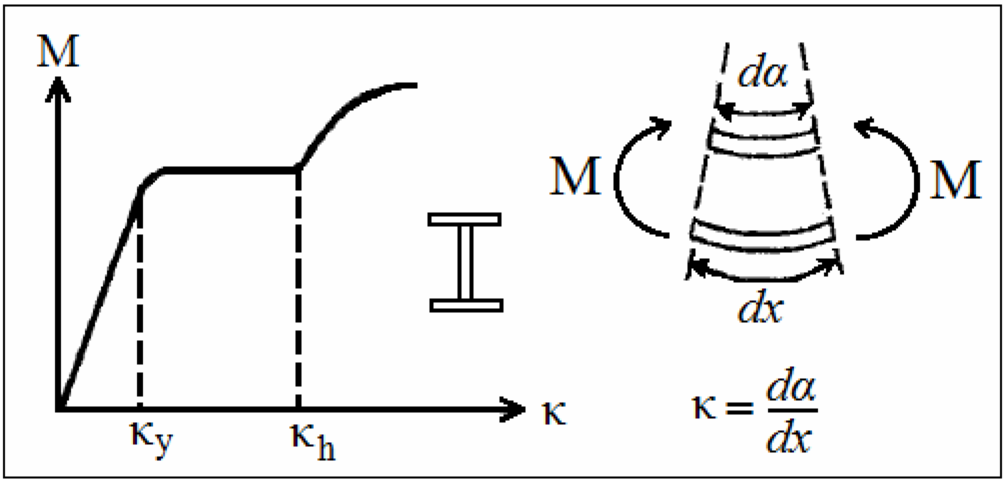


Figure 2.9: Cross-section ductility

○ Member ductility (rotation ductility). Rotation ductility corresponds to the beams rotation at specified locations along the axis of the beam. Figure 2.10 shows the moment-rotation curve for a member, where rotation ductility can be calculated accordingly.

$$\mu_\theta = \frac{\theta}{\theta_y} \qquad \text{(Eq. 2.5)}$$

Where

θ = Rotation

θ_y = Yield rotation

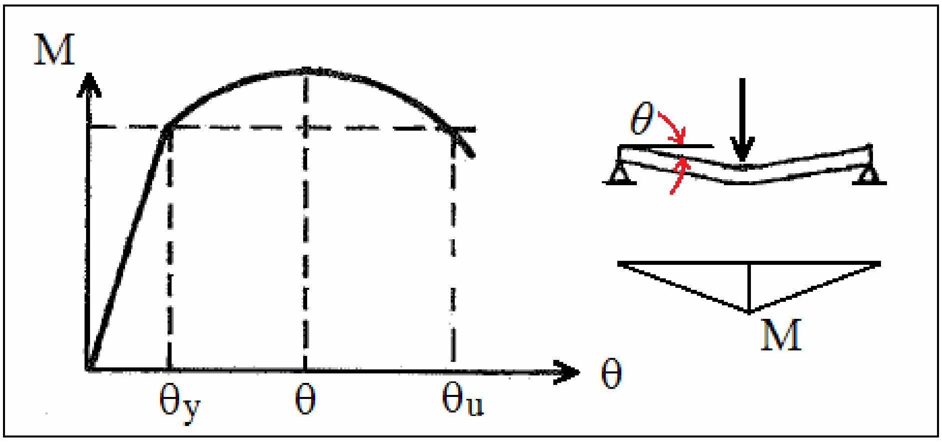


Figure 2.10: member ductility

○ Structure ductility (displacement ductility) which considers the overall behavior of the structure. This type generally characterizes the top displacement of the structure. Figure 2.11 shows the ductility employed by the system in terms of top displacement. It is desired to note that this ductility is termed "global", while the previously mentioned ductilities are called "local".

$$\mu_\Delta = \frac{\Delta}{\Delta_y}$$

(Eq. 2.6)

Where

Δ = Displacement

Δy = Yield displacement

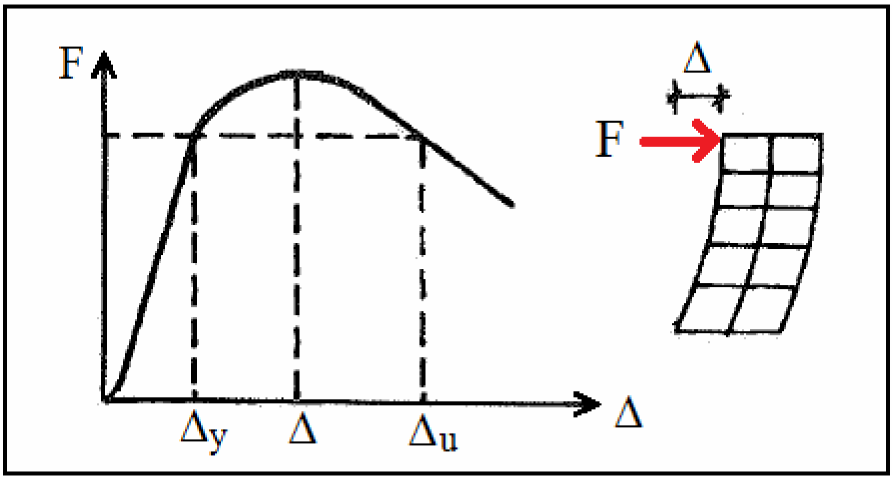


Figure 2.11: Structure ductility

○ Energy ductility (hysteretic ductility), which considers the level of dissipated seismic energy.

A relationship among the different types of ductility exists. Generally, the global ductility capacity (structure ductility) is function of local ductility capacities. Member ductility, also, depends on cross-section ductility, μκ, and material ductility, μ□.

2.2.2.3 Ductility Limits

A very important value in seismic design is the ductility limit. To ensure safe design, the system must exhibit adequate ductility capacity, μ_c, that covers the ductility demand, μ_d.

$$\mu_c \geq \mu_d$$

(Eq. 2.7)

These two ductility limits can be defined as follows:

- Ductility capacity, μ_c. This limit results from the behavior of structures and concerns the system response. Various parameters are controlling this type of ductility, such as material properties, cross-section type and degradation in stiffness and strength due to plastic excursions.
- Ductility demand, μ_c. This limit results from seismic events generally, and describes many factors influencing these excitations: magnitude, ground motion type, soil influence, natural period of structure versus ground motion.

2.2.2.4 Force Reduction Factor

In order to achieve a reasonable design of structures that eliminates high cost resulting from elastic response, a reduction of force must be employed to account for inelastic response; such reduction can be implemented, mainly, by recognizing the ductility of the system (Armouti, 2004).

Figure 2.12 shows the force reduction factor, R, which is defined as the ratio of the elastic strength demand to the available yield level of the system. R can also be expressed in terms of displacements:

$$R = \frac{F_e}{F_y} = \frac{\Delta_e}{\Delta_y}$$

(Eq. 2.8)

Where

F_e = maximum force due to the linear elastic response of the system

F_y = force at the yield level of the system

Δ_e = maximum displacement due to linear elastic response of the system

Δ_m = maximum displacement of the system

Δ_y = yield displacement of the system

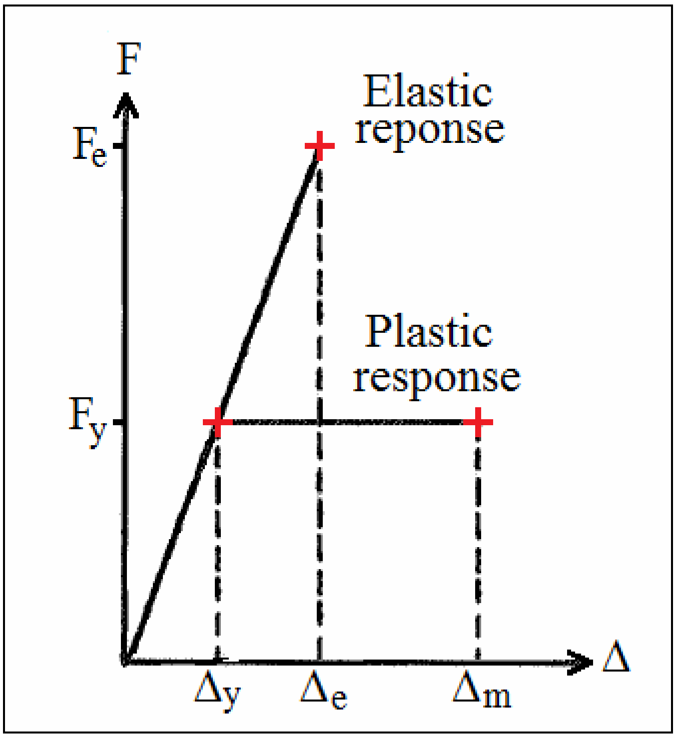


Figure 2.12: Force reduction factor

Ductility demand is function of the amount of force reduction. For long period structures, (greater than that corresponding to peak elastic spectral response), Newmark has found that the maximum displacement reached by the inelastic system are equal to

those obtained from an elastic system with the same stiffness as the initial elastic stiffness of the inelastic system, but with unlimited strength (Armouti, 2004). This criterion is termed *equal displacement criterion*. Referring to Figure 2.13a, the force reduction factor achieved by the inelastic system is, in statistical sense, equal to the ductility.

$$R = \mu_d$$

(Eq. 2.9)

For shorter-period structures, (shorter than the peak spectral response period), the displacement ductility demand is greater than the force reduction factor. Newmark has observed that the peak displacement ductility factor achieved can be estimated reasonably well by equating the area under the inelastic force-deflection curve and the area under the elastic relationship with equal initial stiffness. This criterion is termed *equal energy criterion*. By equating areas under the curves shown in Figure 2.13b, which represent absorbed energy, the force reduction factor will be, (Armouti, 2004):

$$R = \sqrt{2\mu_d - 1}$$

(Eq. 2.10)

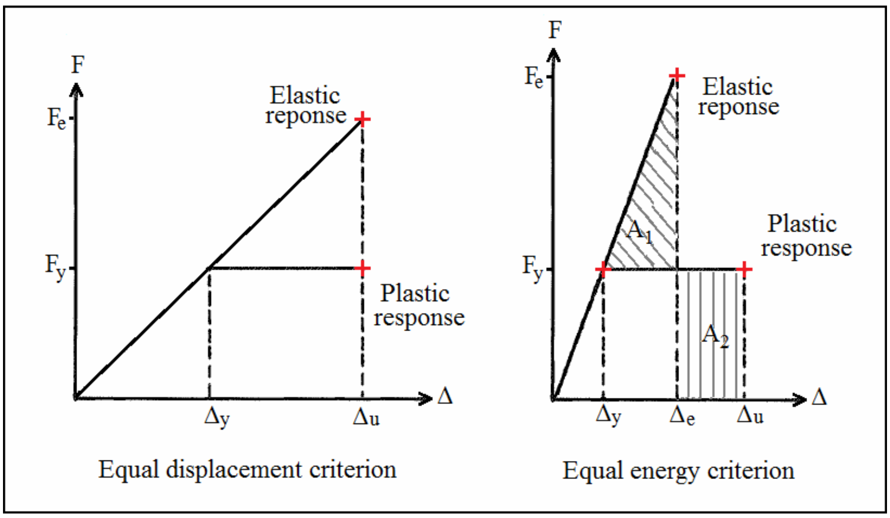


Figure 2.13: Equal displacement and equal energy criteria

2.3 Structural Elements Response under Seismic Excitations

2.3.1 Structural Steel Response

2.3.1.1 Steel Response: Material Level

2.3.1.1.1 Introduction

In seismic design, a convenient selection of material promises in a good ductility capacity. An arbitrary selection may result in an undesirable response of the system. This is an arising problem, because steel developers tend to introduce high strength materials, despite the fact that these high strength materials exhibit less ductile behavior (Gioncu and Mazzolani, 2002).

2.3.1.1.2 Factors Influencing Material Properties

Mechanical factors that affect steel properties, which contribute directly to the erosion of the quality of the produced material, may be listed as follows:

- Strain-rate $\acute{\varepsilon}$

Strain rate expresses the velocity of loading action; this term can define the type of loading introduced to the structure (static, dynamic). According to Figure 2.14, it is clear that for strain rates lower than 0.10 /sec, the excitation of the system shall be considered static and the inertial forces can be disregarded (Gioncu and Mazzolani, 2002).

- Plastic strain accumulation

Many researchers have classified the failure of members under loading cycles of an earthquake as due to low-cycle fatigue. However, this assumption is questionable. Earthquake cycles which can be less than 5 cycles induced plastic excursions in short

duration earthquake, or no more than 20 cycles of large plasticity present for long duration earthquake, as shown in Figure 2.15. These low cycles with high inelastic deformations presented by seismic excitations cause an accumulation of these deformations along the yield line, introducing cracking or rupture in the buckled elements. However, fatigue failure will occur because of the reduction of the material strength due to cyclic stresses (Gioncu and Mazzolani, 2002).

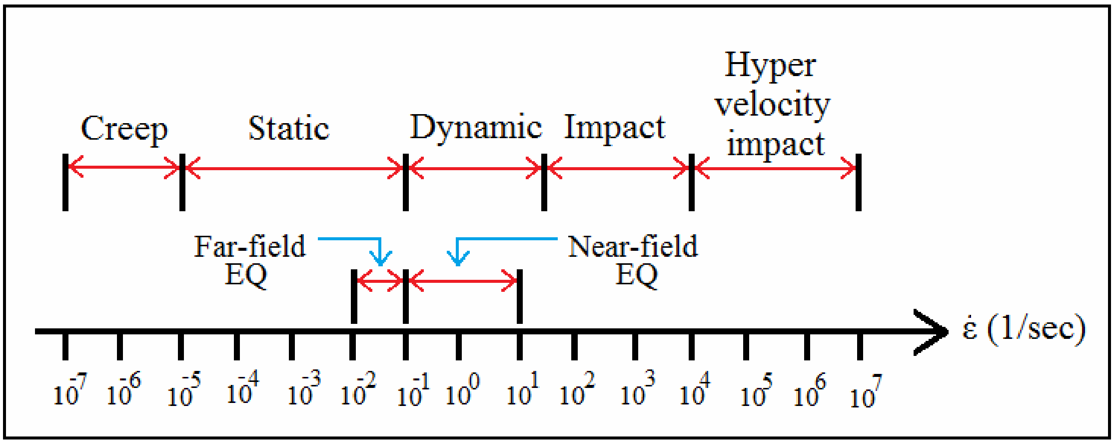


Figure 2.14: Strain rate effect (Gioncu and Mazzolani, 2002)

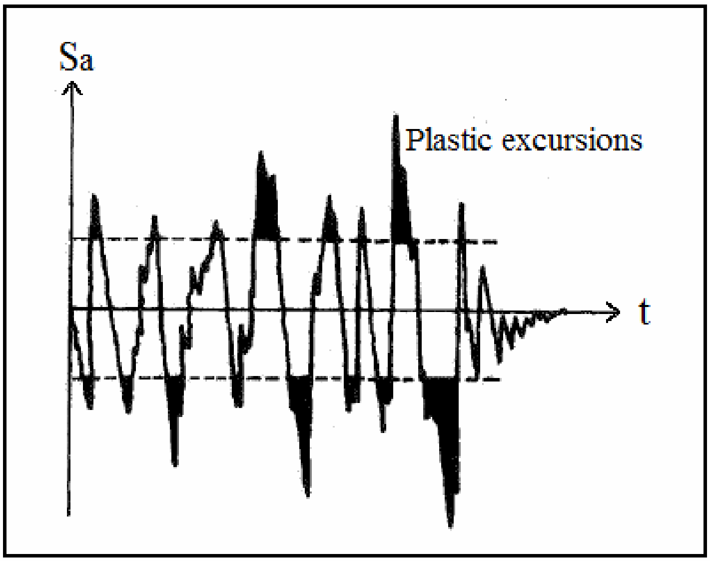


Figure 2.15: Earthquake record

2.3.1.1.3 Yield Ratio

Yield ratio is expressed by the yield stress of the steel proportioned to the ultimate tensile strength:

$$\rho_y = \frac{f_y}{f_u}$$

(Eq. 2.11)

Where

f_y = Yield stress

f_u = Ultimate stress

It was recognized that for low values of ρ_y, a good ductility is introduced by the material. If $\rho_y < 0.75$, then the yield ratio is considered to be low, while it is high for $\rho_y > 0.75$. As a consequence, ductility demand will be subjected to substantial softening by increasing the yield ratio. However, according to material selection for seismic resistant structures, a yield ratio that ensures a good ductility behavior is below 0.70.

The yield ratio topic is a hot issue these days, where the steel producers introduce high tensile strength (≈ 600 MPa) with yield ratios greater than (0.9). These high strength materials show a very poor structural ductility. For this reason (AISC seismic provisions, 2005) limits the steel material usage with steel grade 345 MPa (50 ksi) as maximum. However, recent developments in the production of steel members results in high strength steel with a reasonable yield ratio (≈0.75) which can be considered acceptable in seismic design.

There is another parameter that has an adverse influence on the yield ratio; which is the high strain rates that might generate in the near-field quakes, which ranges from

10^{-1}/sec to 10^{1}/sec. These strain rates will harmfully reduce the ductility capacity of the structure due to yield ratio decreasing.

2.3.1.1.4 Influence of Cyclic Loading

Loading, unloading and reloading in the reversed direction (for example: tension, unloading, compression…), as shown in Figure 2.16, will generate a semi loading loop. In the reversal stress, degradation in stiffness is presented due to the earlier yielding. If the specimen is loaded in tension again, then the curve will deviate from the linear response far beneath the virgin yield stress, but it will be able to reach the stress and strain obtained in the first tension loading cycle, this phenomenon happens when the reversal occurs within yield plateau region, while for the usual case, the reversed action tends to occur within the strain-hardening region. In this case, the shape of the reversal curve is independent of the virgin stress-strain curve; the yield plateau disappears in both directions. The reversal curve, shown in Figure 2.16, depends on the maximum tensile load that has been reached (Gioncu and Mazzolani, 2002).

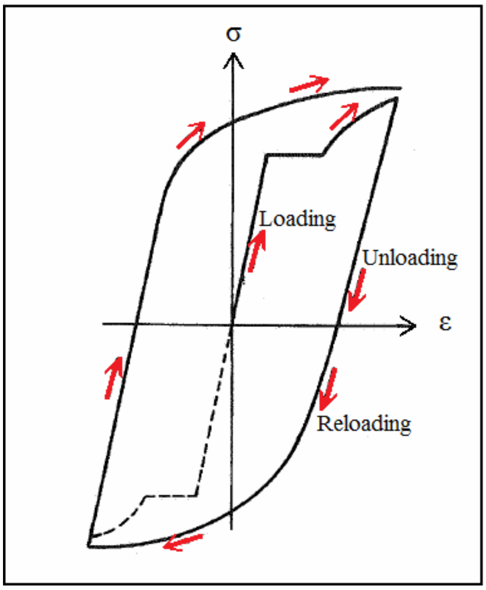


Figure 2.16: Reversal stress-strain curves, (Gioncu and Mazzolani, 2002)

The loading, unloading and reloading curves outline a hysteretic loop, as shown in Figure 2.17. Hysteretic loops, generally expresses hysteretic ductility, while the area enclosed within these curves is equal to the dissipated energy.

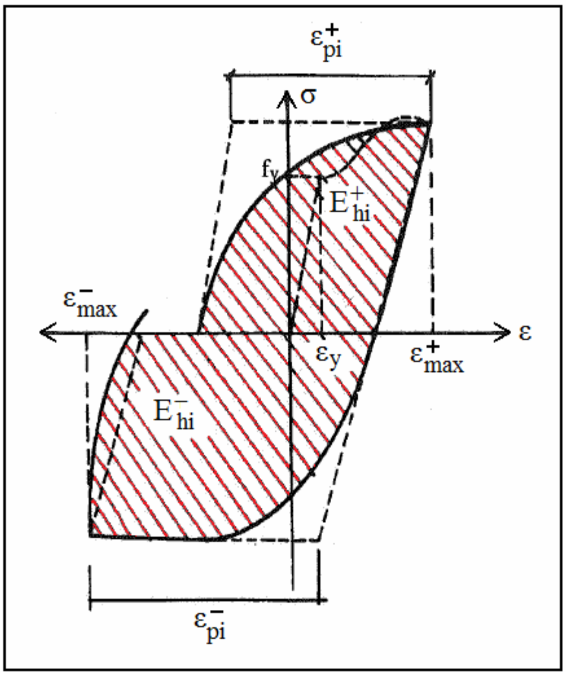


Figure 2.17: Hysteretic energy, (Gioncu and Mazzolani, 2002)

Cyclic loading types vary according to the Control Parameter (CP) which represents the amplitude of the waves (stress or strain); this control parameter can be:

(1) *Constant CP* (fixed value). This type of cyclic loading, which is shown in Figure 2.18, is employed for determining the low cycle fatigue effects.

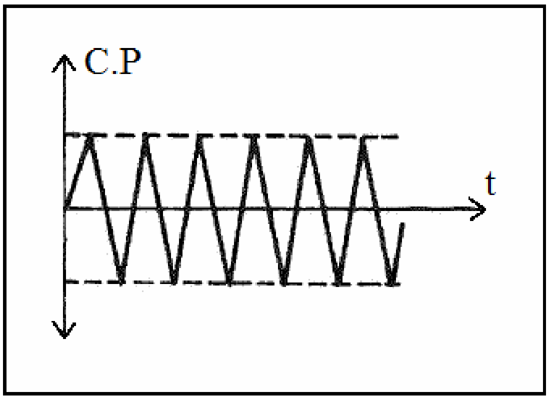


Figure 2.18: Fixed control parameter cyclic loading

(2) *Increasing CP*. This type can be represented by increasing the CP value after each cycle, as shown in Figure 2.19, or after three cycles. This type of cyclic loading is generally a good representation for far-field earthquake excitations.

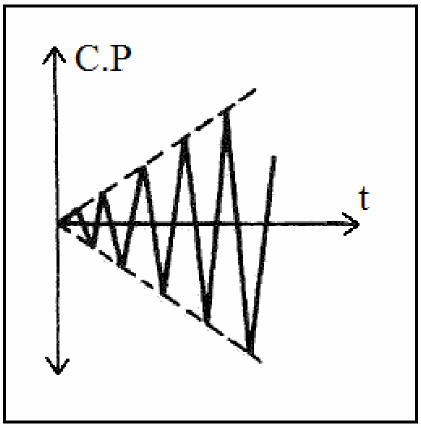


Figure 2.19: Increasing control parameter cyclic loading

(3) *Decreasing CP*. This type can be represented by decreasing the CP value after each cycle, as shown in Figure 2.20, or after three cycles. This type of cyclic loading expresses the excitations of near-field earthquakes, in a good manner.

It is worth to mention that the control parameters of cyclic test can be performed by means of controlling either strain or stress. Laboratory tests, generally, carries tests under the strain control parameter, while the stress control is more realistic for

expressing the behavior of structures under real seismic actions (Gioncu and Mazzolani, 2002).

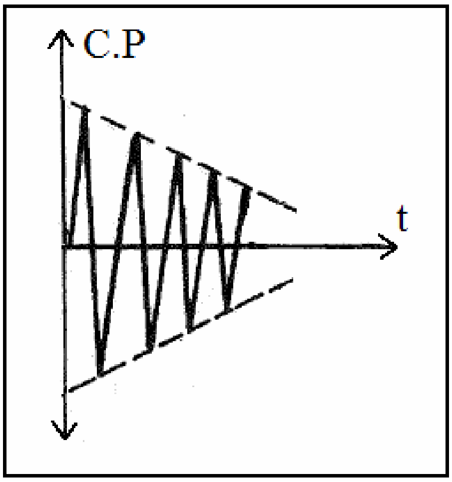


Figure 2.20: Decreasing control parameter

2.3.1.1.5 Fractures in Steel Elements

Steel structure subjected to strong earthquakes can collapse either by ductile mode or brittle mode of fracture (Plumier, 2000). The failure mode is governed by stress level, strain-rate, temperature, and many other factors (Gioncu and Mazzolani, 2002).

If fracture takes place when the available strength is exceeded by the first plastic deformation, then this is the definition of the "single plastic excursion failure" (Gioncu and Mazzolani, 2002). This case may represent structures subjected to seismic actions which are near to source (Gioncu and Mazzolani, 2002). Three sequential phases are composed for this type of fracture: (1) initiation of a ductile crack, then (2) stable growth of the crack, and finally (3) sudden propagation of the crack in a brittle manner. This kind of fracture is released by ductile cracks at strain concentration.

However, if the collapse occurs due to cumulative effects of a number of excursions in plastic range, then this represents the "more plastic excursion" failure

(Gioncu and Mazzolani, 2002). This type of failure is characteristic for structures in situation of intermediate or far field ground motions, where the collapse is dominated by cyclic loading.

Cumulative strain capacity under plastic cycles in the ductile crack range seems to be basically equal to the monotonic strain capacity, when the accumulation is due only to tension field (Gioncu and Mazzolani, 2002). This observation is crucial, because the plastic strain capacity preceding the crack onset under cyclic seismic loading can be predicted from the crack initiation strain obtained under monotonic loading. So, the monotonic loading test could be used to qualify steel for seismic applications (Kuwamura, 1997) mentioned in (Gioncu and Mazzolani, 2002).

2.3.1.1.6 Element Ductility

All properties obtained from tests representing materials are generally kept also for elements, but with some differences that can be summarized as follows:

- Behavior in tension and compression. Element ductility can be seriously affected by the mode of failure, because compression failure is characterized by buckling in plastic regions, while tension mode of failure is dominated by the mechanical properties.
- Element type. Two elements compose all types of structural steel: (i) Plate with two supported edges, such as web of wide flange section or edges of box section, and (ii) One free edge plate, expressing flange of wide flange section, leg of angle section.
- Loading type. The element loading type is always an in-plane type and can be characterized by uniform axial compression or tension, bending, and bending and axial force.

2.3.1.1.7 Behavior of Plates under Cyclic Loading

Due to Cyclic loading, all mechanical properties of steel plates deteriorate, including ductility.

- Cyclic behavior under constant strain amplitude.

During tests, it is noticed that the maximum load capacity in compression side decreases and the residual deflection increases, as the number of cycles increases (Gioncu and Mazzolani, 2002). This reduction of load capacity in compression is due to the sensitivity to the initial deflection. However, plate ductility decreases continuously during cyclic loading due to the erosion of compressive load capacity.

It must be mentioned that the tensile capacity of the plate will not be heavily affected by the cyclic loading (Gioncu and Mazzolani, 2002).

- Cyclic behavior under various strain amplitude.

The loading carrying capacity at the compression side decreases as the strain amplitude increases. However, it is worth to mention that the reduction being more important than under monotonic loading, as shown in stress-strain curves presented in Figure 2.21. This is due to the fact that the initial deflection for each cycle increases due to the former cycle. Consequently, the plate ductility may be rapidly deteriorates during cyclic loading, as shown in Figure 2.21.

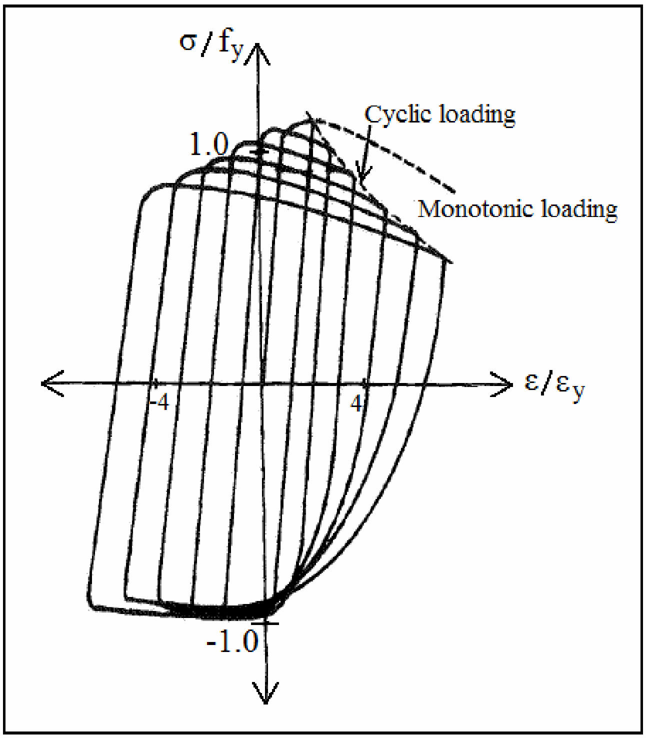


Figure 2.21: Stress-strain under cyclic loading for plates (Gioncu and Mazzolani, 2002)

- Accumulation of plastic deflections.

Due to residual plastic deflection forming, the initial deflection at each new cycle is greater than the former cycle. It is observed that after the buckling occurrence, the direction of deflection can never be reversed under the action of the opposite load, each cycle producing the increasing of the initial deflection for the next cycle. This phenomenon causes a decreasing of the maximum load capacity.

- Asymmetry in cyclic behavior

In monotonic loading, and according to local buckling of the plate, a part of the width of the compressed flange becomes ineffective which causes the neutral axis to be shifted toward the flange in tension, as explained by strain-curvature curve shown in Figure 2.22a. This condition employs different deformations at the two plates, the compressive strain being larger than the tensile one. So, the tensile strain must remain

constant, while the compressive strain increases with the increase of curvature demand. This behavior exhibits an asymmetry in strain over the section (Gioncu and Mazzolani, 2002).

In the case of cyclic loading, this asymmetry in deformations is preserved, the compression strains always being much larger than the tension strains, as presented by strain-cycle number curve shown in Figure 2.22b. So, the tension stresses fails to straighten the buckled surface.

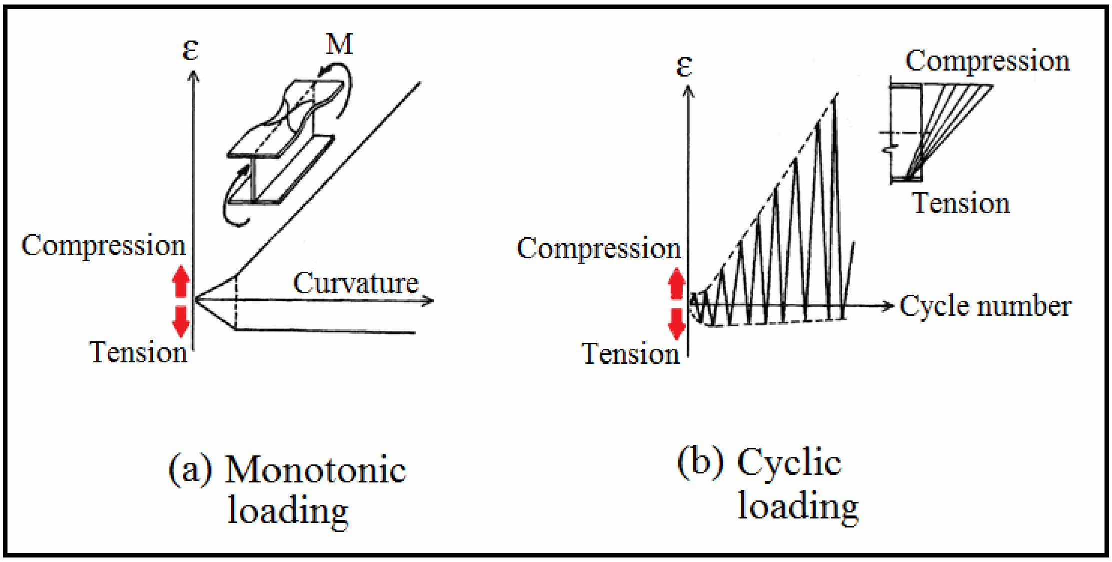


Figure 2.22: Asymmetry in cyclic behavior (Gioncu and Mazzolani, 2002)

2.3.1.2 Steel Response: Section Level

2.3.1.2.1 Introduction

This section discusses factors that increases deterioration of mechanical properties at the section level, this deterioration may be represented mainly by plastic buckling phenomenon, refer to Figure 2.23 for more clarification.

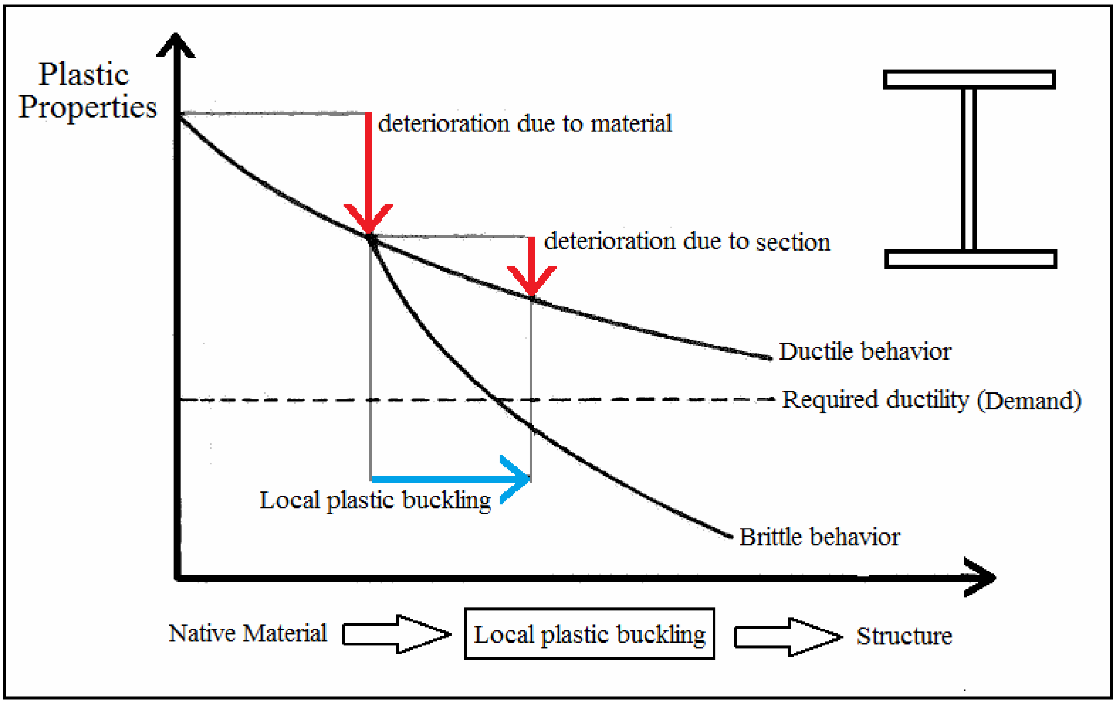


Figure 2.23: Ductility deterioration due to section behavior
(Gioncu and Mazzolani, 2002)

2.3.1.2.2 Factors Influencing Section Ductility

The collapse of steel structures occurs either due to local buckling or to fracture of elements. The main factors influencing section ductility are:

- Cross-section: wide flange sections, hollow box and channels.
- Fabrication process: hot-rolling, cold forming or welded plates.
- Buckling mode: buckling may occur in flange, web, or interaction between both.

2.3.1.2.3 Plastic Behavior of Sections

Pure flexural yielding:

Prior to yield, in the elastic region, the stress and strain relationships are linear over the depth of the section. Only the extreme fibers may reach yield, as shown in Figure 2.24 where $\sigma \leq f_y$, and the corresponding moment at the extreme fibers is:

$$M_y = Sf_y$$

(Eq. 2.12)

Where

S = *Elastic* section modulus

fy = Yield stress

In the ultimate case, strain increases after plastic yielding, while stresses remain constant, as shown in Figure 2.24. The case of plastic hinge formation is shown in Figure 2.24 where ($\sigma = f_y$), and the full plastic moment, M_p, is reached:

$$M_p = Zf_y$$

(Eq. 2.13)

Where

Z = *Plastic* section modulus

fy = Yield stress

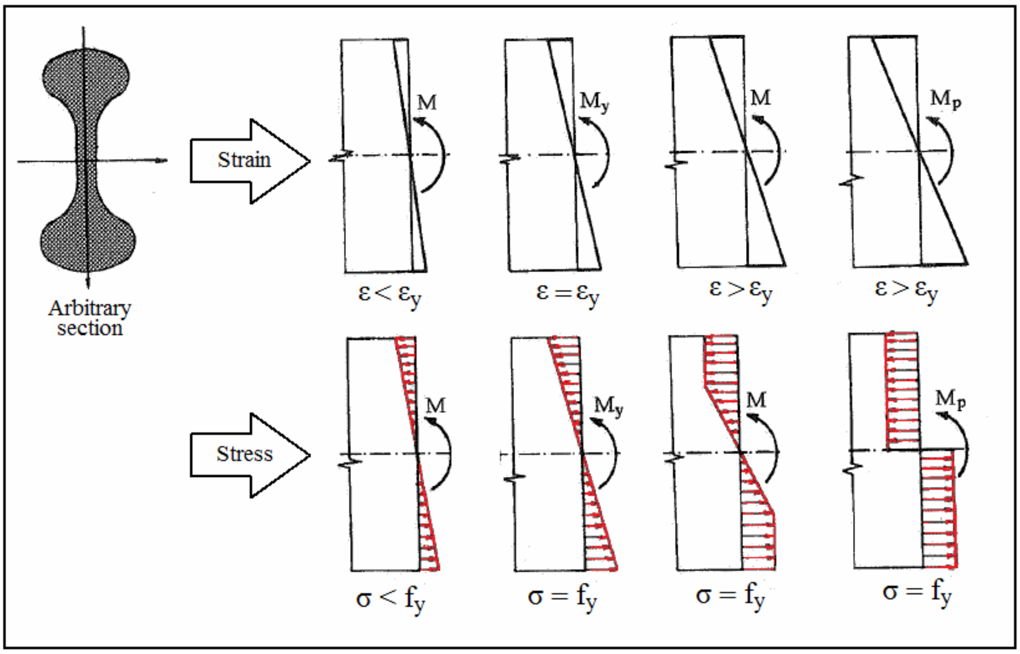


Figure 2.24: Stress and strain under pure bending (Chen and Sohal, 1994)

Axial force influence:

Most of the structural steel components in buildings exhibit beam-column behavior, in which sections have to carry significant axial forces in addition to the bending moment. Plastic axial force that sections can carry:

$$N_p = Af_y$$

(Eq. 2.14)

Where

A = Area

*f*y = Yield stress

Shear force influence:

Shear forces must be carried by all sections excluding the zones of constant moment (i.e. plastic zones). Thus, when yield occurs in bending, the remaining elastic zones only undertake the shear stresses. This means that a combination, between axial stress, σ, due to moment and shear stress, τ, due to shear forces, exists. For ductile material, the Tresca and Von Mises criteria are the most common failure criteria to determine the start of yield (Boresi and Schmidt, 2003):

$$(\frac{\sigma}{f_y})^2 + (\frac{\tau}{\tau_y})^2 = 1$$

(Eq. 2.15)

$$\tau_y = \frac{f_y}{\sqrt{3}} = 0.577 f_y$$

(Eq. 2.16)

Where

σ = Normal stress

τ = Shear stress

fy = Yield stress

τ_y = Yield shear stress

Influence of local buckling:

The ultimate moment is, somehow, an idealized case that cannot be reached due to the existence of plastic buckling phenomenon in the strain hardening range.

2.3.1.2.4 Ductility Classes of Sections

The ductility capacity of a section is expressed in terms of curvature, and can be defined as the ability of the section to undergo large curvature beyond its yield curvature limit (Naiem, 2001).

The element ductility can be used for the classification of cross-sections in different behavioral classes as stated by (Gioncu and Mazzolani, 2002):

(i) Plastic elements, characterized by plastic buckling with high plastic deformations at collapse;

(ii) Compact elements, which provide plastic buckling with moderate plastic deformation at collapse;

(iii) Semi-compact elements, for which yield stress may be attained, but the buckling is mainly elastic; and finally the

(iv) Slender elements, for which the collapse occurs for elastic buckling.

Figure 2.25 shows the effect of slenderness of member components on the curvature ductility; the thinner provided element the lesser ductility capacity gained.

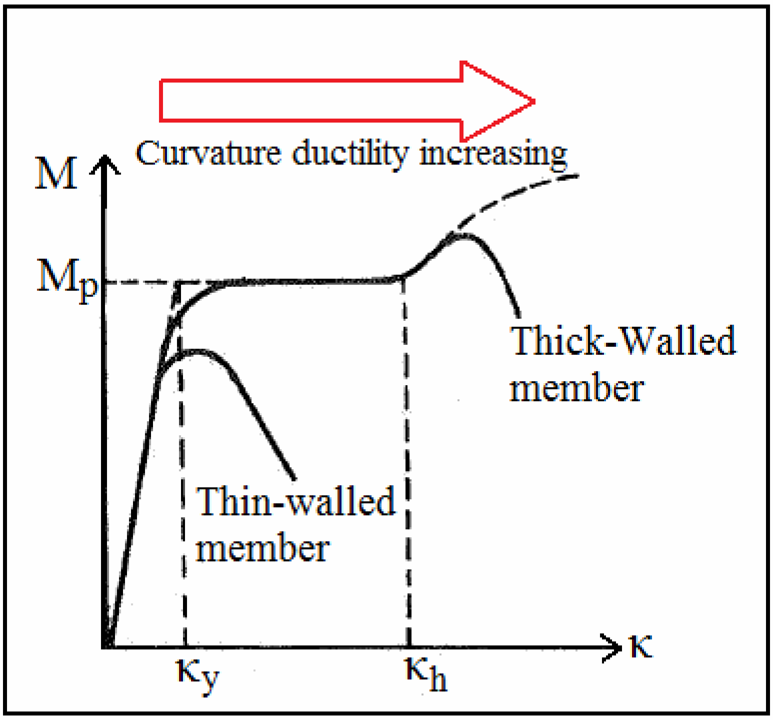


Figure 2.25: Slenderness influence on curvature ductility

(Gioncu and Mazzolani, 2002)

Euro Code (EC8) implements a classification for sections in terms of curvature ductility, $\mu\kappa$ as following:

Class A (ductile section): $\mu\kappa \geq 15$

Class B (Compact section): $\mu\kappa \geq 6$

Class C (Semi-compact): $\mu\kappa \geq 3$

Modern codes classifies section ductility in terms of slenderness ratio (height/thickness) for each element in the sections under consideration, (either two edge supported element or one free edge element). This is conventional because the curvature ductility is function of slenderness ratio, as presented in Figure 2.25, and such

demonstration must be smoother to the designers. However, the assumption that each mode of buckling is independent of the others is unreasonable, because, evidently, in wide flange section for example, the flange is restrained by the web and the web is restrained by the flanges. Figure 2.26 shows buckling modes of wide flange section, which are affected by element slenderness.

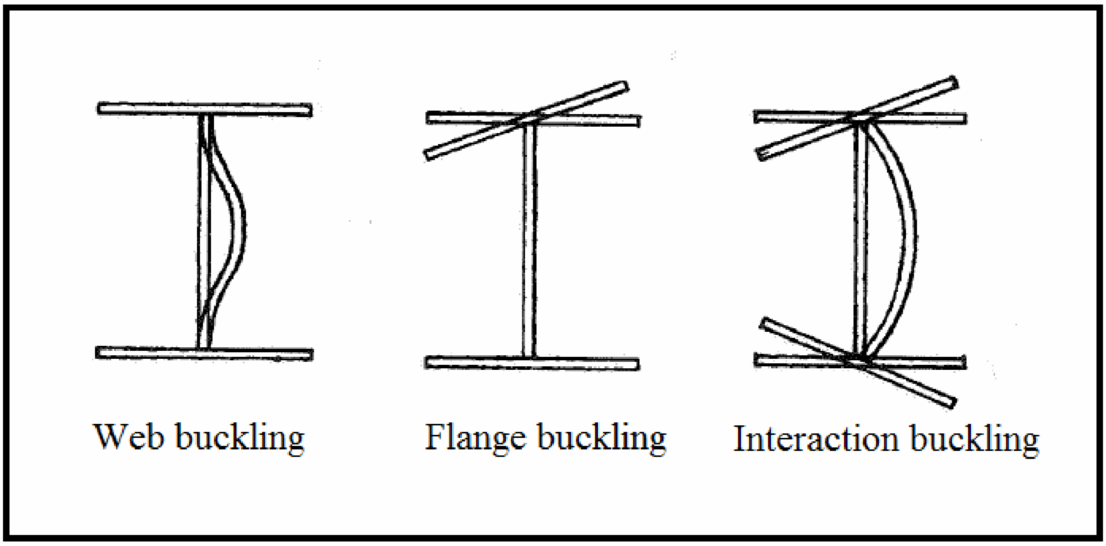


Figure 2.26: Buckling modes in wide flange section (Gioncu and Mazzolani, 2002)

Finally, it is important to mention that modern codes also neglect the effect of the ratio of section depth to unrestrained flange width (i.e. 2d / b_f). Increasing the section depth will decrease the axial local ductility capacity.

2.3.1.3 Steel Response: Member Level

2.3.1.3.1 Plastic Properties Deterioration

In plastic design, it is evidently proved that material ductility cannot describe, by its own, the overall capacity of the structure (Gioncu and Mazzolani, 2002). Due to this fact, modern code provisions take into account the ductility capacity at the level of the section. Unfortunately, neither the material ductility nor the section ductility can

provide a final description on the behavior of the structure under earthquake ductility demands (Gioncu and Mazzolani, 2002).

The deterioration of ductility at the level of the member, as shown in Figure 2.27, which is mainly caused by the dynamic characteristics of seismic actions, must be recognized in order to fulfill the understanding of the overall behavior of structures. To control this type of ductility, many factors must be taken into account, such as the multiple buckling modes, the continuous changing in moment gradient during earthquake excitations and accumulation of plastic behavior due to hysteretic behavior.

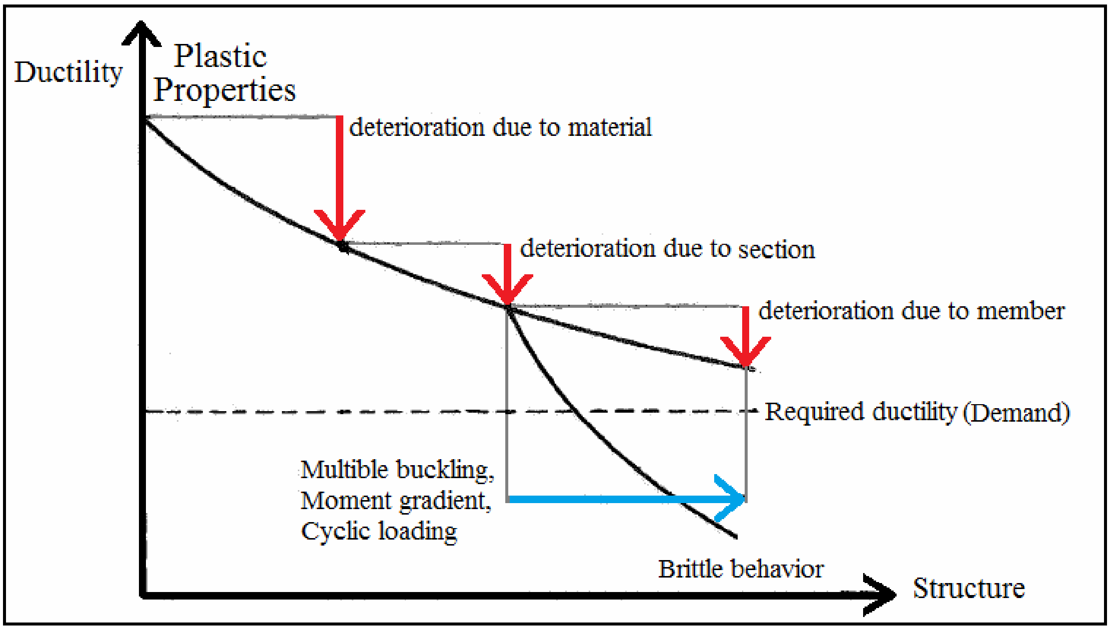


Figure 2.27: Ductility deterioration due to member behavior

2.3.1.3.2 Factors Influencing Member Ductility

All factors were discussed at the level of material and at the level of section can be applied directly to the behavior of steel at the level of the member. But there are some additional factors which are solely related to the member behavior, such as:

- Member type. Whether it is beam or beam-column.

Plastic analysis treats the beam as linear element with points of inelastic rotation at the ends which represents plastic hinges. But in reality, the plastic deformations are

extended at a given length of the beam, which is plastic hinge length, and not concentrated in a point (Chen and Sohal, 1994). Refer to Figure 28. A given amount of strain hardening is required for the plastic zone to extend along the length of the beam (Gioncu and Mazzolani, 2002).

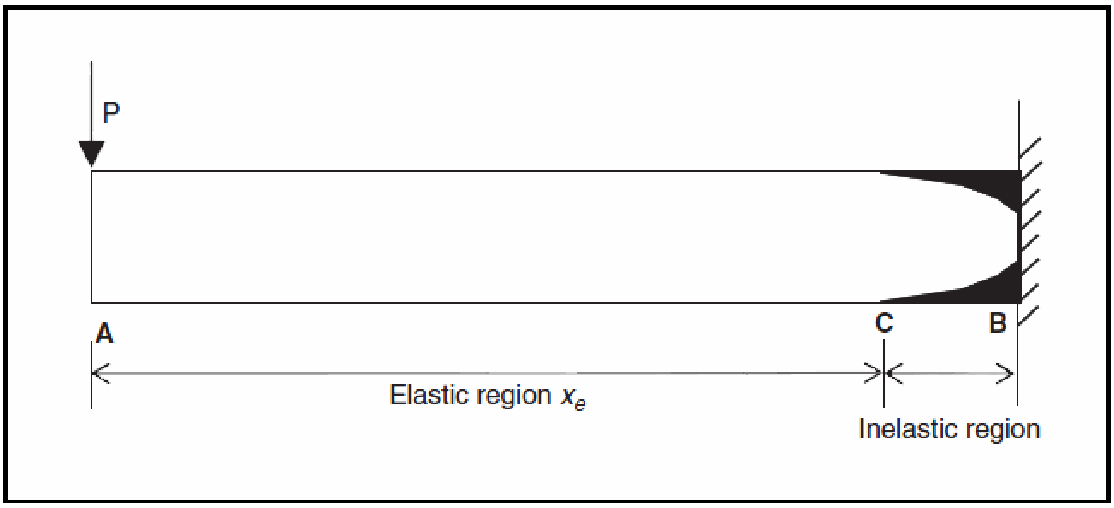


Figure 2.28: Plastic Hinge Length (Wong, 2009)

The ultimate seismic load can be achieved when the plastic hinge loses its rotational capacity, either due to local buckling of compression flange or due to fracture that might occur in the tensioned flange (Gioncu and Mazzolani, 2002).

When shear deformations are dominant and the rigidity amounts of beams and columns are close (or if beam rigidity is higher than column's), the moment diagrams in columns have a double curvature; this features the unfavorable case of weak column–strong beam as shown in Figure 2.29. However, in the preferable case of strong column-weak beam (SC-WB), when flexural deformations are dominant, the moment diagrams in the column exhibit a single curvature, as shown in Figure 2.29. The longest plastic zone, which is the preferable one, occurs for single moment curvature, while the shortest one occurs when two plastic zone form in each column, at their ends.

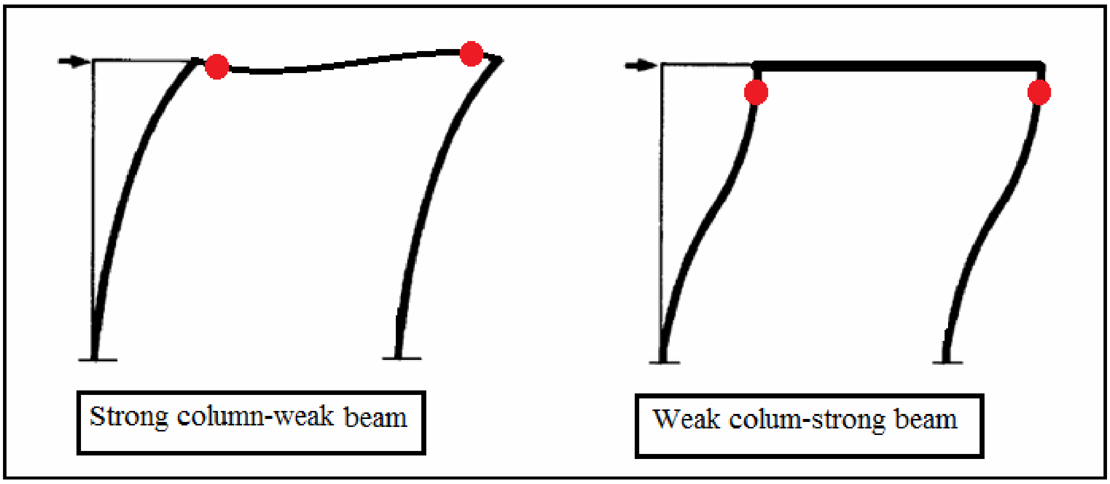


Figure 2.29: Flexure and shear deformations

2.3.1.4 Steel Response: Structure Level

2.3.1.4.1 General

Indeed, current seismic design practice accepts the principle of multi-level seismic design, which has been discussed in details. According to this philosophy, the building must resist minor earthquake without significant damage, moderate earthquakes with repairable damage and major earthquakes without collapse.

This level of response represents the global response, while the whole previously discussed levels (material, section and member) are local levels. Nevertheless, the global response is function of local response, and all factors influencing the plastic properties have been discussed at the levels of material, section and member are affecting the overall structural behavior certainly.

Additional factors are demonstrated under this level of response, which mainly concern lateral displacement issues, such as top displacement and story drift.

Plastic regions must be predetermined, fully detailed to assure the adequate energy dissipation under earthquake loading, while the rest of the structure must be

overstrengthened to ensure its elastic response and to prevent any unfavorable mode of failure (Paulay and Priestley, 1992).

One of the most important features in the response of structures is selecting the adequate lateral resisting system which ensures reasonable stiffness, strength and ductility under any type of loading. This topic will be discussed extensively in following sections.

2.3.1.4.2 P-Δ Effects

When flexible structures are subjected to lateral forces, as shown in Figure 2.30, the resulting horizontal displacements lead to additional lateral overturning moments because the gravity loads P_g is also displaced, then base moment, M_b, equals:

$$M_b = F_e H + P_g \Delta$$

(Eq. 2.17)

Where

F_e = Elastic force

P_g = Gravity force

H = Height of the structure

Δ = Displacement

This moment increment will produce additional lateral displacement, and hence, Δ will increase further. In extreme cases, this will lead to instability, resulting eventually in collapse of the structure.

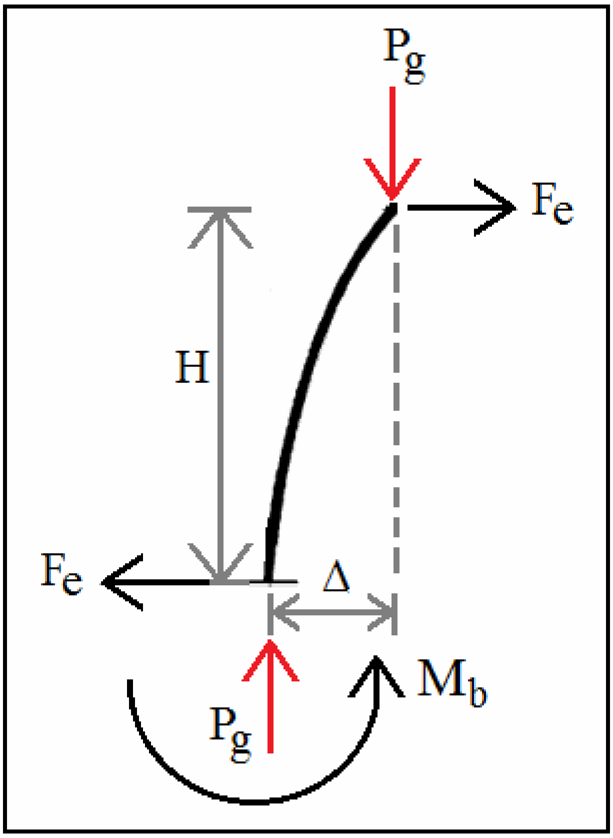


Figure 2.30: P-Δ effect

2.3.2 Reinforced Concrete Response

2.3.2.1 Introduction

This section will introduce a general background on concrete and reinforced concrete plastic mechanics, and to emphasize on the ductility feature of this material to promote the understanding of reinforced concrete response under various ductility demand events.

While this section summarizes general guidelines and basic required knowledge at the preliminary stages of seismic design, subsequent sections will introduce structural systems, in which their behavior depends basically on the reinforced concrete response described herein.

2.3.2.2 Confined and Unconfined Concrete

The term "confined concrete" represents the concrete which is enclosed by closed stirrups or spiral reinforcement, as shown in Figure 2.31. The lateral strain in the concrete is restrained by such confining reinforcement, therefore, an enhancement of mechanical properties of concrete take place which can be expressed in terms of enhancement in stiffness, strength and ductility (Taranath, 2010).

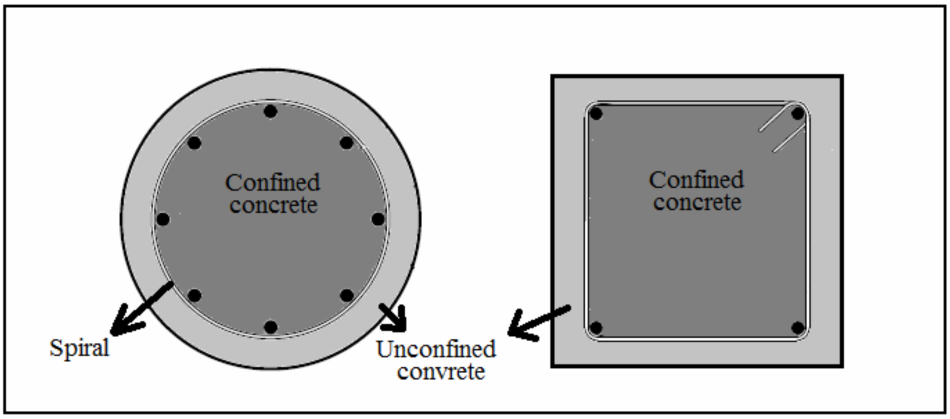


Figure 2.31: Confined and unconfined concrete (Taranath, 2010)

Compression strain for unconfined concrete cannot achieve the required ductility capacity under seismic events without spalling of the cover concrete (Taranath, 2010). Adequate transverse reinforcement to confine the compressed concrete core is needed to exhibit the preferred response under seismic ductility demands, otherwise failure may occur.

Loading unconfined concrete in compression stresses near its crushing strength employs high lateral tensile strain resulting from longitudinal cracks propagation. This abrupt behavior that is presented by unconfined concrete produces instability of the compression zone that leads to failure (Paulay and Priestley, 1992).

So, transverse reinforcement is used to restrict the expansion of the concrete in the lateral direction, introducing higher compression stresses, and much higher strain levels which play an important role in improving ductility capacity.

Referring to Figure 2.32, and according to stress-strain curves, confined concrete can provide higher strain levels compared to unconfined concrete.

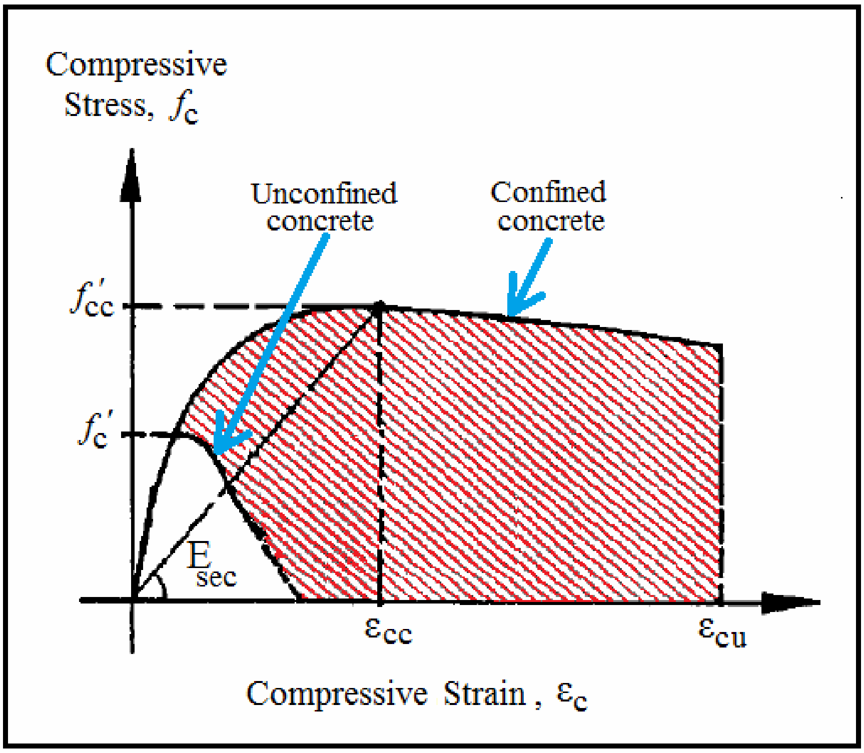


Figure 2.32: Stress strain curves for concrete (Paulay and Priestley, 1992)

Confined concrete must be used in the plastic regions of the structures where possibility of high ductility demand may arise, thus assuring adequate plastic behavior of the structure in terms of ductility, energy dissipation and self centering (Paulay and Priestley, 1992) and (Armouti, 2004).

It was found that buckling of longitudinal reinforcement under compression load may limit the spacing of the transverse reinforcement. However, experiments have indicated that within expected plastic zones this spacing should never exceed six times the diameter of the longitudinal bar to avoid buckling.

2.3.2.3 Influence of Cyclic Loading and Loading Velocity

(1) Cyclic loading influence

Experiments on unconfined and confined concrete under cyclic loading have shown that monotonic loading stress-strain curves form an envelope to the cyclic loading stress-strain curves. As a consequence, no modification to the stress-strain curve is required when calculating the flexural strength of concrete elements subjected to the stress reversal typical of seismic loading (Paulay and Priestley, 1992).

(2) Loading Velocity influence

Concrete employs a remarkable increase in strength and stiffness when loaded at increased loading velocity, (i.e. higher strain rates), as shown in Figure 2.14, which generally arises in near-field earthquakes.

2.3.2.4 Ductility Relationships

The following discussion is concerned with the ductility of confined and unconfined concrete elements at all levels of concern; material, section, member and overall structural level.

i. Material Ductility

Material ductility is described in terms of strain, referring to (Eq. 2.1)

$$\mu_\varepsilon = \frac{\varepsilon}{\varepsilon_y}$$

As stated previously, unconfined concrete fails to employ a reliable ductility strain in compression. But, if appropriately confined, the strain ductility can be increased to remarkable levels under compression.

ii. Section Ductility

Section ductility, or curvature ductility, predominately concerns curvature of sections within plastic hinges, referring to (Eq. 2.2)

$$\mu_\kappa = \frac{\kappa}{\kappa_y}$$

It must be mentioned that the first significant yield does not necessarily mean the formation of the first plastic hinge in the system (Armouti, 2004). Figure 2.33 shows the moment-curvature curves for the actual behavior and the idealized one; where idealized yield exist.

Factors influencing section ductility:

a. Axial Force. If the section is supposed to carry axial forces, then its curvature ductility capacity will be reduced accordingly, since the presence of axial forces increase the yield curvature, κy, and reduce the ultimate curvature, κu (Armouti, 2004).

b. Compression strength of concrete. By increasing the concrete strength, the neutral axis will shift up toward the compression extreme fiber, which will reduce the yield curvature and increase the ultimate curvature. Hence, increase the section ductility (Paulay and Priestley, 1992).

c. Yield strength of reinforcement. Increasing reinforcement steel grade will reduce the curvature ductility of the section (Paulay and Priestley, 1992).

iii. Member Ductility

Member ductility which is expressed in terms of rotation over the member axis, referring to (Eq. 2.2)

$$\mu_\theta = \frac{\theta}{\theta_y}$$

In concrete elements, member ductility is function of section ductility and material ductility. The latter, which is represented by strains, significantly affects the member ductility which cannot be achieved if plastic strains cannot be extended over a reasonable length of that member. This particular length is the plastic hinge length. If

such length is restricted to a small portion of the beam axis, extreme large ductility demand may arise (Paulay and Priestley, 1992).

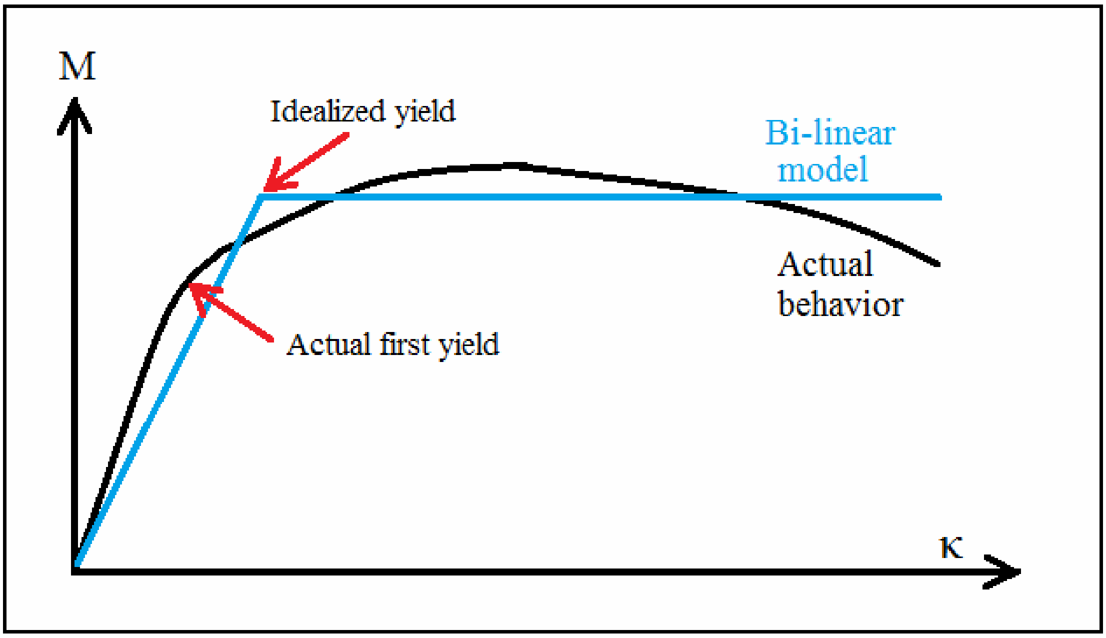


Figure 2.33: Idealized and actual moment curvature curves

iv. Structure Ductility

This type of ductility describes the global behavior of the system and generally represents the top displacement of the structure. Referring to (Eq. 2.4)

$$\mu_\Delta = \frac{\Delta}{\Delta_y}$$

This global ductility capacity is surely dominated by local ductility discussed earlier. For example if a local member exhibits a sufficient ductility by dissipating a reasonable dynamic energy through plastic hinges, then the structure ductility will be positively affected. This relation between structure ductility and member ductility, for a beam element, can be expressed by integrating the curvature along the beam axis (Paulay and Priestley, 1992):

$$\mu_\Delta = \frac{\Delta_m}{\Delta_y} = \frac{\int \kappa(x)xdx}{\int \kappa_e(x)xdx} = \frac{c_1\kappa_m}{c_2\kappa_y} = \frac{c_1}{c_2}.\mu_\kappa$$

(Eq. 2.18)

Where

Δm = Maximum displacement

Δy = Yield displacement

κm = Maximum curvature

κy = Yield curvature

$\mu\kappa$ = Curvature ductility

c1 and c2 = constants

Introducing a convenient structural system to resist expected ductility demands is one of engineer duties through the design process. At this particular stage, the need for considering structure ductility arises to ensure inelastic ductile response and to prevent any brittle mode of failure during various earthquake excitations. Selected systems will be introduced in subsequent sections.

2.4 Seismic Resistant Systems

2.4.1 Structural Steel Bracing Systems

2.4.1.1 General

Bracing is a competent and economical system of resisting lateral forces if enhanced in a frame structure, see Figure 2.34. These provided diagonal braces tend to work in axial stresses, and therefore calling for minimum member sizes of elements, rather than members working in flexural manner (Smith and Coull, 1991).

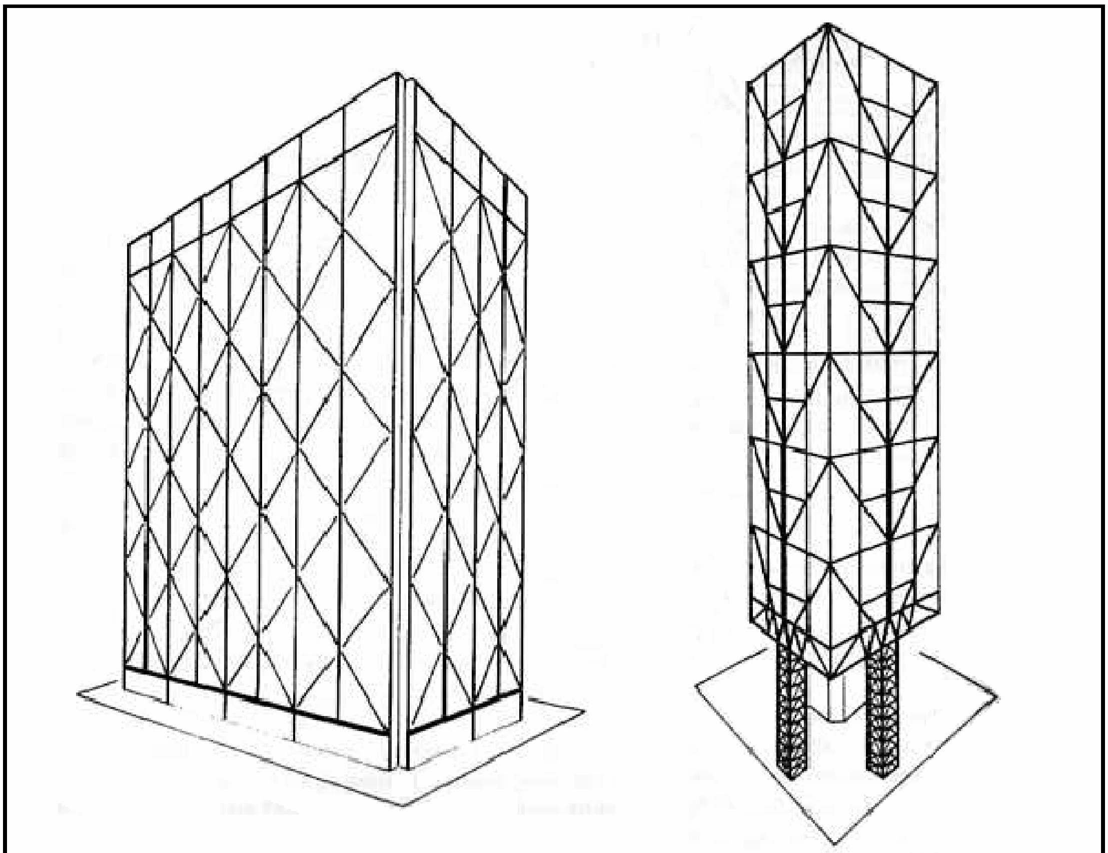


Figure 2.34: Samples for bracing in buildings

Some of bracing types are shown in Figure 2.35; these types have numerous structural uses, relating to efficiency and feasibility due to architectural and limitation issues. As it is clear from Figure 2.35, bracing types are divided into two major sets: (1) Concentrically Braced Frames (CBF), see Figure 2.35a, b, c and d, and (2) eccentrically braced frames (EBF), see Figure 2.35e, f, g and h.

Names of such types of bracing are granted solely according to the geometric shape, for example: Figure 2.35a is named D-Type Bracing. While inverted V, and V-types stand for shapes (c) and (d), respectively. In the eccentric bracing types: K-Type is the name of the shapes (e) and (g) shown in Figure 2.35.

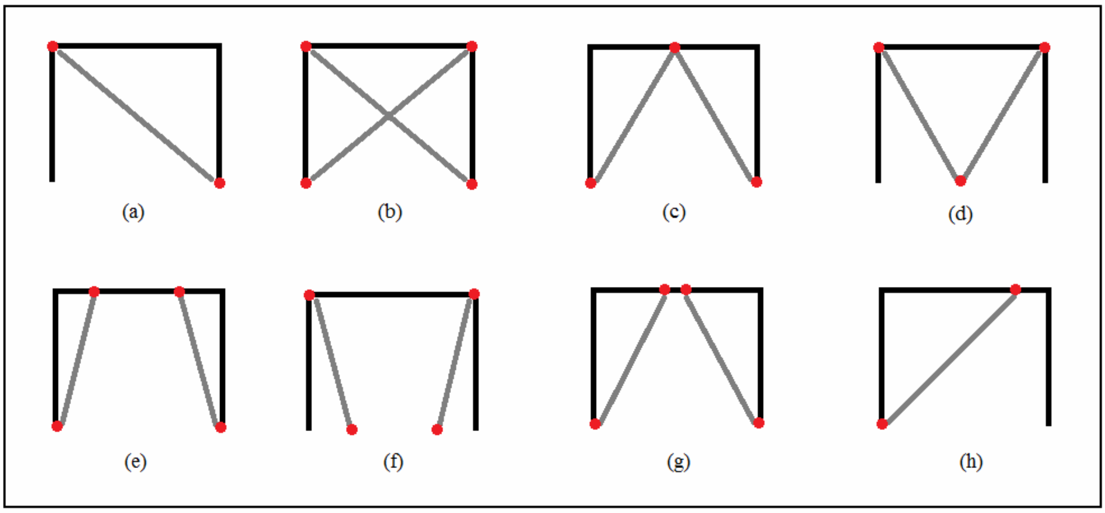


Figure 2.35: Selected types of bracing

There is a significant advantage for the fully triangulated bracing types (i.e. concentric braced frames) that is the girder moments and shears are independent of the lateral forces which are taken by both; diagonals and columns. Where diagonals behave as web, columns tend to act as boundary chords (Smith and Coull, 1991).

Link, in EBF, is defined as the segment of a beam that is located between the ends of two diagonal braces or between the end of a diagonal brace and a column (ASIC seismic provisions, 2005).

2.4.1.2 Eccentrically Braced Frames EBF

2.4.1.2.1 Introduction

Eccentrically braced frame systems (i.e. systems in which the braces are not attached at the same joint) are widely used in earthquake resistant frame structures, mainly, to control drift in minor earthquake and wind excitations. In high seismic events, and while the diagonal braces remain in the elastic range as same as the rest of the structure, only the short link in the girder is pursued to serve as a *fuse*, see Figure

2.36, in which it undergoes high inelastic shear deformations assisting the whole system to provide a ductile response.

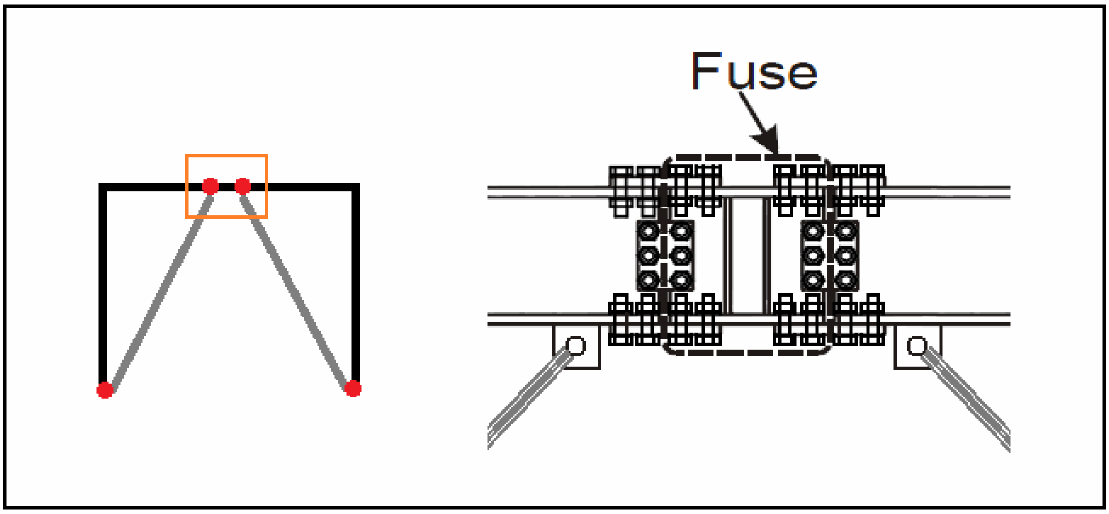


Figure 2.36: Schematic drawing for fuse (Gong and Shahrooz, 2001)

Eccentric bracing systems combine both high elastic stiffness and large inelastic energy dissipation capacity that can sustain many cycles generated by seismic events without sudden collapse, as will be shown later in this thesis.

There are general requirements according to seismic provisions for structural steel buildings (AISC seismic provisions, 2005) for links. These requirements can be summarized, as follows:

1. Links shall be designed with steel grade not exceeding 345 MPa (50ksi), to ensure ductile behavior in the inelastic regions.
2. Links shall meet the requirements regarding width-thickness ratios as presented by AISC provisions.
3. The web of a link shall be single thickness. Doubler-plate reinforcement and web penetrations are not permitted.

2.4.1.2.2 Link Behavior

Free-body diagram of a link is shown in Figure 2.37. When both M_A and M_B reach the plastic moment, M_P, a flexural hinge is said to form at two ends of the link. On the other hand, a shear hinge will form when the shear reaches V_P.

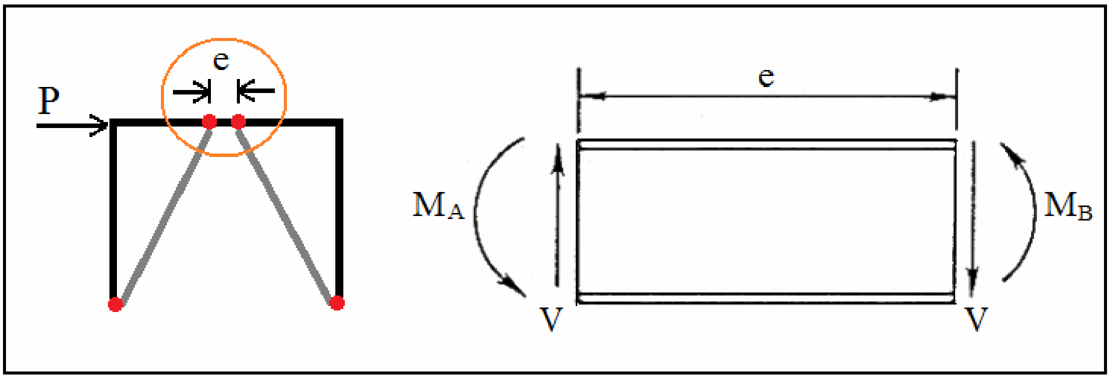


Figure 2.37: Link free-body diagram

For more information on the effects of axial forces and the interaction between moment and shear it is highly recommended to refer to seismic provision for structural steel buildings, (AISC seismic provisions, 2005). It must be noted that the effects of axial forces and the interaction between moment and shear in the link are ignored in the following calculations:

Employing simple static equilibrium the following equation can be written:

$$V.e = M_A + M_B$$

(Eq. 2.19)

Where

V = Shear force

e = Length of link

M_A and M_B = End moments

The plastic moment and shear capacities are computed respectively as follows (AISC seismic provisions, 2005):

$$M_p = f_y Z$$

(Eq. 2.20)

Where

Z = *Plastic* section modulus

*f*y = Yield stress

$$V_p = 0.6 f_y \left(d - 2t_f\right) t_w$$

(Eq. 2.21)

Where

V_P = Plastic shear force

*f*y = Yield stress

d = Section depth

t_f = Thickness of flange

t_w = Thickness of the web

The length of the link, corresponding to balanced yielding condition, in which flexural hinge occurs simultaneously with shear hinge, is:

$$e_0 = \frac{2M_p}{V_p}$$

(Eq. 2.22)

Where

V_P = Plastic shear force

M_P = Plastic moment

When $e \leq e_0$, then a shear yielding will form providing short link:

$$V = V_p \qquad M < M_p$$

While if $e \geq e_0$, then link will yield in flexure first, forming a long link:

$$V < V_p \qquad M = M_p$$

Experimental results showed that a properly stiffed short link can develop shear strength equal to $1.5V_P$, due to strain hardening effect (Naiem, 2001). The end moments of a link that has yielded in shear can continue to increase due to strain hardening. However, the end moments are limited to $1.2M_p$ to avoid low-cycle fatigue (Naiem, 2001). The maximum length for a short length will be modified as follows:

$$e_0 = \frac{2(1.2M_p)}{1.5V_p} = \frac{1.6M_p}{V_p}$$

Where

V_P = Plastic shear force

M_P = Plastic moment

(Eq. 2.23)

Experimental results showed that flexural yielding cannot provide adequate levels of ductility, and the inelastic deformation capacity of an EBF can be radically reduced when long link used ($e > e_0$). On the other hand, and if a short link is considered, shear yielding can provide a perfect response under plastic excursions of seismic events, and can undergo a noticeable inelastic deformation without failure, if the link is well detailed (Naiem, 2001).

2.4.1.2.3 Link Rotation Angle

The link rotation angle, γ_P, can be defined as the deviation of the ends of the link from the line connecting the end of the link, as shown in Figure 2.38. Applying simple plastic theory, the kinematics of the plastic mechanism requires that:

$$\theta_P = \frac{\Delta_P}{h}$$

(Eq. 2.24)

Since γ_P can be given in the following form:

$$\gamma_P = \frac{L}{e}\,\theta_P$$

(Eq. 2.25)

Where:

θ_p = plastic rotation

Δ_p = plastic displacement

h = frame height

e = length of the link

L = span length

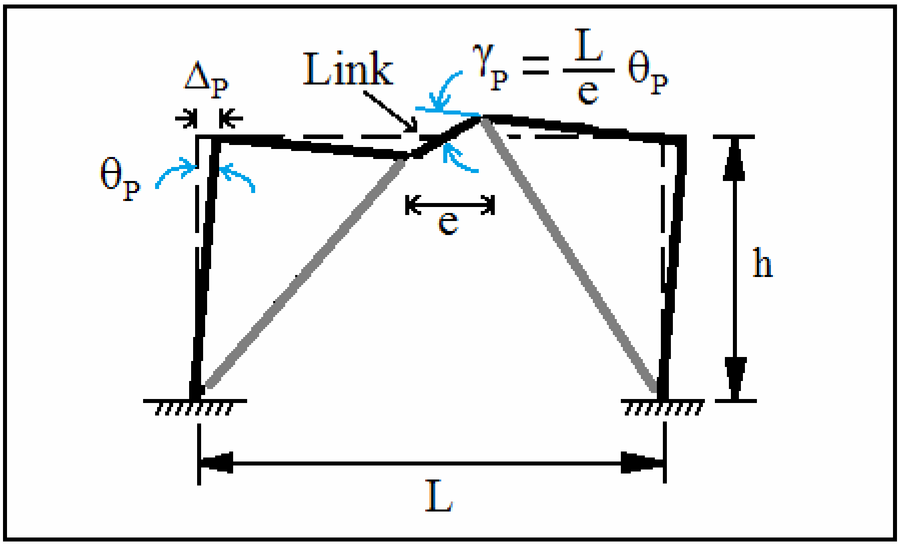


Figure 2.38: link Rotation Angle in EBF (Naiem, 2001)

According to seismic provisions for structural steel buildings, (AISC seismic provisions, 2005), the link rotation angle shall be governed by the following:

For short link: $e \leq 1.6M_P / V_P$ $\gamma_P \leq 0.08$

For long link: $e \geq 2.6M_P / V_P$ $\gamma_P \leq 0.02$

Linear interpolation must be carried for the values in between.

2.4.1.2.4 Link Stiffeners

Link stiffeners are divided into two parts: End and Intermediate stiffeners.

i. End Stiffener

Full-depth web stiffeners shall be provided on both sides of the link web at the diagonal brace ends of the link, as shown in Figure 2.39. End stiffener shall also meet the following limitations of (AISC seismic provisions, 2005):

$$b_{st} \geq b_f - 2t_w$$

$$t_{st} \geq \text{the larger of}\,(\,0.75t_w, 10mm)$$

Where:

b_f = width of the link flange

t_w = thickness of the link web

b_{st} = width of the stiffener

t_{st} = thickness of the stiffener

ii. Intermediate Stiffener

Intermediate stiffeners are shown in Figure 2.39.

a) For short link: ($e \leq 1.6M_P / V_P$), the inelastic response is dominated by shear yielding. The spacing of the stiffener is governed by the rotation angle as follows:

For $\gamma_P \leq 0.08$, $s \leq 30t_w - d/5$

For $\gamma_P \geq 0.02$, $s \leq 52t_w - d/5$

Linear interpolation to be permitted for values in between.

b) For Intermediate length, where ($e \leq 5M_P / V_P$ and $\geq 2.6\ M_p / V_p$), the inelastic response is solely controlled by flexural yielding. Stiffeners spacing is:

$s = 1.5\ b_f$

c) For Intermediate length, where ($e \leq 2.6M_P / V_P$ and $\geq 1.6\ M_p / V_p$), the inelastic response results from a combination of shear and flexure yielding. The stiffeners shall be provided as mentioned previously in (a) and (b).

d) For long link, where ($e \geq 5M_P / V_P$). No stiffeners are required.

For links with depth $d \geq 635$ mm, intermediate stiffeners shall be provided on both ends of the web of the link. Otherwise only one side stiffeners are required, and shall follow the following thickness regulations:

$$b_{st} \geq \frac{b_f}{2} - t_w$$

$$t_{st} \geq \text{the larger of}\,(t_w, 10mm)$$

Where:

d = Overall depth of the link

b_f = Width of the link flange

t_w = Thickness of the link web

b_{st} = Width of the stiffener

t_{st} = Thickness of the stiffener

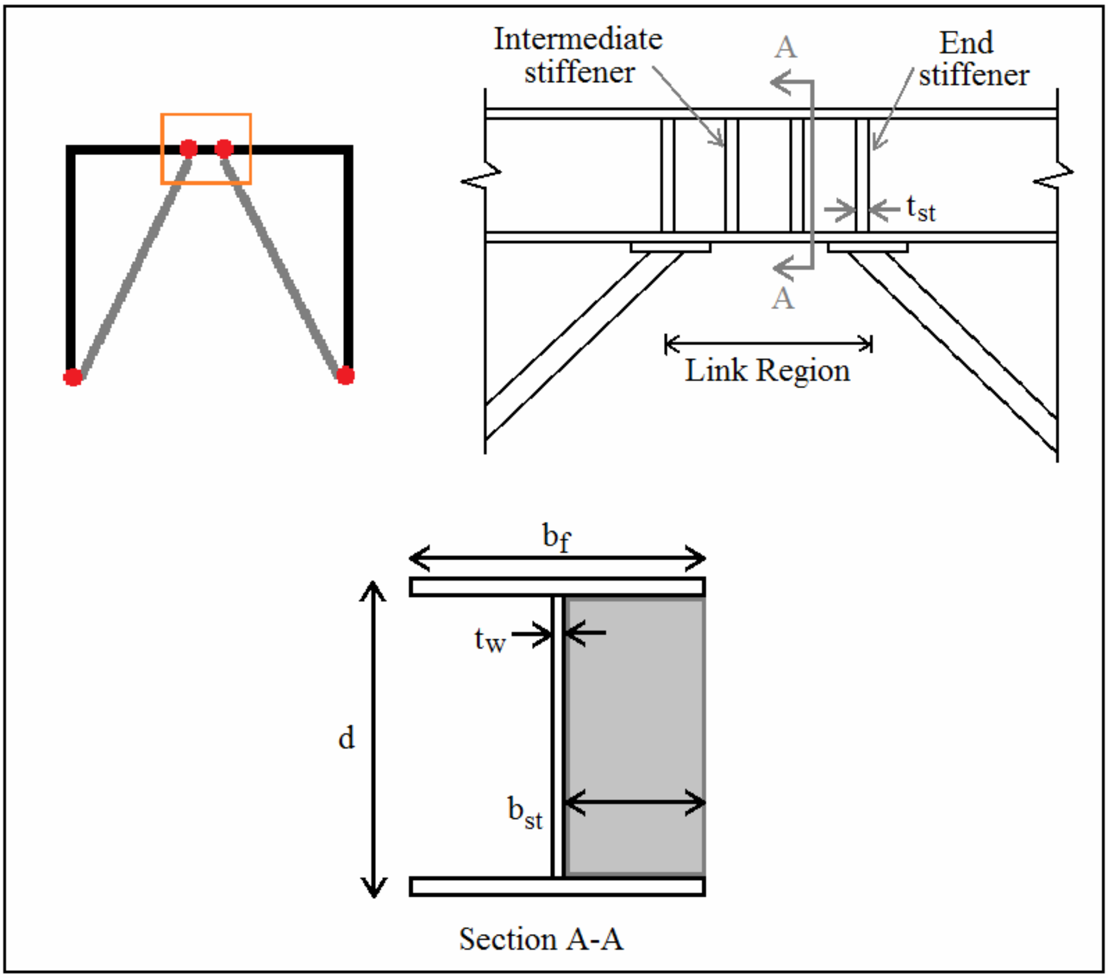


Figure 2.39: Link stiffeners

2.4.2 Structural Wall Systems

2.4.2.1 Cantilever Shear Walls

2.4.2.1.1 Introduction

A substantial change in structural design for resisting lateral forces from moment resisting frames to flexible frames with stiff shear walls has occurred in the last decades (CIRIA, 1984). For buildings of 10 to 30 stories height, the use of shear wall elements is a common practice. For buildings over 30 stories, it may become inappropriate to use such system due to economical and structural design issues, such as lateral deflection

control. Figure 2.40 shows a sample building that contains structural walls and corewalls that are used to resist lateral forces.

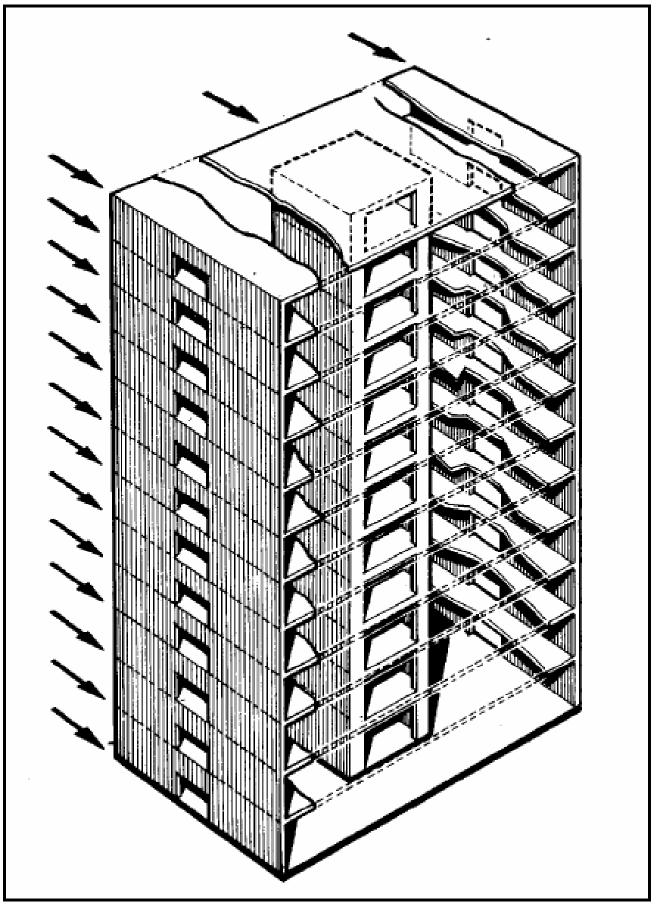


Figure 2.40: Systems of structural walls in building

Frames typically deform in a shear manner, whereas shear walls generally deform in a flexural mode. Shear walls tend to attract lateral forces, while frames shed these forces because it is more flexible.

Monolithic shear walls can be classified as short, squat or cantilever, as shown in Figure 2.41, according to their aspect (height/depth) ratio. The shapes of walls may be planar, flanged or core.

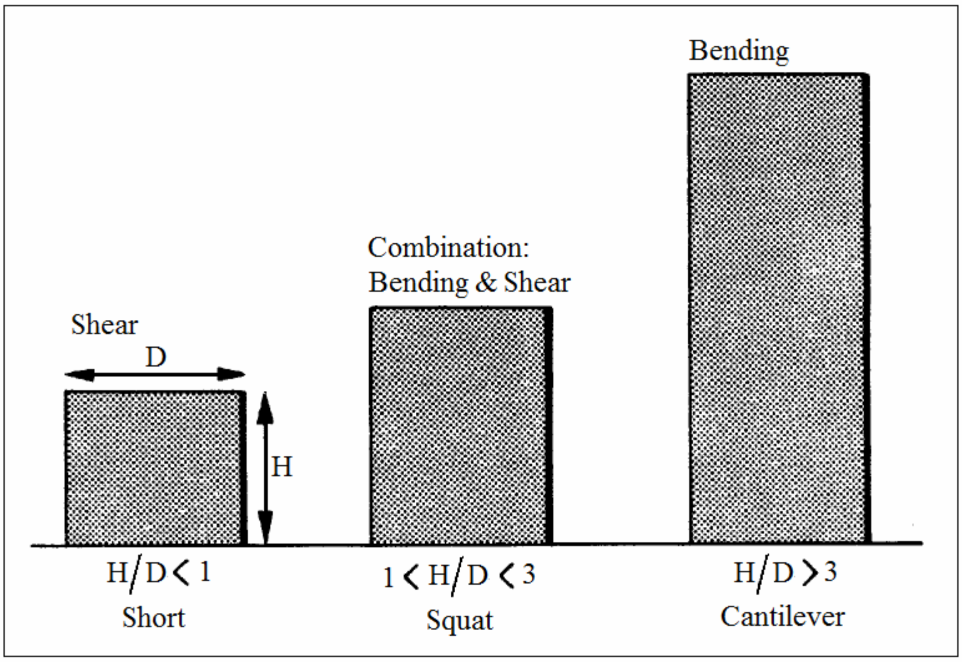


Figure 2.41: Shear Walls Classification

It should be appreciated that while it easy to accommodate any kind of wall arrangement to resist wind forces, it is much more difficult to ensure satisfactory overall building response to large earthquakes when wall locations deviate considerably from those dictated by seismic considerations. The difference in concern arises from the fact that in the case of wind, a fully elastic response is expected, while during large earthquake demands, inelastic deformations will arise (Paulay and Priestley, 1992).

The lateral deflection of shear wall structures under wind or minor earthquakes is important to be controlled to prevent any damage might occur due to sway in brittle partitions, windows or doors. Such deflection arises under elastic response is to be considered as a serviceability limit state. However, lateral deflection occurring under severe seismic events is not considered as a serviceability limit state, but a survivability limit state, and it is important to be taken into account to prevent any unfavorable damage due to excessive deflection (Paulay and Priestley, 1992).

When plastic excursions arises in a structure due to major earthquakes, and where the structure has no redundancy, as cantilever shear wall, it cannot continue to resist load after failure of one element. Survival limit state proposed number of approaches to ensure structural integrity. One of these approaches suggested developing alternate load paths following removal of a critical element (Wight and MacGregor, 2009).

2.4.2.1.2 Failure Modes

In a laterally loaded cantilever wall, flexural yielding shall be clearly defined at the plastic hinge region (i.e. base of the wall) controlling strength and ensuring ductility capacity, and hence energy dissipation in the system.

Yielding of flexural reinforcement at the base of cantilever wall must be the principal source of energy dissipation. Other types of failure such as horizontal and vertical shear, diagonal tension or diagonal compression caused by shear, instability of thinned sections, sliding shear along construction joints, and shear failure along lapped splices must be prevented. Samples of these failure modes are shown in Figure 2.42.

For example, shear walls controlled by shear strength cannot provide the desirable hysteretic loops needed in cyclic loading, thus causing severe reduction in the ability of the system to dissipate energy.

2.4.2.1.3 Shear Wall Ductility

The displacement ductility capacity, μ_Δ, of walls depends on the rotational capacity of the plastic hinge formed at the base of the wall. It has been found that the relationship between curvature ductility, μ_θ, and displacement ductility, μ_Δ, depends on the aspect ratio (height/depth) of the wall (Paulay and Priestley, 1992).

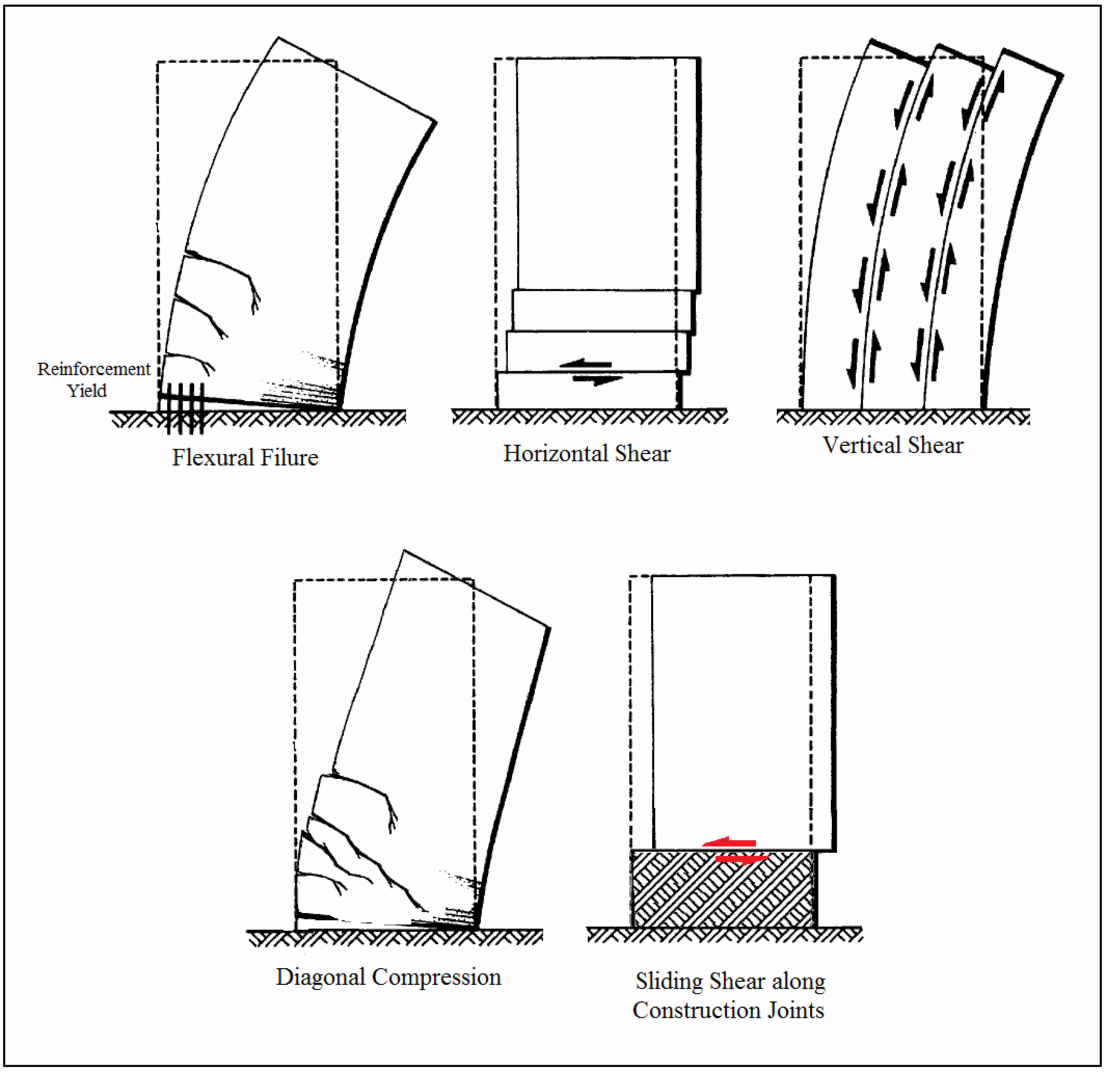


Figure 2.42: Possible Shear wall failures

Length of the plastic hinge, l_p, is the most important parameter affecting displacement ductilities in shear walls. By its turn, the length of the plastic hinge is generally controlled by many parameters, such as in-plane depth of the wall, D, as shown in Figure 2.43, and axial load intensity. It is not possible to define an exact section above the base of the wall where the inelastic response exactly diminishes, but there are typical values of the plastic hinge length (Paulay and Priestley, 1992):

$$0.3 < \frac{l_p}{D} < 0.8$$

Where

l_P = Plastic hinge length

M_P = Wall in-plane depth

2.4.2.1.4 Boundary Elements

Shear wall boundaries must be well confined with adequate detailing and extra reinforcing compared to the web elements, as shown in Figure 2.43. Boundary elements perform as chord members in tension or compression to increase the flexural capacity of the wall, while the web elements deal with in-plane shear stresses. Enlarged, or flanged boundary elements increase the compression capacity of these regions, and improve the ductility capacity of the overall system. However, if the boundary elements are not carefully detailed, or a confined concrete is not provided, or not adequately reinforced, this will result in premature yielding of the reinforcement, and unfavorable brittle failure of the system will occur (Paulay and Priestley, 1992).

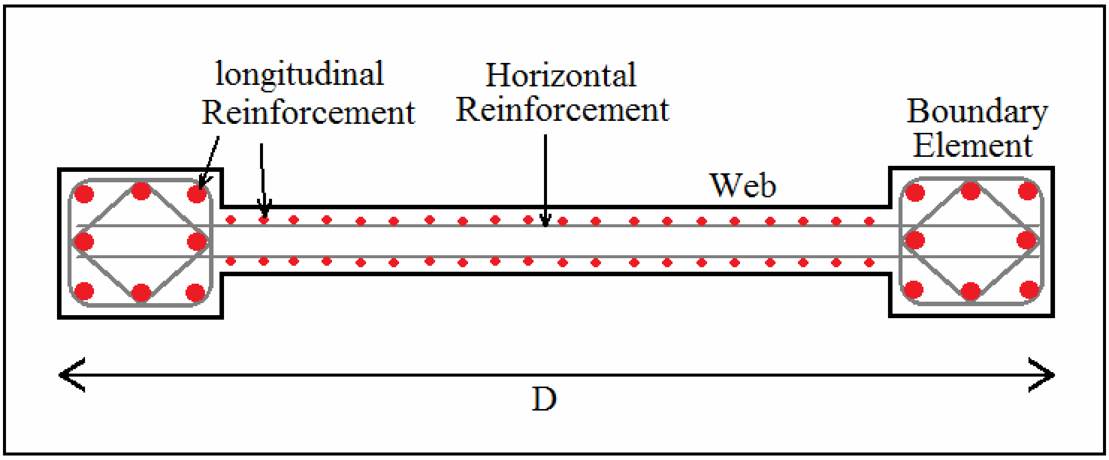


Figure 2.43: Plan view for shear wall

2.4.2.2 Coupled Shear Walls

2.4.2.2.1 Introduction

In many cases, walls are pierced by regular pattern of openings due to architectural reasons, as shown in Figure 2.44. These openings weaken the system. The behavior of the wall is governed by the degree of coupling, depending on the proportions of the walls and the coupling beam (Shahrooz, 2006).

The designer must ensure the adequacy of flexural strength due to reduction of wall area at the extreme boundaries of the wall. Also, the vertical and horizontal shear strength must not control the design.

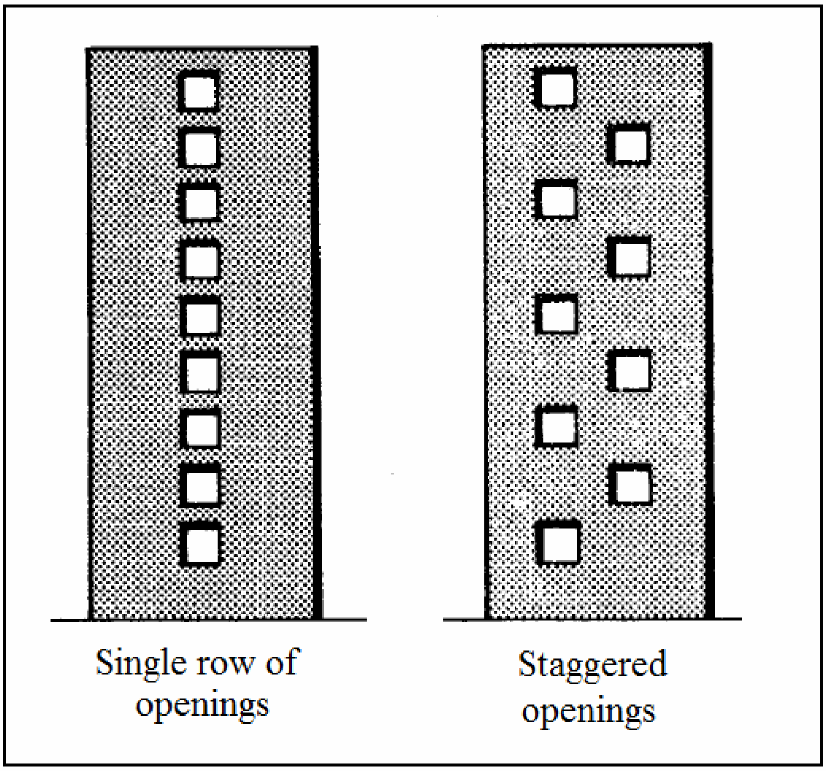


Figure 2.44: Openings in shear walls

In their simplest form, a single row of openings may be modeled for analysis as a continuous flexible medium, thus reducing the problem from a highly statically indeterminate structure to the solution of a single differential equation.

Many researchers have suggested solving the problem using "*wide-column*" frame method; the implication of this method is by representing the walls as wide columns, while the coupling beam acts as a girder. This method may be good in improving the strong-column weak-beam action, but it poorly represents the true behavior of the system (CIRIA, 1984).

It has been previously mentioned in this study that frames deform in an almost pure shear manner, whereas shear walls generally deform in a flexural mode. However, coupled shear walls deform in a shear-flexural manner, depending on the degree of coupling. Figure 2.45 shows these modes of deflection.

2.4.2.2.2 Degree of Coupling

The coupling beams are essentially weaker than the walls. The walls which behave solely as cantilevers, can then impose sufficient rotations on these connecting beams to make them yield before walls do. If properly detailed, the beams are capable of dissipating energy over the entire height of the wall, rather than a plastic hinge to form at the base (Paulay and Priestley, 1992).

Experimental results showed that the stiffness of even relatively shallow coupling beam can provide a considerable increase in the overall stiffness of the shear wall, and a corresponding reduction in the stress variation at the base (CIRIA, 1984).

Depending on the modes of deflection shown in Figure 2.45 the system can be classified either as a coupled shear walls, or as one pierced shear wall. If the mode of

deflection is close to flexural mode then it is more logically to represent the structural model as a pierced wall. If not, then the coupled wall system shall be recognized.

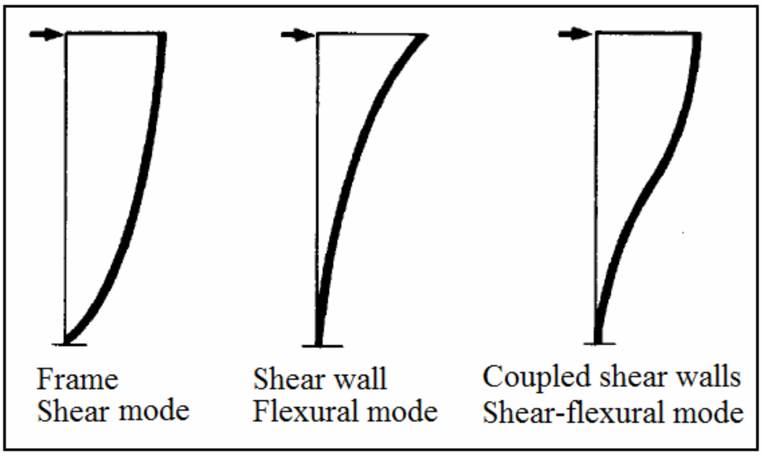


Figure 2.45: Lateral deflection shapes

In traditional structural walls, the total overturning moment, M_0, is resisted at the base of the cantilever wall. While in the coupled walls system, axial force arises at each wall to be resisted as well as the moments, as shown in Figure 2.46.

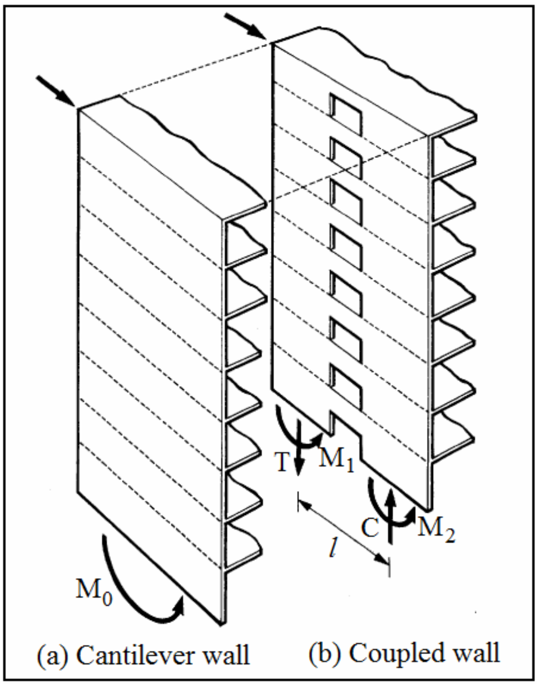


Figure 2.46: Coupled walls

Between the coupled shear wall and the pierced cantilever wall, the following simple equilibrium equation must be satisfied:

$$M_0 = M_1 + M_2 + l.T$$

(Eq. 2.26)

Where

M_0 = Overturning moment of cantilever wall

M_1, M_2 = Overturning moment of walls 1 and 2 respectively

T, C = Axial forces

l = Lever arm length

Now, the degree of coupling ratio can be defined as follows:

$$\beta = \frac{T.l}{M_o}$$

(Eq. 2.27)

When the coupling is relatively weak (coupling by slabs for example), the coupling ratio, β, will be small, since the major portion of the moment resistance is provided by moment components of walls M_1 and M_2.

Paulay and Priestley (1992) have mentioned that the New Zealand code of practice has suggested that the coupling walls can be treated as a ductile concrete frames. Accordingly, the force reduction factor, R, for ductility given in the New Zealand standards may be taken as intermediate value between the limits recommended for slender cantilever walls and ductile frames, depending on the efficiency of coupling defined by the previous equation, Eq. 2.28**:**

$$5 \le R = 3\beta + 4 \le 6$$

When

$$\frac{1}{3} \leq \beta = \frac{T.l}{M_o} \leq \frac{2}{3}$$

Relating to Figure 2.46 the moment sharing components M and T.l varies according to the degree of coupling. The force in the most highly stressed coupling beam and the position of such coupling beam can be found with respect to the coupling ratio.

It is seen that with deep beams the shear forces, q_u, are large in the lower third of the structure and reduce rapidly toward the top; this is explained in Figure 2.47. This is due to the fact that under the increased axial load on the walls, axial deformations in the top stories become more significant and this relieves the load on the coupling beams, (Paulay and Priestley, 1992).

As the coupling between the walls increases, the position of the most highly stressed coupling beam moves down towards the base of the wall. This statement provides a logical guideline concerning the behavior of such system; that if the walls are radically coupled to form a pierced cantilever wall, then the most highly stressed region will be lowered to be at the base of the wall to form a plastic hinge. This choice, however, conflicts with the principle of using the system of coupled walls, which is dissipating the energy over the entire height of the wall.

So, the strength of the coupling beams should never exceed the demand, because this will result into a stiffer system, which may increase the overturning capacity of the system, thus overloading the foundations (ASCE, 2005).

Experiments have shown that with concrete coupling beams with 500 mm depth or deeper, a suitable degree of coupling is exhibited. However, when beams shallower than 250 mm (for example 150-mm slabs) are used, the moment demand on the walls ($M_1 + M_2$) increases rapidly.

Coupling beams should be proportioned to avoid over coupling (i.e. system that acts as a single pierced wall) and light coupling (i.e. a system that performs as a number of isolated walls) (Gong and Shahrooz, 2001).

Elasto-plastic forces in coupling beams of shear wall due to increasing of lateral loading are shown in Figure 2.47, where q_u is the ultimate load in the coupling beams.

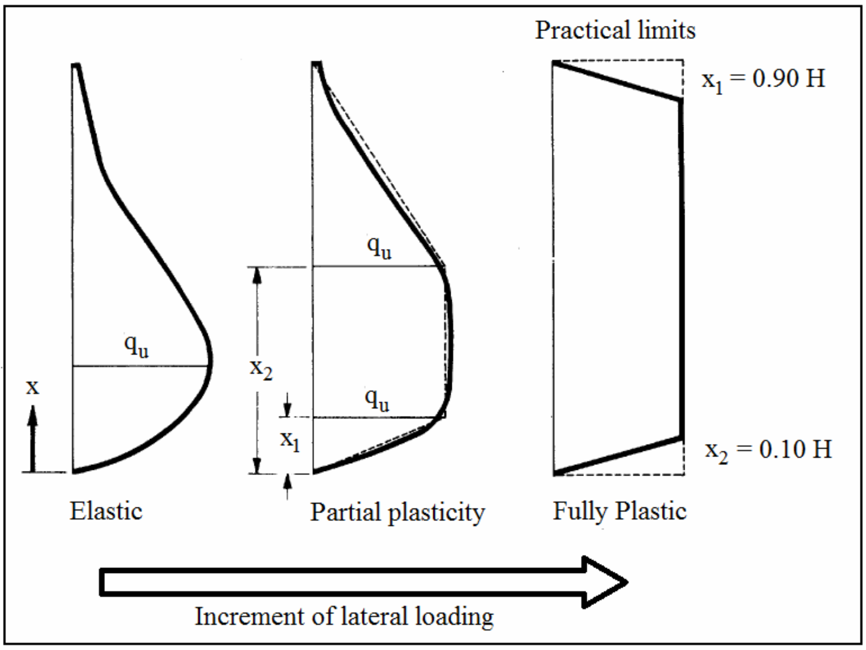


Figure 2.47: Forces in coupling beams (CIRIA, 1984)

2.4.2.3 Hybrid Coupled Shear Walls

2.4.2.3.1 Introduction

Traditionally, reinforced concrete shear walls have been recognized for their large stiffness and strength, which provides an outstanding control on the lateral deflections matter (CIRIA, 1984).

In cantilever walls, the plastic response arises at the wall base only, where significant rotations and yielding of reinforcement take place. The overall structural response depends predominantly on the response of this region to provide a reasonable stiffness, strength and ductility that serves the energy dissipation.

In coupled wall systems, reinforced concrete coupling beams are utilized to distribute stresses and deformations throughout the entire height of the shear wall rather than concentrating it at the base of the wall.

In order to ensure stable hysteretic response of reinforced concrete beams under reserved loading, high level of detailing must be provided. This often lead to deep beams with heavy reinforcement. For this reason, recent studies focus on structural steel beams usage. Structural steel beams possess the required combination of stiffness, strength and ductility in order to provide a stable response under seismic events. The resulting system; reinforced concrete shear walls coupled by structural steel beams, is termed hybrid coupled shear wall system.

In a pierced shear walls, for example, the ultimate strength of the available critical coupling beam may be reached at a trivial proportion of the overall capacity of the wall, thus it is an arising necessity to account for the inelastic response of the coupling beams based on redistribution of forces in the walls.

Structural steel elements, if well selected, have proved that they can perfectly sustain inelastic deformations during seismic events, by absorbing energy transferred to

the system and dissipate it through plastic hinges, without any brittle response or premature yielding which might be represented by local buckling.

As shown in Figure 2.48, onset of plasticity in the coupling beams is not in itself an ultimate limit state criterion, because a remarkable reserve of strength against overall collapse exists. The potential for internal forces redistribution in coupling beams and walls can be assessed before the ultimate strength of the wall is attained. Anyhow, failure in coupling beams does not cause an overall collapse in the structure. Figure 2.48 shows the ductility capacity gained in the coupled wall system.

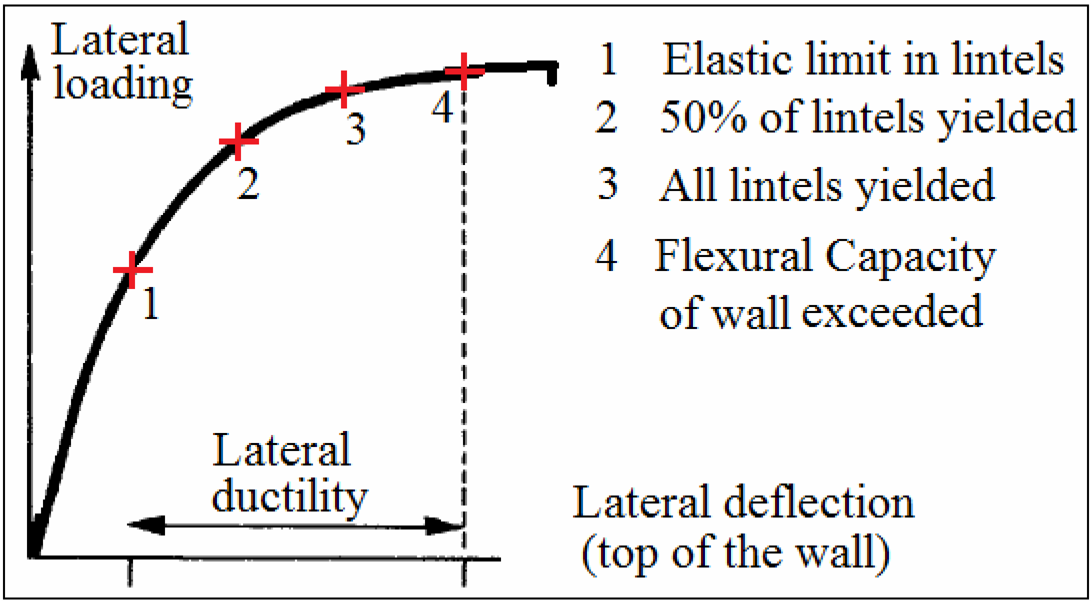


Figure 2.48: Behavior of coupled wall under monotonic loading

2.4.2.3.2 Steel Coupling Beams

The advantages of steel or hybrid coupling beams becomes particularly apparent in cases where height restrictions do not permit the use of deep reinforced concrete beams, or where the required capacity, stiffness, or deformation capacity cannot be developed economically with a concrete beam (Shahrooz, 2006).

The coupled systems are employed such that the coupling beams yield before plastic hinge formation at the base of the wall. Such coupling beams are utilized to yield in shear in the stem prior to flexural yielding, according to the (AISC seismic provisions, 2005) for short links in eccentrically braced frames.

This procedure results in coupling beams with thin webs and thick flanges. However, premature yielding in webs (local buckling, web crippling…) must *not* be permitted (AISC seismic provisions, 2005).

In the same field, considering the short link behavior to dissipate energy provides coupling beams with fuses technology as shown in Figure 2.36. As mentioned previously in eccentrically braced frames section, in order to control the level of the damage. These fuses are detailed to eliminate the damage to the rest of the structure (steel coupling beams and RC walls), and to ensure ease of replacement.

Inelastic flexural capacity of the fuse must be greater than the corresponding value for the coupling beam, and the plastic shear capacity of the fuse is taken proportional to the plastic shear capacity of the coupling beams, to prevent any failure in the coupling beam (Shahrooz, 2006).

2.4.3 Hybrid Brace-Coupled Shear Walls Systems

2.4.3.1 Introduction

Shear walls are traditionally used in tall concrete buildings to resist lateral loads. Due to the presence of regular openings (door or window), a shear wall is often pierced and divided into number of units coupled together by coupling beams. During a major earthquake, if the coupling beams are sufficiently designed and detailed, they are able to

yield and dissipate the excessive vibration energy before the wall units do, thereby reducing the stresses handled by the walls and protecting the walls from damage, especially, in plastic hinge region at the base of the wall. Ensuring that coupling beams are designed to yield prior to the wall is vital, because rendering the repair of the wall after seismic events is complex and much difficult than coupling beams repairing; however, the coupling beams will be exposed to a considerable ductility demand that must be recognized in order to form plastic hinges.

Under seismic events, the response of the system of coupled shear wall is tragically dependent on the nonlinear inelastic behavior, especially the strength and ductility which provides the ability to dissipate energy at these regions. However, structural steel coupling beams, if well chosen, proved to possess a perfect manner under such excitations.

It is desired to mention that the width of the openings commonly ranges from 1.0 m to 2.0 m; hence the majority of the coupling beams are quite short and deep with lower levels of span-to-depth ratios. From this aspect these short coupling beams (links) tend to fail in shear rather than in flexure.

However, if an irregular openings pattern in the walls exists, as shown in Figure 2.49, or if the gap between the coupled walls is grand, then the behavior of the coupling beams will be no more controlled by shear yielding, and flexural yield will be dominant. Unfortunately, experimental results have shown that the inelastic deformation capacity of an eccentrically braced frame can be greatly reduced when long links are used (Naiem, 2001).

Definitely, Diagonal reinforcement always provides remarkable solutions for such curious problems if the reinforced concrete coupling beam solutions was the case. However, this research intends to continue studying same problems using structural

steel solution, as structural steel proved to be a favorable powerful system to be used in numerous cases.

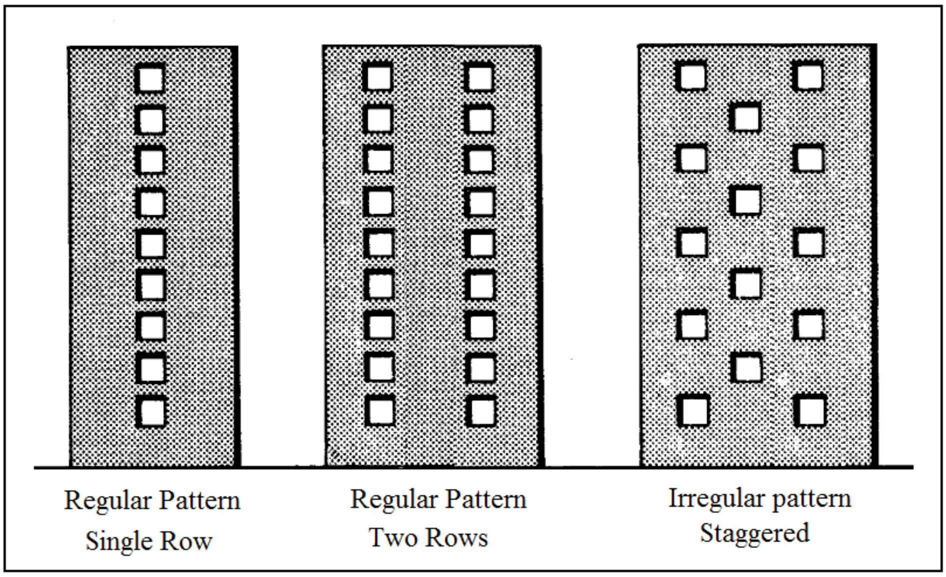


Figure 2.49: Openings Patterns

Shear walls coupled using eccentric steel bracing system introducing a hybrid brace-coupling system will be the structural steel alternative for such cases.

2.4.3.2 Structural Behavior

Simply, the structural steel coupling beam which couple remote piers, shall be enhanced with two diagonal braces, to form an eccentrically braced frame that will enrich the overall stiffness of the system, by improving the ability to resist lateral force side by side with existing structural walls, as shown in Figure 2.50.

Consequently, the ultimate advantage of this combination would be the short link formed between the adjacent braces on the steel girder (coupling beam) which transforms the overall behavior of the coupling beam from flexural yielding (long link) to shear yielding (in the short link). Short link is able to provide the adequate strength and ductility to sustain reserved cyclic loading under undesirable excitations, by forming a plastic hinge to dissipate energy through.

Failure in these added diagonal braces is prohibited; energy dissipation must only be through the short link located in the girder between these braces. Plasticization of one of these braces may result in an unstable response and undesirable hysteretic loops. Thus, in design process these diagonal elements must remain elastic during various excitations.

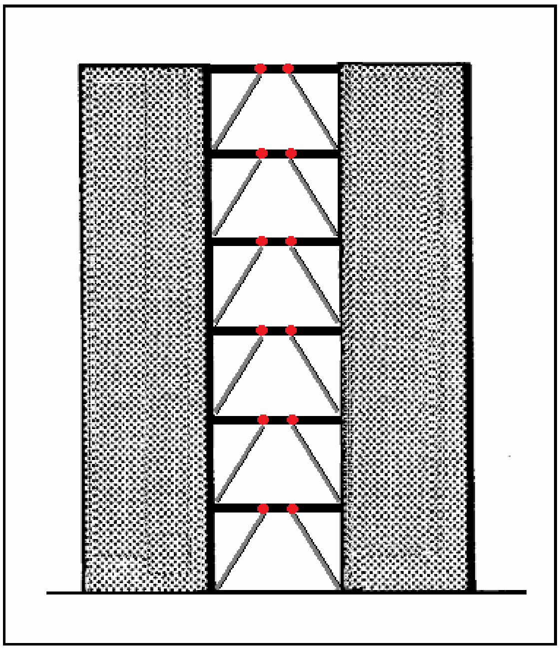


Figure 2.50: Hybrid Brace-Coupled Shear Walls system

Shear yielding links, as suggested by AISC seismic provisions, must be designed so that they do not undergo premature yielding which results in a brittle failure (such as local web buckling or lateral torsional buckling). It is corollary that diagonal braces also must not face instability matters, for example to buckle under compression stresses. Web local buckling in the shear link and buckling in the diagonal chords can be limited by encasing steel sections in a well confined concrete.

Overall response of the proposed hybrid brace-coupled shear walls system using eccentric steel bracing shall follow all the guidance, recommendations and limitations have been mentioned through the previous sections discussion on the traditional seismic

resistant systems of shear walls, coupled walls and eccentrically braced frames, accordingly.

The scope of this paper is to study the behavior of hybrid coupled shear walls using eccentric steel bracing system under seismic excitation, the study will implement pushover analysis in the first stage to account for stiffness, strength and ductility. Then cyclic analysis is applied to study the energy dissipation through the system, as will be shown next in the modeling chapter.

CHAPTER THREE
MODELS DESCRIPTION AND RESULTS DISCUSSION

3.1 Introduction

This chapter is partitioned into two main parts. The first part; "models description" describes the models proposed in this thesis, implementing the finite element environment, description of material, structural element types and other identifications corresponded to the modeled specimens.

The results of the provided models will be discussed in the second part of this chapter, and a comparison between various responses of the models is carried out.

3.2 Models Description

3.2.1 ADINA Environment

ADINA (2005) stands for *Advanced Dynamic Incremental Nonlinear Analysis*. ADINA is a FE computer program suite developed by Department of Mechanical Engineering at the Massachusetts Institute of Technology (MIT).

ADINA was adopted in this research because it describes the actual behavior of structures in a reasonable manner, and the inelastic behavior is introduced clearly in its environment.

In the concrete field, ADINA has formulated a nonlinear concrete material model that can expresses the behavior of two dimensional problems, such as planar shear walls, in a perfect manner (Khatri and Anderson, 1995).

The advantages of using ADINA concrete model can be summarized as following:

- Material calibration capability, which provides the option to model various concrete strength and ductility parameters.
- ADINA can account for multiaxial stress state. For example, a shear wall experiences a two dimensional stress condition with in-plane shear flexure and vertical axial loads. High vertical loads stress the concrete beneath in compression and increase its resistance to shear in horizontal direction. ADINA accounts for this complexity.
- ADINA concrete model offers the full range of linear and nonlinear static, dynamic, buckling and frequency analysis capabilities.
- ADINA program can show crack patterns and configurations, which enables the researcher to locate critical areas of failure.

From an overall perspective, ADINA has developed an outstanding finite element program that is the first significant step towards providing a comprehensive nonlinear FE program for use in practical structural design (Khatri and Anderson, 1995).

Nevertheless, it must be mentioned that a noticeable disadvantage may arise when ADINA package is used, which is the tendency to diverge through analysis process due to high degree of complexity and stiffness matrix rapid degradation in post yield regions (Khatri and Anderson, 1995).

UNITS

ADINA system in its graphical user interface seems to be an almost unitless program, containing no specified units to be adopted. However, when using the system,

(ADINA TMG, 2005) states that it is important to enter all physical quantities (lengths, forces, masses, times) using a consistent set of units.

For example, when working with the SI system of units, enter lengths in meters, forces in Newtons, masses in kg, times in seconds. When working with other systems of units, all mass and mass-related units must be consistent with the length, force and time units (ADINA TMG, 2005).

3.2.2 Material and Elements Description

3.2.2.1 Introduction

Through material modeling, ADINA FE procedures can define the capability of the system to undertake excitations within nonlinear inelastic response regions. However, few of FE program suits employ such inelastic response due to complexity and time consuming which lead to an elevated level of cost.

ADINA FE environment was constructed to handle various types of responses, such as elastic response (isotropic, orthotropic and nonlinear); plastic response (bilinear, multilinear and orthotropic); creep and other numerous types of material response, such as concrete.

All material guidelines mentioned herein and in the preceding sections, or adopted in the proposed models of this research, are relative to material description introduced by (Chen and Han, 1988).

All modeling procedures and general guidelines mentioned herein and in the preceding sections, to be adopted consequently in the proposed models of this research, are described by (ADINA TMG, 2005).

3.2.2.2 Structural Steel Modeling

3.2.2.2.1 General

Steel elements in ADINA can simply be idealized to bilinear or multilinear response taking into account the elasto-plastic behavior.

Steel grade selected for structural steel elements in thesis models is: grade 345 MPa, see Figure 3.1. The corresponding material ductility can be calculated as following:

$\varepsilon_y \approx 2x10^{-3}$ m/m

$\varepsilon \approx 50x10^{-3}$ m/m

$$\mu_\varepsilon = \frac{\varepsilon}{\varepsilon_y} = \frac{50x10^{-3}}{2x10^{-3}} = 25$$

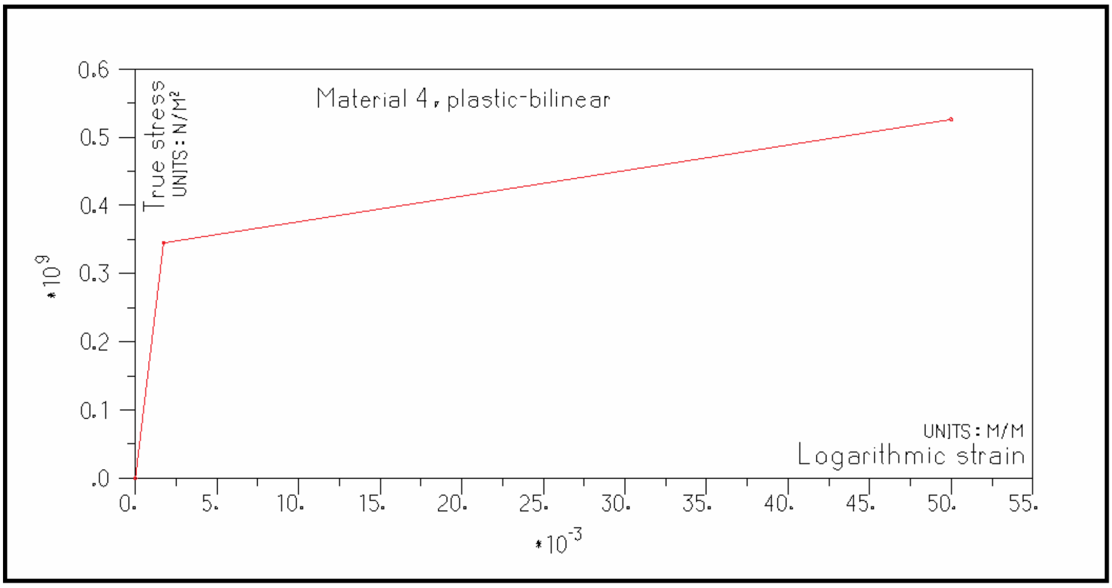


Figure 3.1: Bilinear steel model f_y= 345 MPa

3.2.2.2.2 Bracing Element

Steel bracing elements, which take axial compression or tension only, is simply defined in the models of this thesis using the ADINA truss element with bilinear behavior shown in Figure 3.1, based on Von-Mises elasto-plastic failure criteria. However, it must be mentioned that the effect of buckling in bracing elements, through this research, is neutralized.

3.2.2.2.3 Beam-Column Element

Modeling nonlinear elasto-plastic beam element in ADINA is, unfortunately, restricted to rectangular and pipe cross sections only (ADINA TMG, 2005). On the other hand, this research concerns in modeling wide flanged cross section, "I" or "H" shape. The solution of this problem is to model such component using Shell elements.

Modeling wide flange section using shell element components can have two advantages: revealing whether the inelastic response appears in the web or the flanges region and creating the ability to add stiffeners in the link regions.

In the proposed models, structural steel element, representing connecting beams and stiffeners, were modeled using shell elements shown in Figure 3.2.

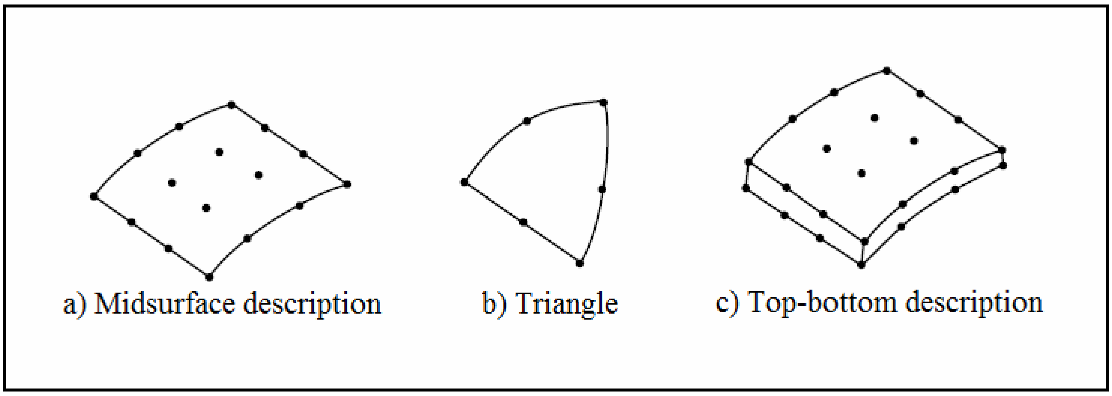


Figure 3.2: Examples of shell elements (ADINA TMG, 2005)

3.2.2.3 Concrete Model

3.2.2.3.1 General

The intricacy of the true behavior of the concrete elements is a foremost matter that faces FE modeling programmers and researchers alike. However, an outstanding nonlinear concrete model was developed by ADINA team which is able to describe the true behavior of two dimensional applications in excellent manner (Khatri and Anderson, 1995).

The formulation consists of a hypoelastic model utilizing up to 27 constants for calibration, as shown in Figure 3.6. For more information, it is recommended to refer to (ADINA TMG, 2005). The concrete elements are meshed as two dimensional plane-stress isoparametric elements which are able to account for in-plane forces, as shown in Figure 3.3.

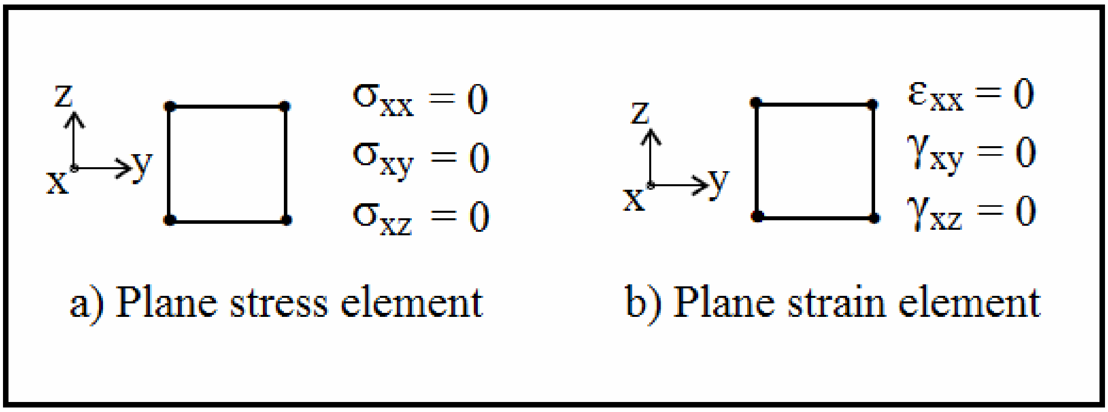


Figure 3.3: Basic assumptions in 2D analysis (ADINA TMG, 2005)

It is important to mention that ADINA restricts the employment of concrete model to 2D-solid element for the planar problems and 3D-solid element for general three dimensional cases, refer to Figure 3.4, the advantage of such restriction is to visualize crack patterns introduced to the concrete.

However, to solve planar problems using 2D-solid material, the mesh shall be defined within YZ plane. This criterion is one of ADINA definitions (ADINA TMG, 2005).

In this research, the concrete was modeled as four-node, plane-stress, 2D-solid elements as shown in Figure 3.4b, with nonlinear truss elements that are attached to boundaries of the plane-stress elements. These truss elements represent the steel reinforcement, and the definition of these elements is similar to steel bracing elements definition. However, ADINA provides the ability to the user to mesh these nonlinear steel trusses as "rebar" elements, this tool is introduced to account for the exact behavior of the composite action and was considered in the work of this research. Still, both options provide acceptable results, refer to Figure 3.5.

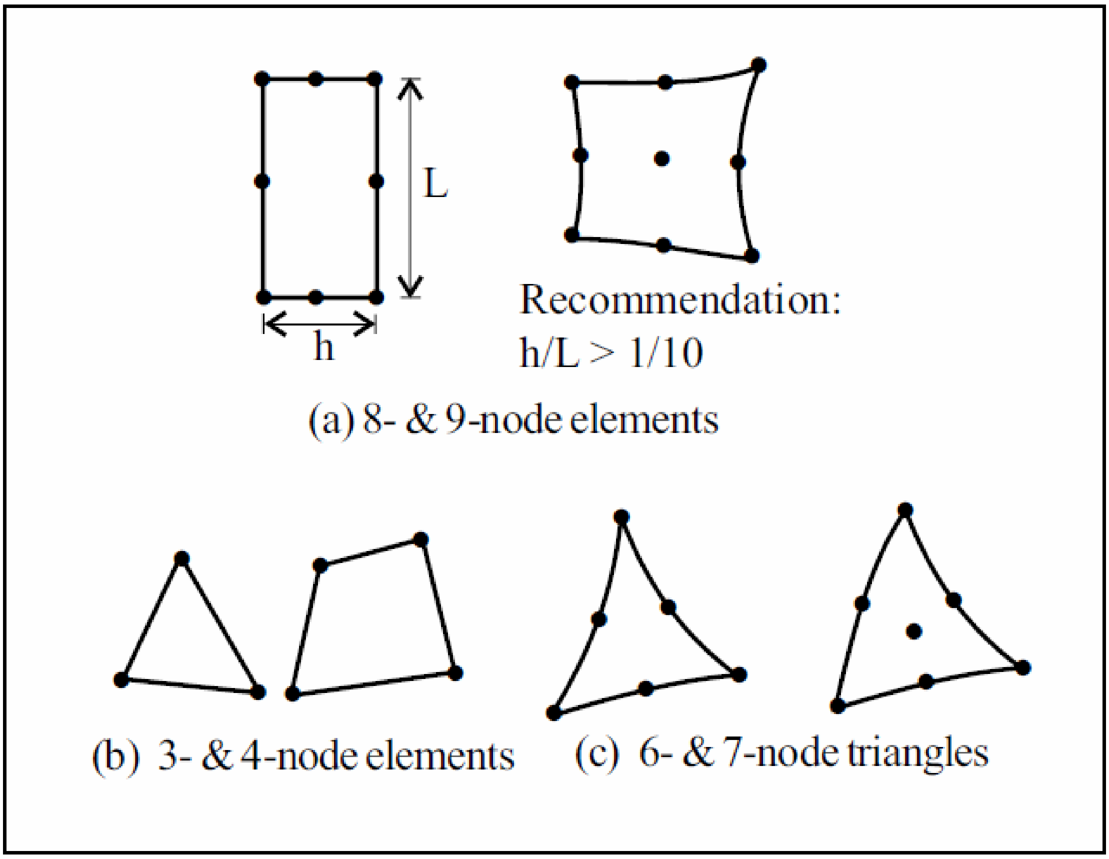


Figure 3.4: 2D-solid elements (ADINA TMG, 2005)

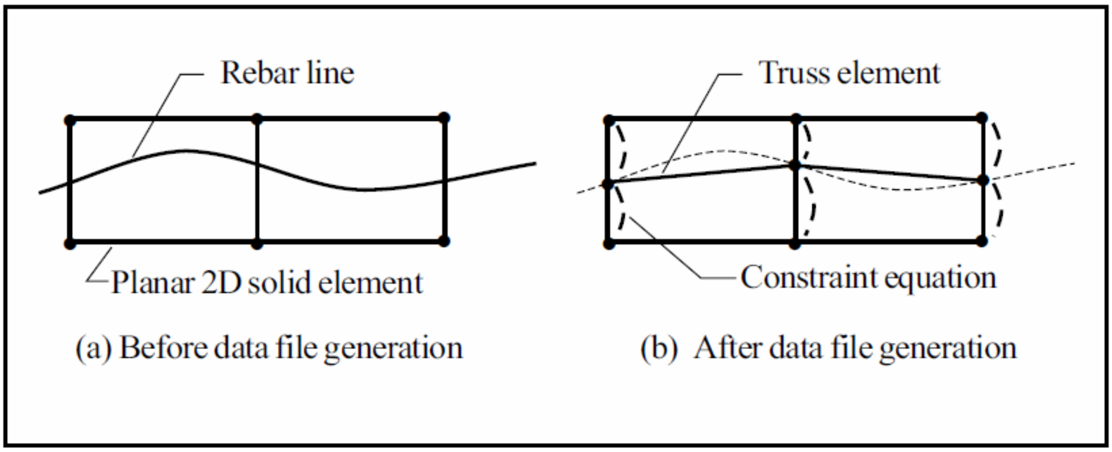


Figure 3.5: Truss and rebar representation (ADINA TMG, 2005)

Together, these two elements; plane stress concrete and steel truss elements provide the composite action of the concrete model, in which steel truss elements handle tension forces while the plane stress concrete is able to resist the compression forces.

Despite the fact that (ADINA TMG, 2005) recommends the use of 3-node nonlinear truss elements to represent rebars that are modeled with higher-order continuum or shell elements, the use of 2-node is more effective for other cases and can also give reasonable results. 2-node nonlinear truss definition was performed in many papers; (Khateri and Anderson, 1995), and this research will follow the same procedure for simplicity in parallel with efficiency.

Reinforced concrete response under monotonic loading can be divided into two phases: prior to yield and postyield. The boundary between these two limits is the yielding in tension steel.

Although steel reinforcement follows a bilinear curve of response, reinforced concrete behaves predominantly in an inelastic fashion.

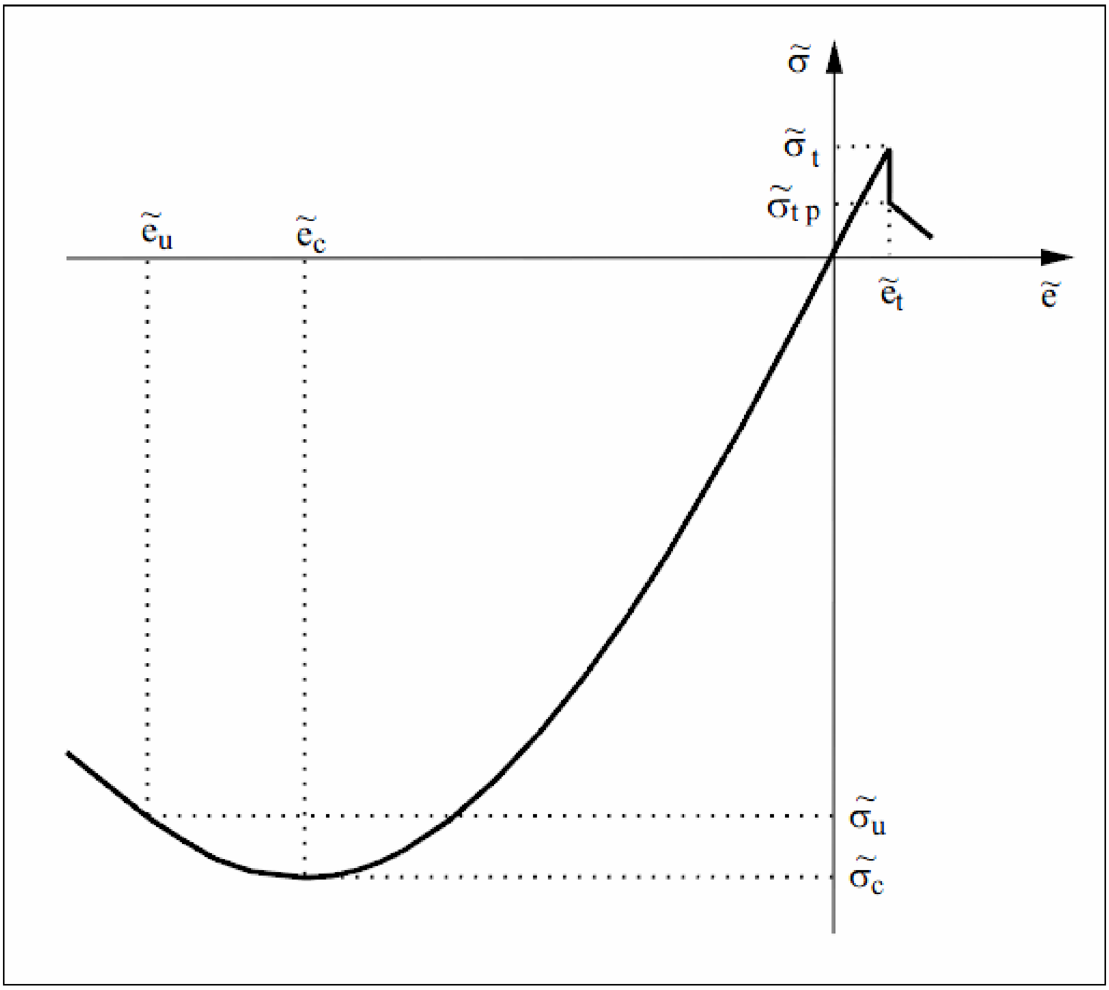


Figure 3.6: Uniaxial stress-strain relation used in concrete model (ADINA TMG, 2005)

Response characteristic in the preyield regions differs than that in the postyield. For example, deflection shape in the preyield phase tends to have an almost purely linear curve, while in the postyield regions large deflections will result from small incremental loads until failure.

Under this behavior, the convergence parameter changes drastically between the preyield and postyield phases. This change will lead to unstable solution with severe divergence in the model in the post yield phase. However, ADINA supports an Automatic Time Stepping procedure (ATS) that helps to provide good results in a reasonable time for all types of models.

ATS method performs perfectly in the preyield regions because the solution has a stable stiffness matrix, but after yielding of steel reinforcement, this stiffness matrix degrades rapidly under loadings increment (Khatri and Anderson, 1995).

In cyclic loading, the case will be more complicated, since these cycles will introduce reversals with plastic excursion in either direction of the loading.

3.2.2.3.2 Concrete Modeling

ADINA provides the tool to model concrete as a 2D-solid element. Through material definition itself; stress and strain can be controlled according to specified curve.

In this research, concrete compressive strength is selected to be 50 MPa for all of the proposed models.

It is widely accepted that concrete is undependable in the field of tension loading type, especially when inelastic response takes place, so its tensile capacity must be neglected respectively. This criterion, surely, will lead to a concrete material stress-strain curve that is not extended into the tension regions. However, in Figure 3.7 the small portion of tensile strength shown in the curve is for stabilizing the solution and to assure convergence in the model.

3.2.2.3.3 Reinforcement

Steel reinforcement was modeled using ADINA nonlinear truss elements, based on Von-Mises elasto-plastic failure criteria. Stress-strain curve for steel reinforcement is shown in Figure 3.8.

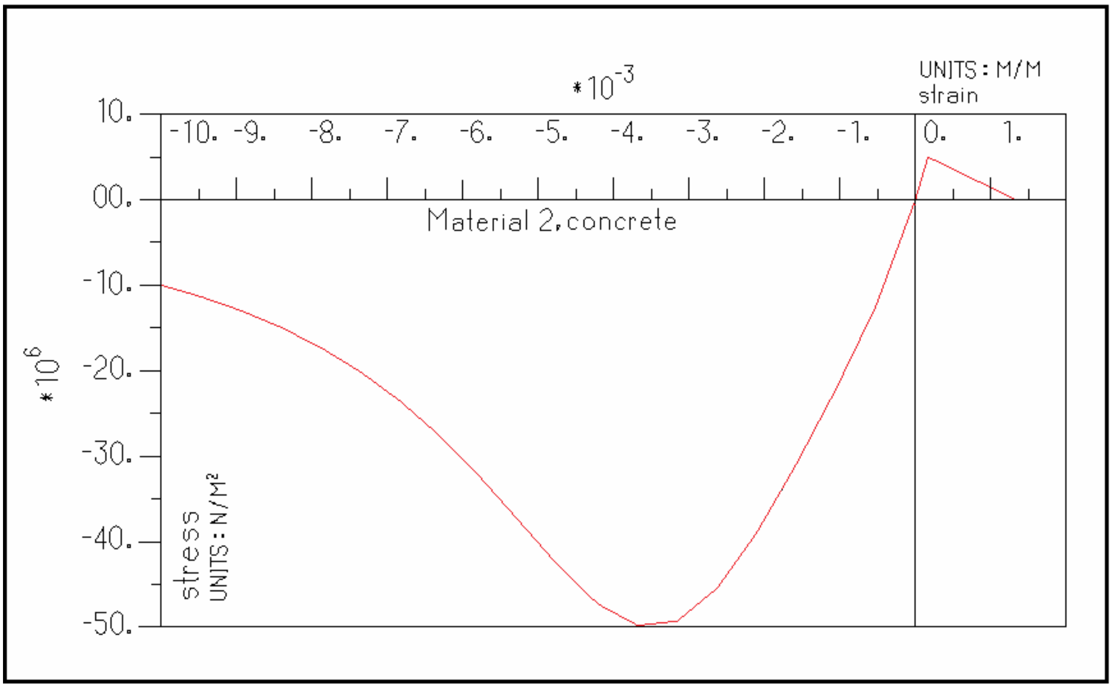


Figure 3.7: Stress strain curve for concrete model

Elasto-plastic bilinear relationship was adopted with a considerable amount of strain hardening. However, modeling the steel elements as elastic-perfectly plastic response is not possible due to convergence issues as stated earlier.

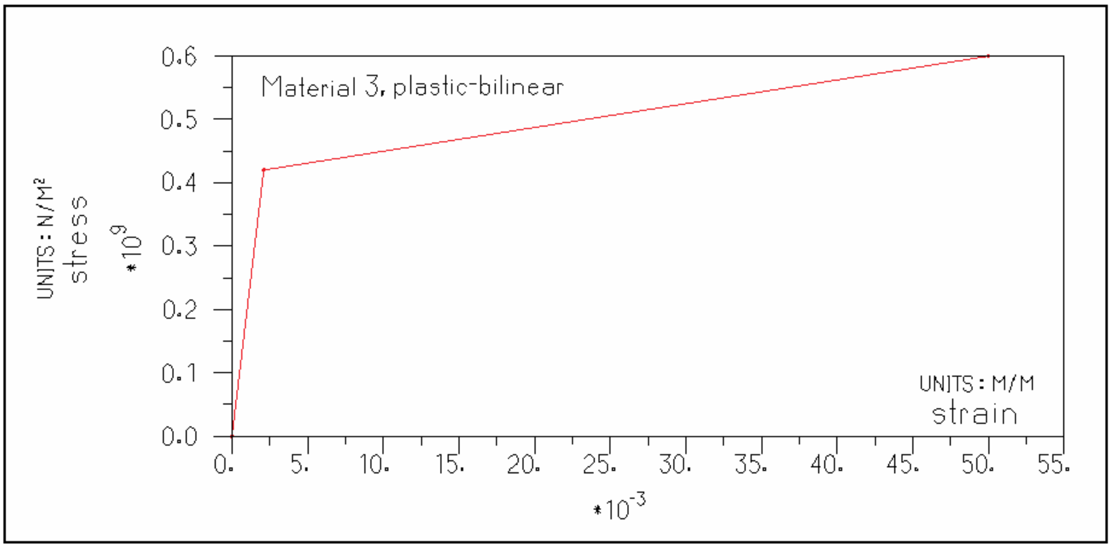


Figure 3.8: Stress strain curve for steel reinforcement f_y = 420 MPa

During meshing the model, plane stress concrete elements will be restricted to a given geometrical size, and therefore steel reinforcement elements must be governed by these concrete elements (i.e. attached to its edges) since it is not feasible to model such reinforcement independently. This will force the size of the reinforcement and their spacing to be restricted to the given mesh.

Due to this criterion, steel reinforcement must be imported to the model in terms of equivalent element area, see Figure 3.9.

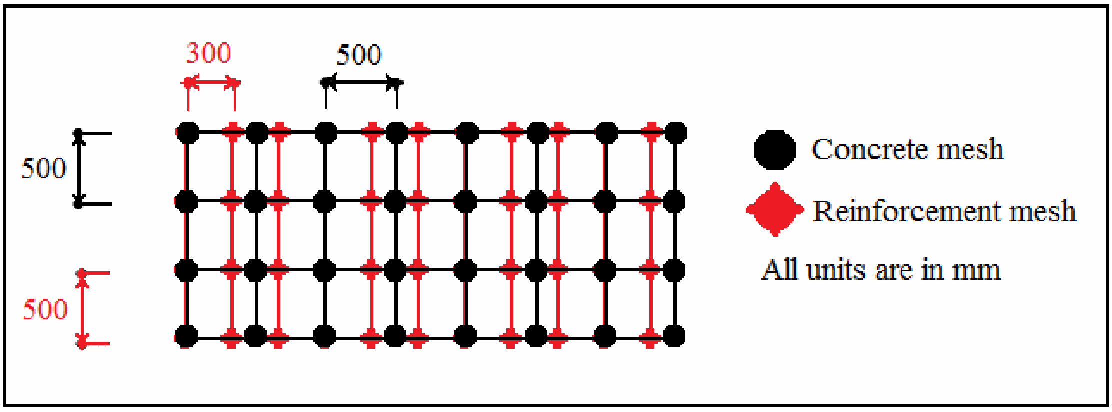


Figure 3.9: Meshed sample representing equivalent reinforcement area

Referring to Figure 3.9 for example, if the vertical reinforcement was 2Φ32@ 300 mm and concrete element mesh size is 500 mm as shown in Figure 3.9, steel reinforcement spacing must follow the concrete mesh size of 500 mm spacing with an equivalent bar size as follows:

$$A_{Actual} = \frac{2\pi}{4}(32)^2 = 1{,}608\ mm^2$$

$$A_{Equivalent} = \frac{500}{300}\ (1{,}608) = 2{,}680\ mm^2$$

The result will be 2,680 mm^2 @ 500 mm instead of 1,608 mm^2@ 300 mm.

3.2.3 Models Description

3.2.3.1 Introduction

The aim of this research is to bring forward a new hybrid seismic resistant system to study. This study will focus on the seismic performance of such system and its feasibility in seismic regions under severe events. In order to introduce the applicability of the system and its advantages it must be compared to the traditional systems. Thus, two classical systems were modeled side by side with the proposed new system for comparison issues.

Therefore, three models will be represented in this research to compare their seismic response under ADINA User Interface (AUI) environment. Two types of loading are introduced: (Monotonic and cyclic loading). Seismic response of these models, will be represented herein in this chapter, in terms of ductility, top displacement, story drift and energy dissipation.

These three modeled systems are:

(1) Cantilever Shear Wall System, as shown in Figure 3.10.

(2) Hybrid Beam-Coupled Shear Wall System, as shown in Figure 3.12.

(3) Hybrid Coupled Shear Walls using Eccentric Steel Bracing System (i.e. Hybrid Brace-Coupled Shear Walls), as shown in Figure 3.14.

3.2.3.2 Model 1: Cantilever Shear Wall

The cantilever shear wall is the main element in the three types of the proposed systems. This wall consists of 2-D solid elements describing the nonlinear concrete material; each element has four nodes, and attached to steel truss elements at its four edges. The steel truss is a 2-node truss element and describes the reinforcement. These

two elements introduce the composite action of the reinforced concrete in the shear wall.

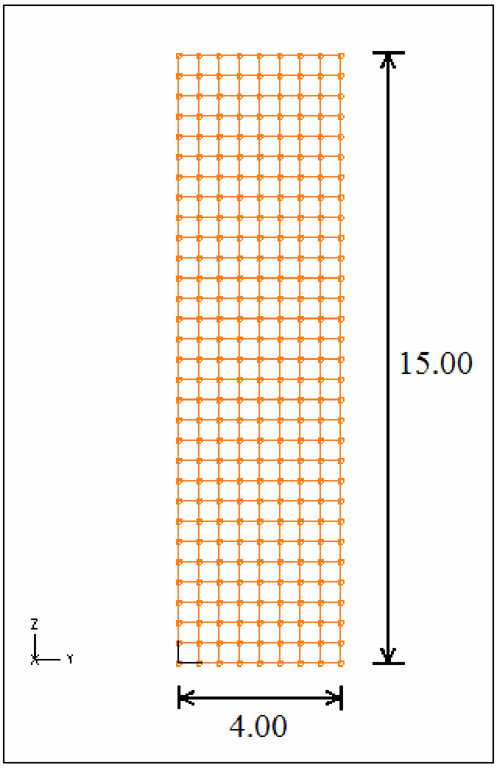


Figure 3.10: Independent cantilever shear walls model by ADINA (all units are in m)

Hinged Support is the fixation type assigned to each node at the base of the wall.

Referring to Figure 3.11, each element in the wall was meshed and numbered accordingly; numbers in violet represents concrete elements and numbers in green represents steel reinforcement.

Wall thickness is selected to be 1.00 m and Steel reinforcement mesh (represented by green numbers) is chosen to be 4Φ32@ 300 mm. Equivalent area of reinforcement according to 500 mm typical spacing is performed and the results are as follows:

$$A_{Actual} = \frac{4\pi}{4}(32)^2 = 3{,}217\ mm^2$$

$$A_{Equivalent} = \frac{500}{300}\,(3{,}217) = 5{,}362\ mm^2$$

The result will be 5,362 mm^2 @500 mm instead of 3,217 mm^2 @ 300 mm.

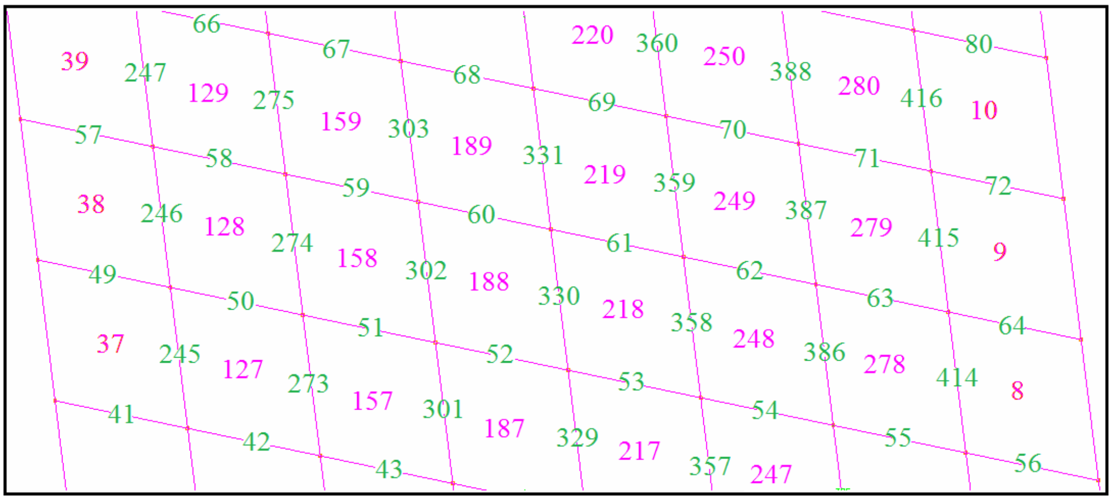


Figure 3.11: Meshing wall elements

3.2.3.3 Model 2: Hybrid Beam-Coupled Shear Walls

Two coupled shear walls are modeled using the same exact procedure considered in the previous model, see Figure 3.12.

Steel coupling beams are meshed using shell elements. To avoid complexity, and as suggested by many papers; (El Tawil, 2002), concrete encasement is not considered in the model.

Web elements (numbered in orange) shown in Figure 3.13 have a total depth of 500 mm, flange elements (numbered in turquoise) are also 500 mm total width, while thickness of these elements is changeable during modeling, but limited to AISC slenderness limitations.

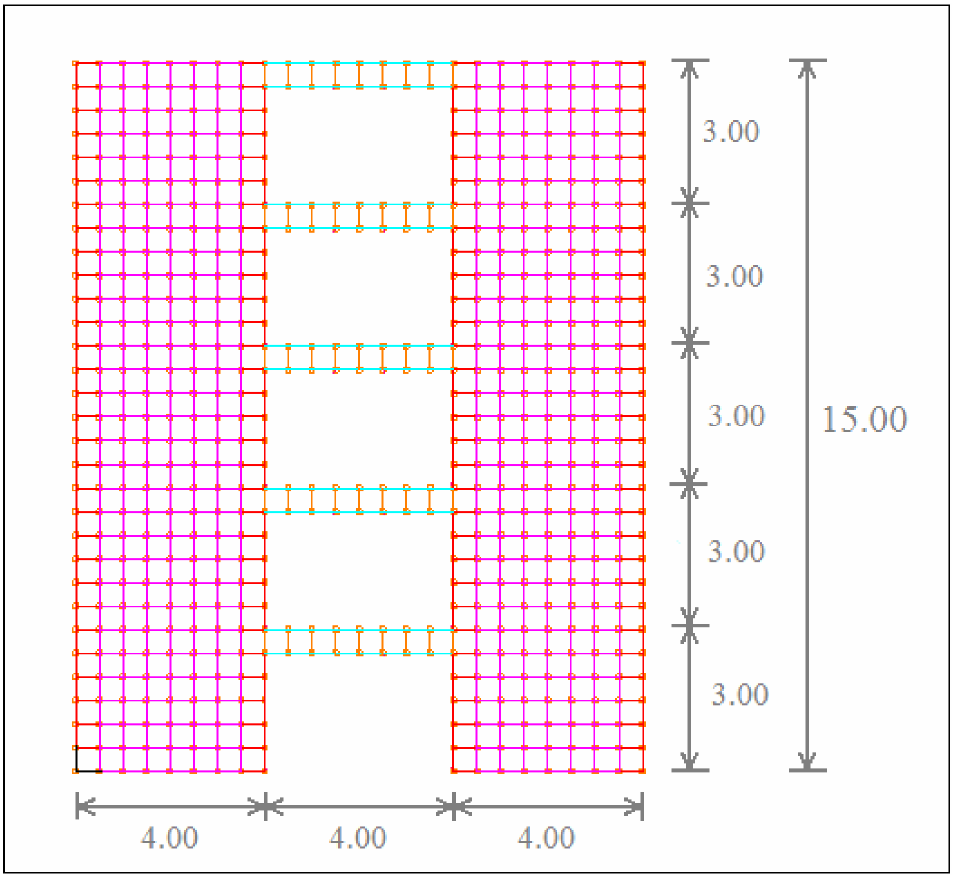


Figure 3.12: Hybrid beam-coupled shear wall model by ADINA (all units are in m)

After a preliminary run for hybrid brace-coupled shear walls model, a flange thickness of 50 mm is adopted, web thickness to be 20 mm and stiffeners thickness, which will be described in the following section, equals the web thickness unless noted otherwise.

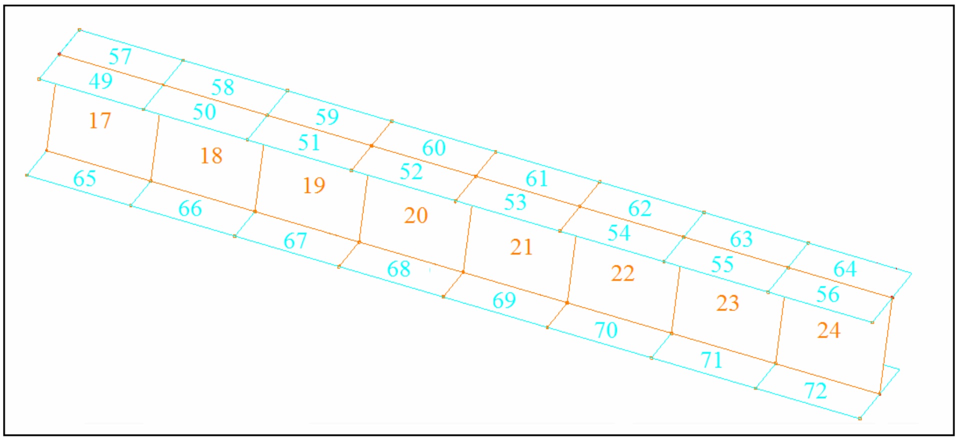


Figure 3.13: Shell elements for coupling beam

3.2.3.4 Model 3: Hybrid Brace-Coupled Shear Walls

For this model, bracing elements are enhanced beneath coupling beams, these braces form a short link in the area between them, and such area must be supported by stiffeners. Refer to Figure 3.14.

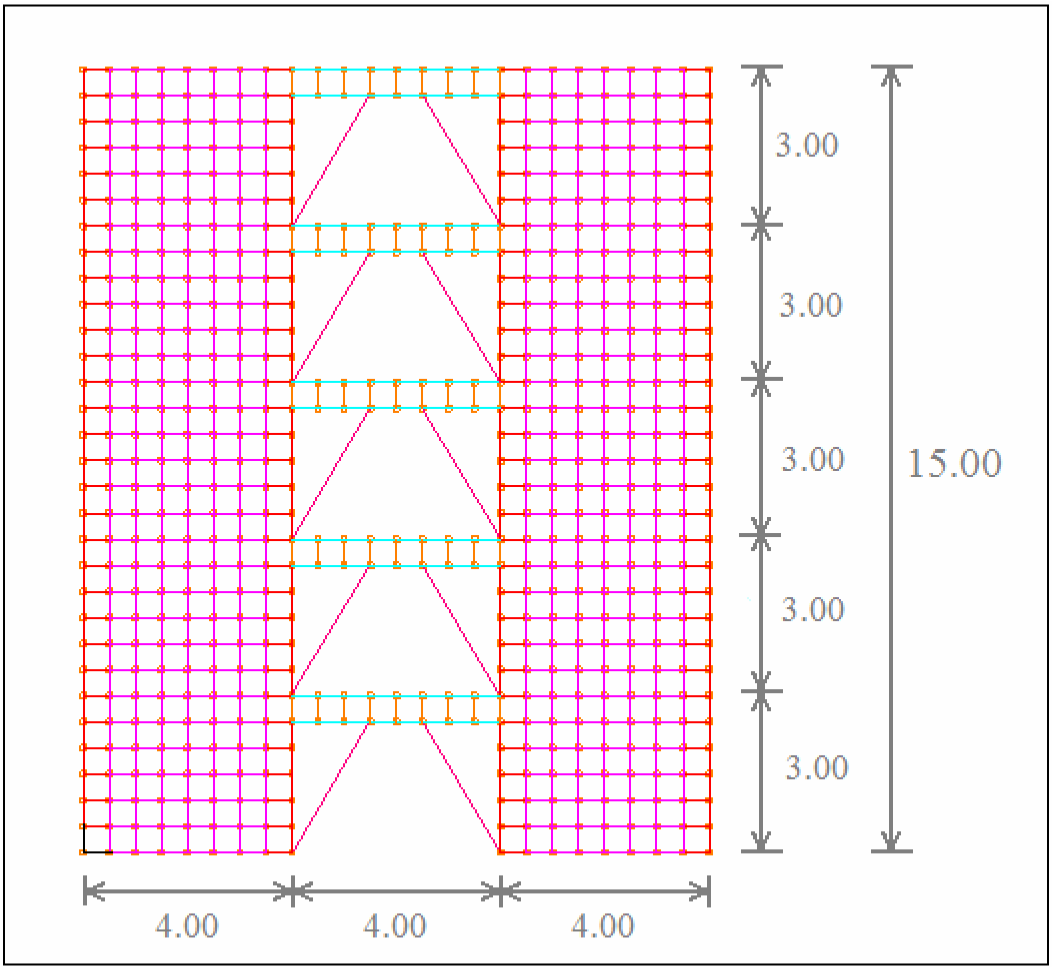


Figure 3.14: Hybrid brace-coupling model by ADINA (all units are in m)

Diagonal bracing modeling is a critical phase in modeling the hybrid brace-coupled shear walls system (i.e. selecting braces size) since the braces must not experience any overstressing that causes them to yield or buckle. Rod cross section is adopted for diagonal braces. For preliminary analysis, the rod section is selected to be 180 mm in diameter. However, if the results show an unfavorable plasticity response in

these braces during analysis, these diagonals must be enlarged by means of overstrength factor implemented in the capacity design.

Stiffeners are modeled as shell elements that are perpendicular to the web of the coupling beam in the short link region. Dimensions of these elements are selected to have the same depth of the web of the coupling beam (i.e. 500 mm), and have the same width of the flange exposure on each side of the coupling beam (i.e. 250 mm), refer to Figure 3.15, while thickness of stiffeners is changeable during modeling, but restricted to the limitations of (AISC seismic provisions, 2005).

Element number "55" shown in orange in Figure 3.15 is an intermediate stiffener modeled in ADINA, while orange colored elements "53" & "57" are end stiffeners, and the region enclosed by the end stiffener elements is the link zone. Also, on the other side of the web, stiffeners are provided accordingly.

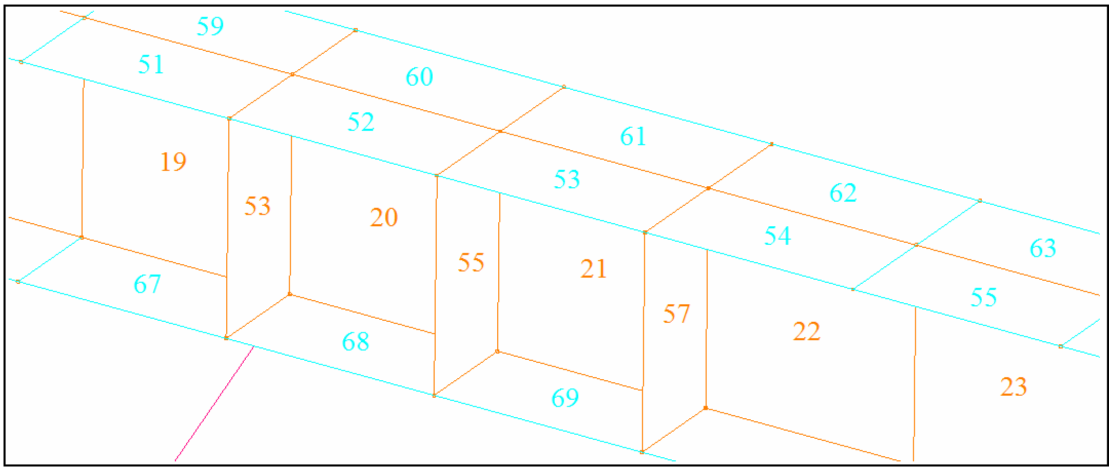


Figure 3.15: Link stiffeners modeling

3.2.4 Excitation Description and Analysis Assumptions

3.2.4.1 Introduction

This section discusses all the matters related to ADINA environment concerning loading definition, numerical analysis, time stepping, and kinematic assumptions. General guidelines are introduced to cover the basic matters which are related to this specific study only. For more information, it is highly recommended to refer to (ADINA TMG, 2005) where detailed requirements, descriptions and assumptions are overwhelming.

3.2.4.2 Excitation Description

3.2.4.2.1 General

Types of loadings applied to the system can be classified into two major types: (1) Gravitational loads and (2) Lateral loads. The latter can describe seismic excitations, while gravitational loads can describe traditional dead loads and live loads.

ADINA program suite differs than other programs; which are solely intended to structural/civil representations, where every type of loading is categorized under certain definitions that consider related modern codes of practice procedures. ADINA is a more generalized program that does not consider civil concerns only; it includes heat transfer problems, solid mechanics and fluids. For this reason, definition of loads in ADINA is absolutely abstracted.

Seismic excitations are the elementary concern in this research. So, definition of any other type of loading is totally related to seismic general rules and guidelines accepted by modern codes. Consequently, full dead load is recognized during

earthquake shaking with portion of live load that ranges between (25-50) percent of the full live load.

Gravitational loads are determined in advance and added as a constant magnitude at four locations directly on the edges of the shear walls, at each floor level, see Figure 3.16.

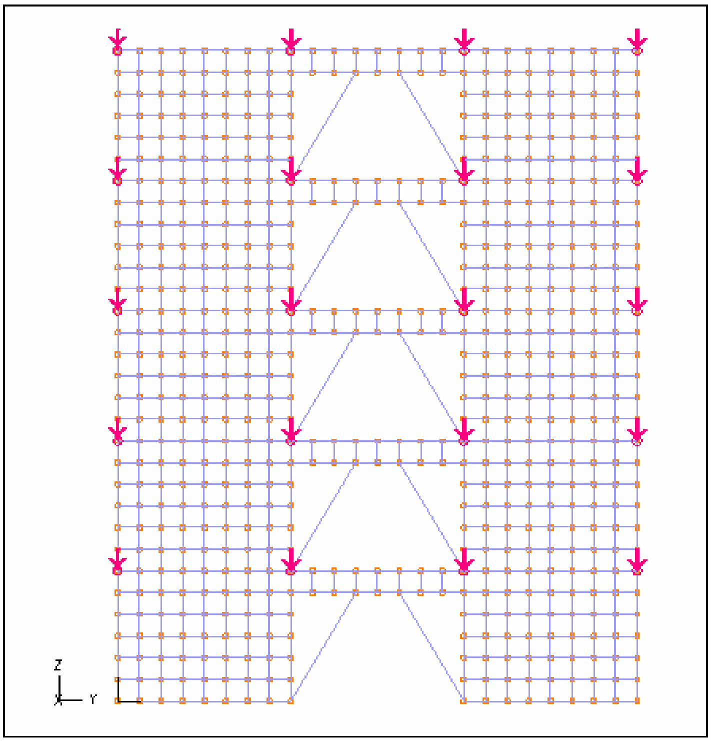


Figure 3.16: Gravitational Loads

Recognizing such type of loading introduces two opposite features: increase the P-Δ effect which has a bad influence on the system and increase the horizontal shear capacity of the wall, due to compression gravitational loads; which has a positive influence on the mechanical properties of the concrete elements (ADINA accounts for this particular complex behavior) (Khatri and Anderson, 1995).

3.2.4.2.2 Monotonic Loading

Monotonic loading is a one way increasing loading until failure. This type of loading is generally applied laterally to the structure. However, this assumption can be defined easily through ADINA by controlling time function of such load, refer to Figure 3.17.

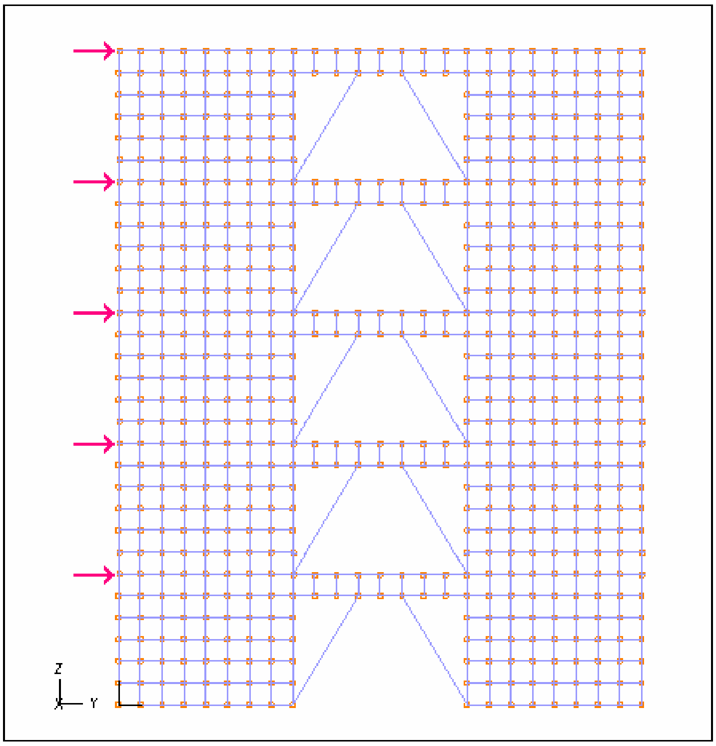


Figure 3.17: Monotonic Loading

Static analysis procedure is considered for this incremental loading; this is the definition of the pushover analysis.

3.2.4.2.3 Cyclic Loading

Cyclic loading can also be provided using time function parameters. One of the options provided is the sinusoidal case, where the loading changes its sign (direction) according to time. Constant control parameter CP is selected for simplicity.

3.2.4.3 Analysis Assumptions

P- Δ

ADINA provides the tool to recognize the well known P-Δ effects by its kinematic assumptions. Under this option the "Displacement/Rotations" default assumption in ADINA is: small. However, to recognize the P-Δ effect, ADINA TMG mentions that it must be changed to: Large.

Automatic Time Stepping

Through this tool ADINA can calculate the proper time step to pursue the convergence while running the analysis.

Time Step

This is one of the most elaborated tools considered in ADINA, since it allows the user to recognize the response of the system during all phases. This tool can be utilized by recording the required number of steps within the required time, and then the response can be extracted at each time step.

3.3 Results Discussion

3.3.1 Hybrid Brace-Coupled Shear Walls Model Results

3.3.1.1 Introduction

This section discusses the results of the three models proposed in this thesis; cantilever shear wall, hybrid beam-coupled shear walls and finally the hybrid brace-

coupled shear walls model shown in Figure 3.18, which is the prescribed hybrid coupled shear walls using eccentric steel bracing.

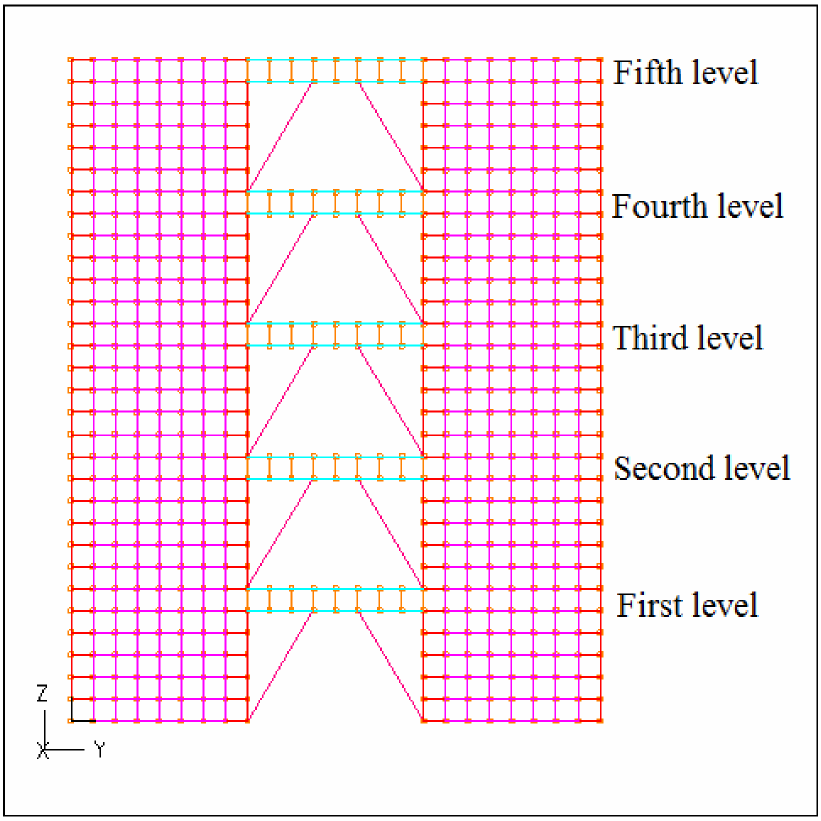


Figure 3.18: Hybrid brace-coupled shear walls model

3.3.1.2 Model Response

The hybrid brace-coupled shear walls model is subjected to an incremental step by step, static loading up to failure, which is functioning toward positive Y direction, refer to Figure 3.17.

(1) First yield

The model shows a linear response until the first plastic formation in the link of the third story coupling beam (i.e. middle coupling beam), followed by another plastic hinge at the link located in the second story coupling beam (i.e. coupling beam

beneath). These are the earliest inelastic excursions during system response, and it must be mentioned that these two plastic hinges, which are presented in predetermined zones to receive inelastic behavior, are associated with yielding of the steel reinforcement at the base of the wall due to wall curvature. See Figures 3.19 and Figure 3.20.

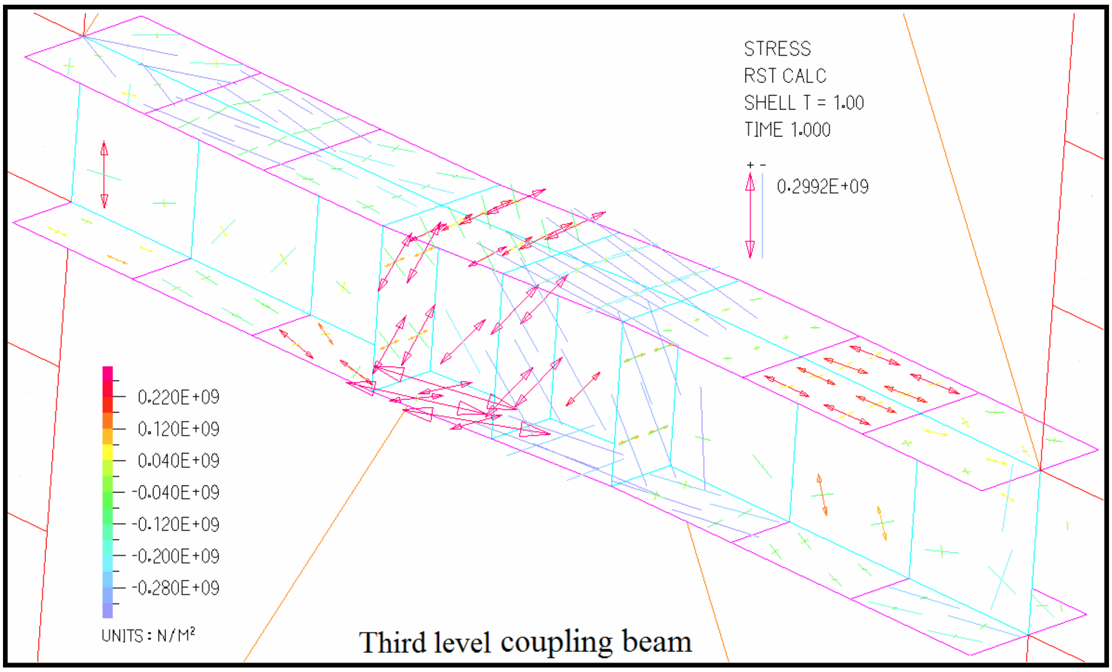


Figure 3.19: Vector plot: Stresses in link region (ADINA output)

In Figure 3.20, violet color representing areas with elastic behavior, while pink colored elements represent the plastic excursion in the structure.

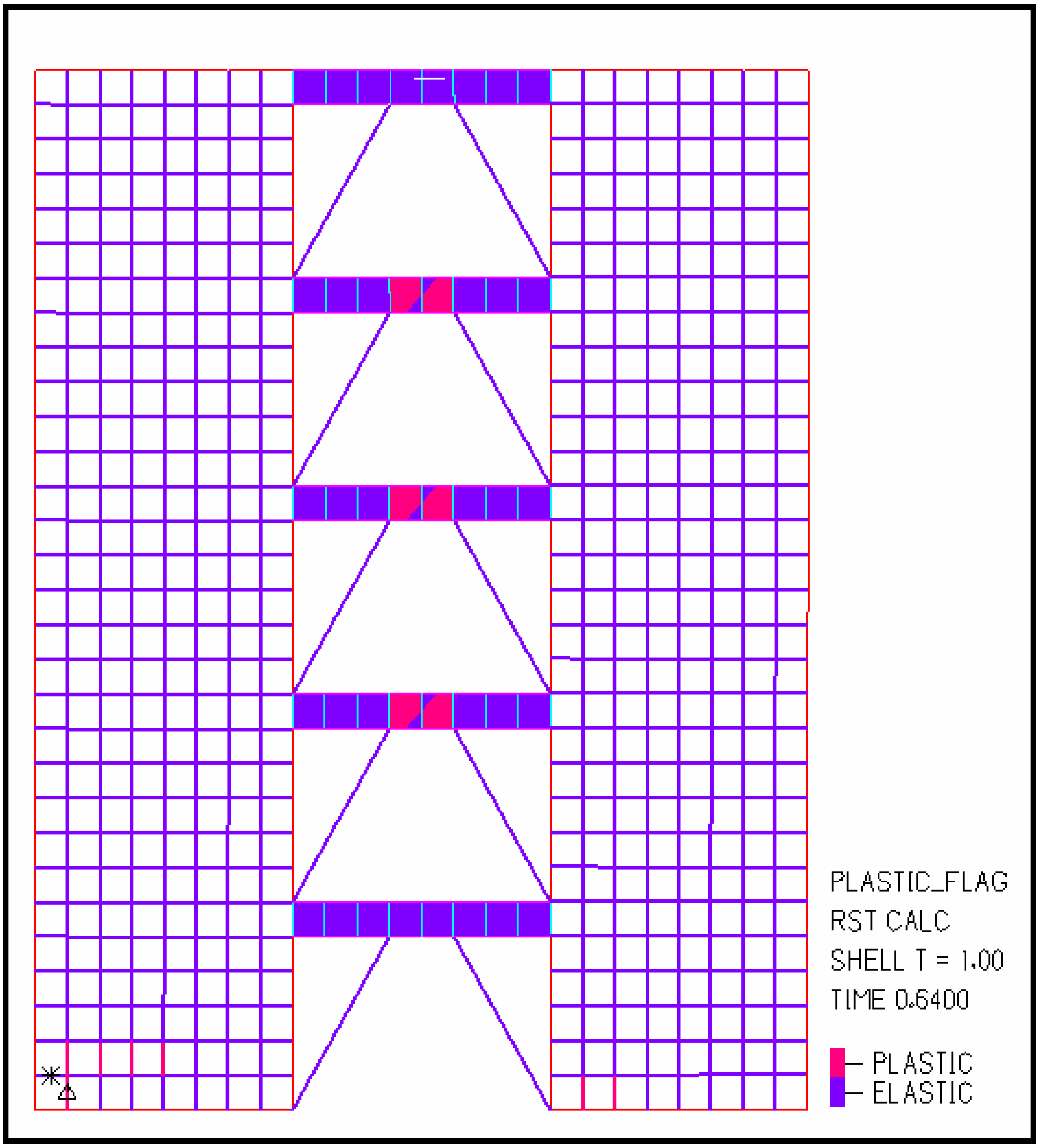


Figure 3.20: Preliminary plastic hinge formation (ADINA output)

(2) Yielding in the remaining links

Posterior to the preliminary hinges formation in the two links, the remaining links exhibit the expected inelastic response after few steps of loading increment. This is a healthy behavior in the system response that proves the capability of the entire system to dissipate energy along the entire height of the wall rather than a solitary plastic hinge formation at the base of the wall only. Refer to Section 2.4.2.2.

At this stage, Yield length in the yielded reinforcement at the base of the wall is elevated also.

Yielding in the links occurs at the web of the wide flange section, not in the flanges, which describes the case of shear dominant behavior of the short link, see Figure 3.21.

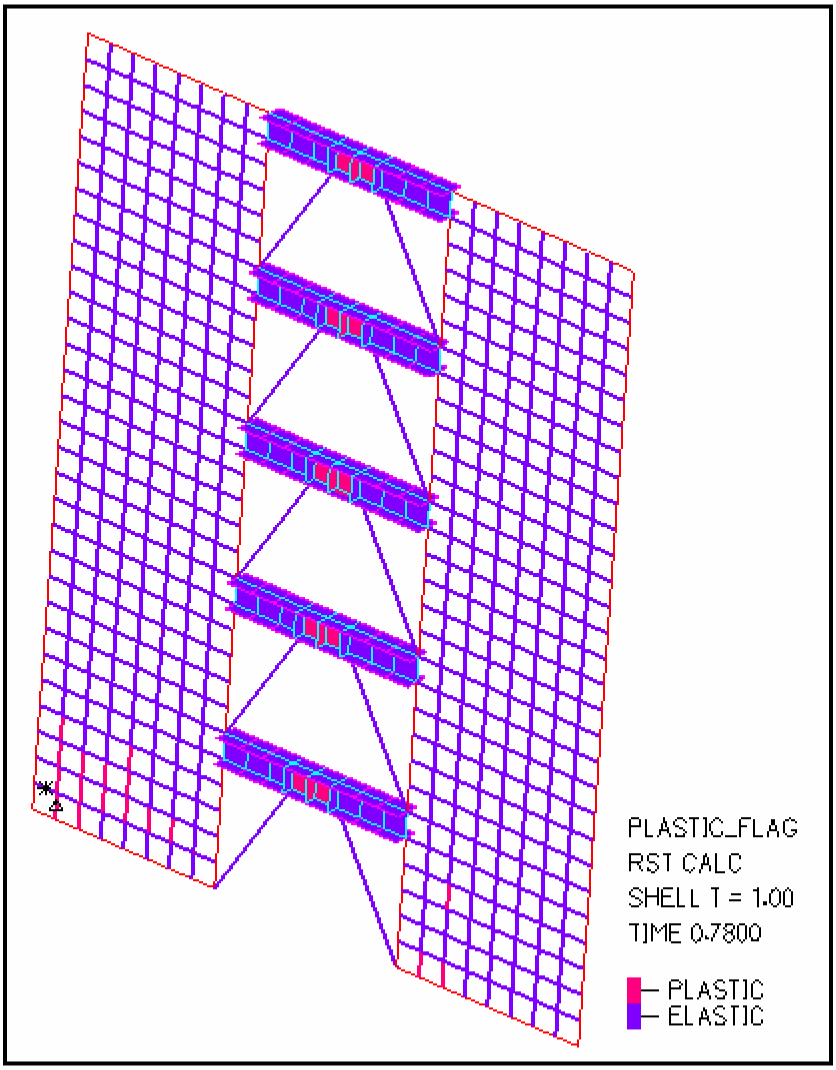


Figure 3.21: Plastic hinges formation (ADINA output)

At this particular stage, the kinematic properties of the system are introduced in terms of ductility in the link zone to sustain large deformations beyond yield, while the rest of the system remains unharmed.

(3) Yielding at the ends of the coupling beams

This type of yielding have occurred mainly at the ends of the coupling beams outer of the zone of the shear link, and can be described to be one of the most significant results in this study.

It was mentioned earlier, in chapter 2, that yielding in the links is not a case of "failure" by itself, even if these links fail to produce the desired plastic capacity, the system still have a reservation of capacity represented by the cantilever walls capacities. However, this distinct type of yielding at the ends of the coupling beams can be classified to be a reservation capacity in the system.

Hybrid beam-coupled shear walls (i.e. coupled without eccentric bracing system enhanced), if well detailed for extreme seismic events, can dissipate energy through the entire height of the wall, and then by introducing a plastic hinge at the base of the wall (El Tawil, 2002).

Eccentrically braced frames (i.e. not coupling shear walls), also, if well detailed to resist sever earthquake events, can dissipate energy, but through the desired short links, then mechanism might occur.

On the other hand, and concerning the proposed hybrid brace-coupled shear walls system, this study observes that this system can dissipate energy over the entire height of the wall on two steps: (1) by forming a plastic hinges at link zone, and (2) by forming plastic hinges at the end of coupling beams.

It is crucial to state that this remarkable re-yielding in coupling beams has exhibited three types of yielding response, as numbered in Figure 3.22: (1) Flexural yielding, (2) shear yielding and (3) combination between both.

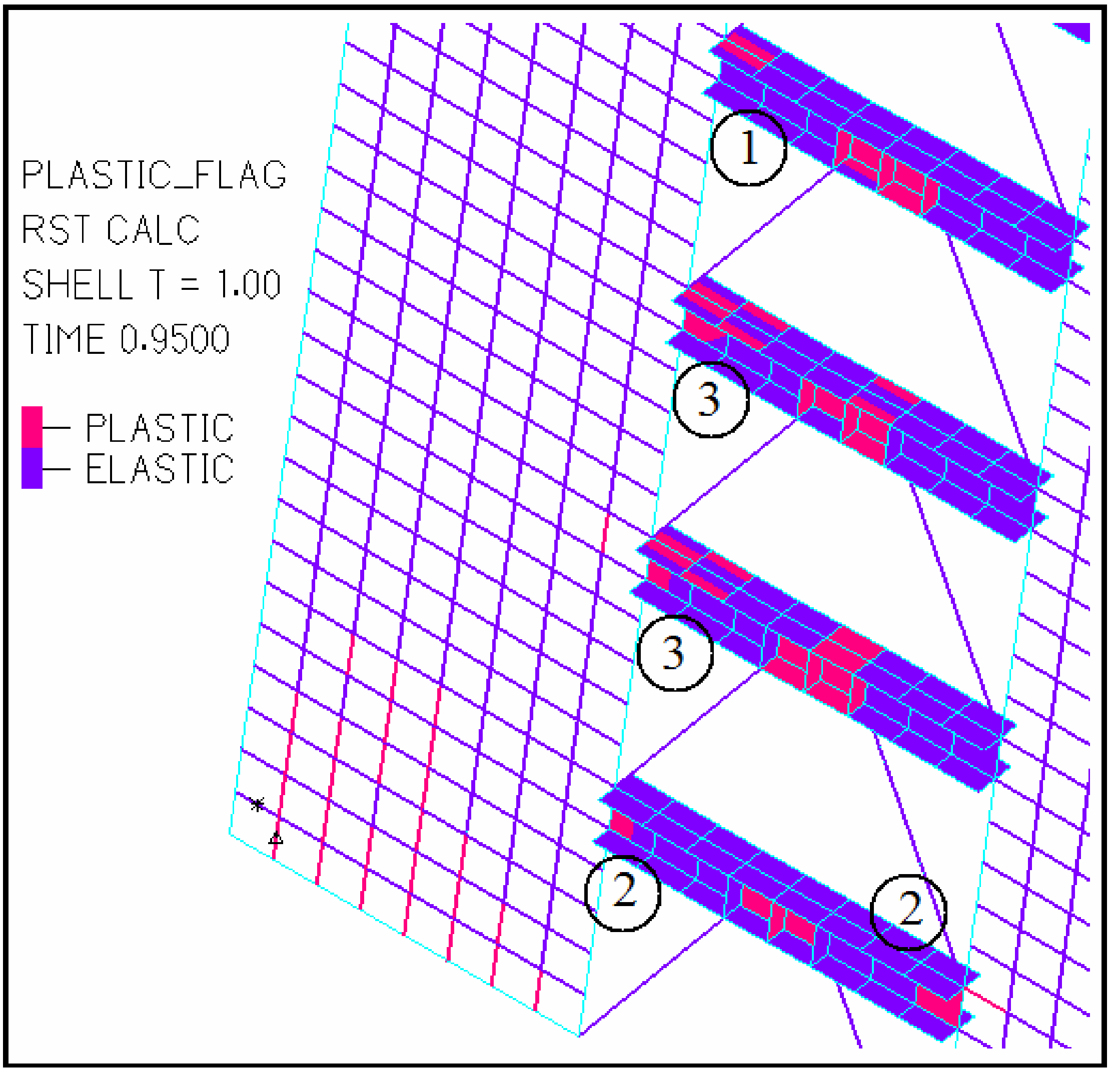


Figure 3.22: Second Phase of plasticization in coupling beams

Figure 3.22, shows the second phase of plasticity in the coupling beams. Flexural yielding type (i.e. number 1) described by flanges plasticization is shown on the fourth coupling beam from the bottom, while shear yielding type (introduced by plastic excursions in web) and combined yielding (that employs plasticity in both web and flanges) have both formed at the lower part of the system. This can be understood since the shear behavior tends to be dominant near the base of the wall at stages near to failure.

However, it must be pointed out that the second phase of plasticization in the coupling beams diminishes with height (i.e. upper floors do not introduce such response).

(4) Failure stage

At this stage, the coupled shear walls are subjected to higher curvature demand. Thus, plastic hinges form at the bases of the two walls; yield of reinforcement mainly in the left wall and crushing in concrete elements in the right wall, see Figures 3.23 to 3.24.

Figure 3.24 demonstrates that yield stresses occur at a level above the first story. This length describes the plastic hinge length. Nevertheless, improper reinforcement curtailment at an arbitrary length of the wall height for economical reasons can obstruct the yielding stresses from growing (Paulay and Priestley, 1992). This improper practice might increase the ductility demand on the wall, which is associated with brittle behavior induced beyond curtailment height (Paulay and Priestley, 1992).

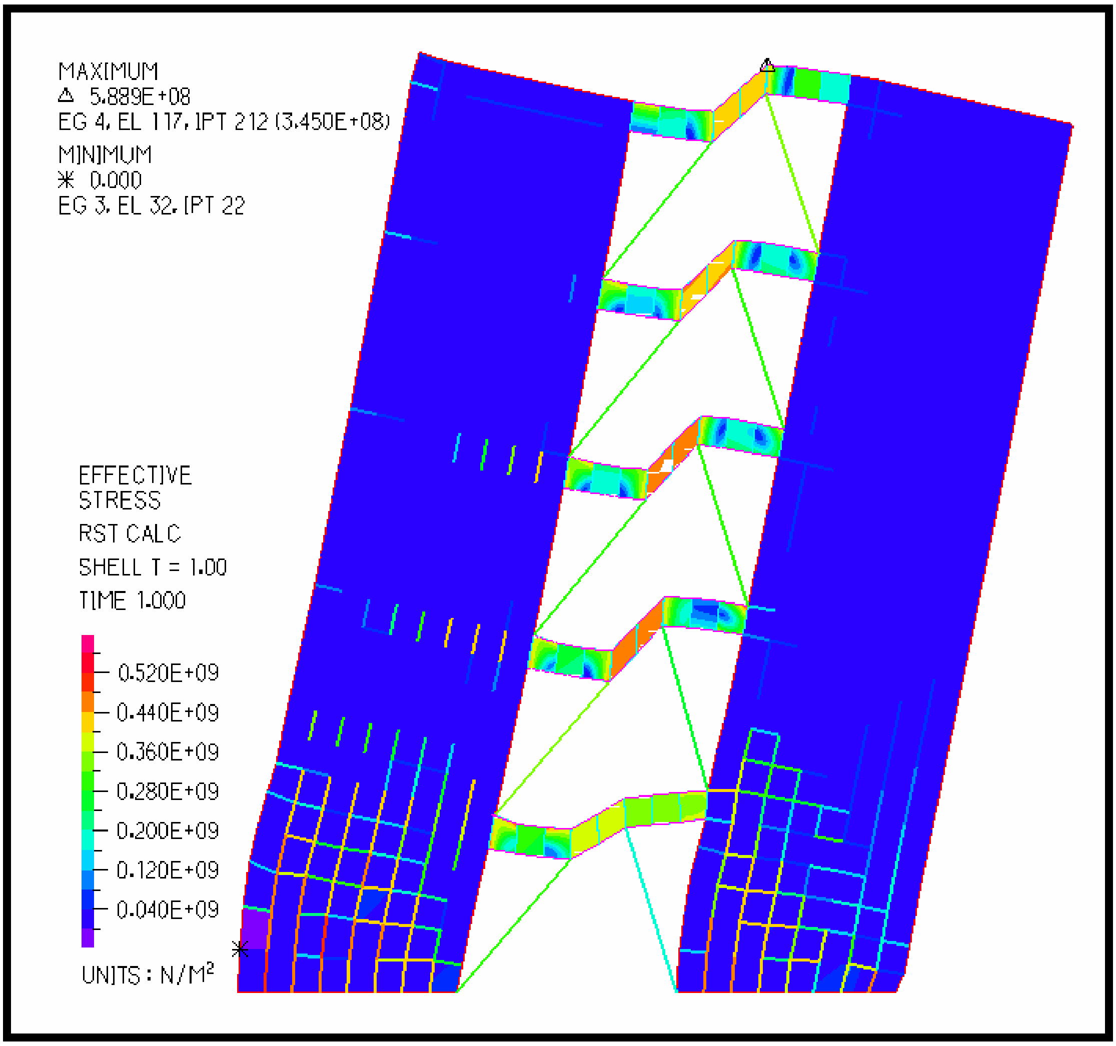


Figure 3.23: Effective stresses at final stages (ADINA output)

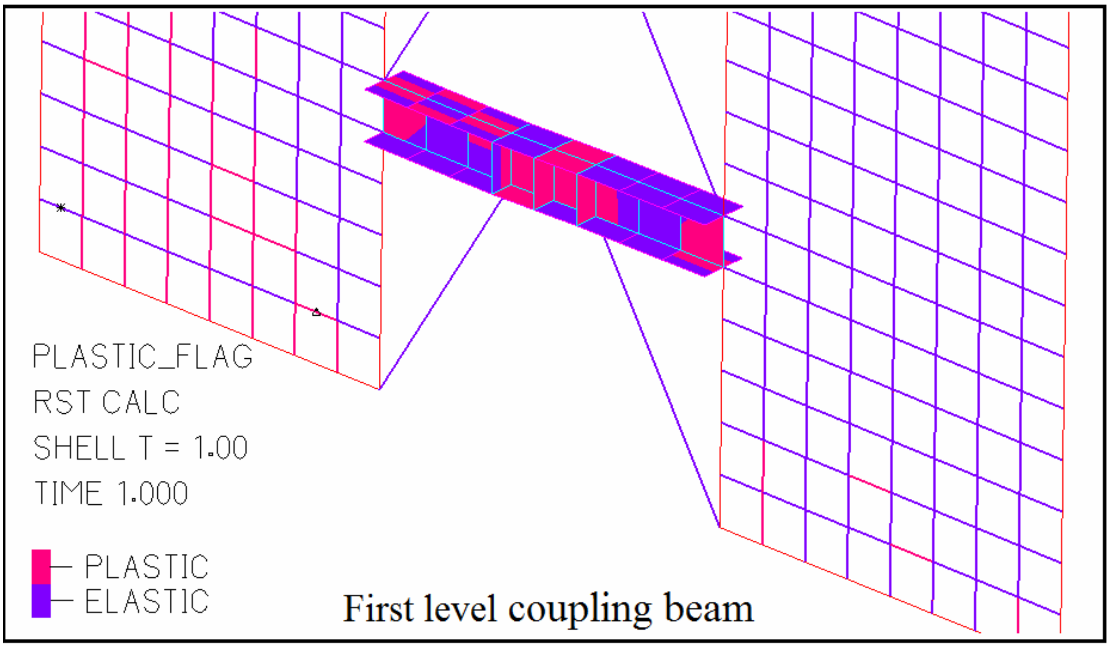


Figure 3.24: Plastic hinge formation at the base (ADINA output)

3.3.1.3 Link Plasticization

Yield must occur in the link region of the coupling beams to ensure that ductility and energy dissipation are going to occur through these specific replaceable elements.

This performance was evident in the behavior of the hybrid brace-coupled shear walls model, and the plastic accumulation has appeared in the coupling beams, specifically, in the link zone.

However, this type of plasticity is a shear dominant type, and this can be illustrated from ADINA results output as shown in Figure 3.25.

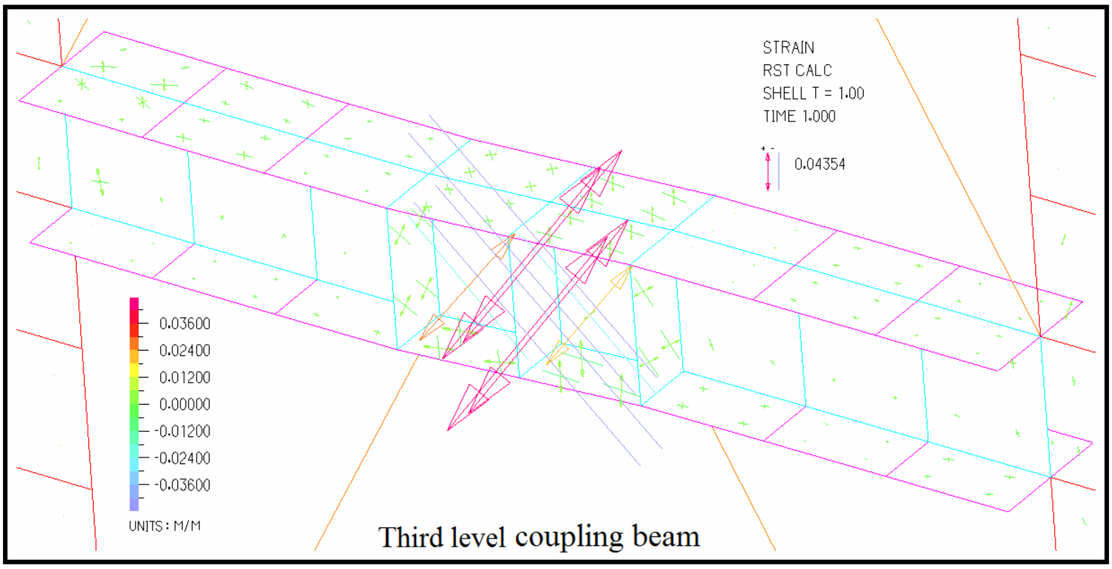


Figure 3.25: Vector plot: Plastic strain accumulation in link region (ADINA output)

Stiffeners provided in the link zone, especially the intermediate ones, demonstrate inelastic response similar to the web elements of the link.

Link rotation angle

The following equations show that inelastic rotation angles of both links is within the limit suggested by AISC seismic provisions.

Lowermost coupling beam, web shell element no. 4 in the link zone, the rotation value is

$$\theta = 5.71\ x\ 10^{-3}\ rad\ (ADINA\ output)$$

$$\gamma_p = \frac{L}{e}\ \theta = \frac{4}{1}\ 5.71\ x\ 10^{-3} = 0.0228\ rad < 0.08\ (O.K)$$

Intermediate coupling beam, web shell element no. 21 in the link zone, the rotation value is

$$\theta = 1.25\ x\ 10^{-2}\ rad\ (ADINA\ output)$$

$$\gamma_p = \frac{L}{e}\ \theta = \frac{4}{1}\ 1.25\ x\ 10^{-2} = 0.05\ rad < 0.08\ (O.K)$$

Subsequent sections will discuss the effect of coupling beam size on the overall behavior of the system thoroughly.

3.3.1.4 Lateral Movement Discussion

Top displacement

Maximum displacement happened prior to collapse of the hybrid brace-coupled shear walls model and was about 165 mm.

Figure 3.26 shows the top displacement increasing per time, it is clear that the displacement tends to follow an almost pure linear increment until plastic hinges take place in all of the links (Time≈ 0.75), then this increment goes in an almost exponential function up to failure.

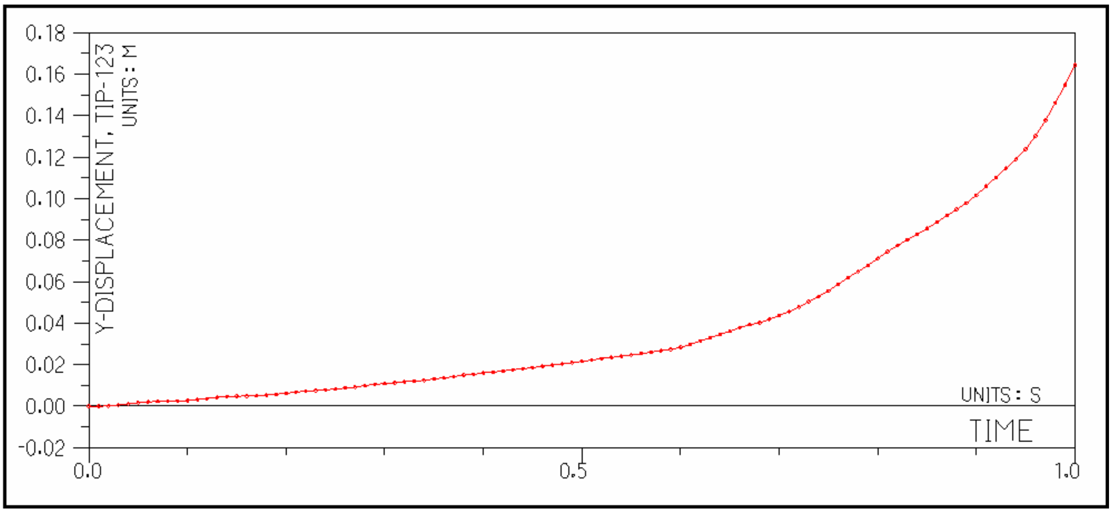


Figure 3.26: Top displacements time history (ADINA output)

Maximum top deflection in the linear response range (i.e. system without plastic excursions) did not exceed 30 mm at time ≈ 0.62.

So, privation in the lateral stiffness of the system happens after plastic hinge formation in all of the links, not after the first plastic hinge formation at the middle link.

Story Drift

Table 3.1: Lateral response

Story no.	Absolute Lateral Displacement (m)	Relative Lateral Displacement (m)	Story Drift Δ/h
5	0.165	0.032	0.011
4	0.133	0.031	0.010
3	0.102	0.032	0.011
2	0.070	0.034	0.011
1	0.036	0.036	0.012

Table 3.1 shows the lateral response of the system, consisting of lateral displacement and story drift ratio.

3.3.1.5 Ductility Evaluations

3.3.1.5.1 Local Ductility

The link zone is supposed to dissipate seismic energy demand during excitation through plastic hinge formation. In the hybrid brace-coupled shear walls model, the stiffened web in the link zone shows the required ductility via shear strains; since the shear behavior is dominant in the short link regions.

According to Von Mises yield criterion:

$$\sigma^2 + 3\tau^2 \leq \sigma_y^2$$

where

σ is axial stress

τ is shear stress

In the case of the pure shear, referring to Eq. 2.16:

$$\tau_y = \frac{\sigma_y}{\sqrt{3}}$$

For steel grade 345 MPa used in this thesis (i.e. σ_y= 345 MPa), pure shear stresses will be:

$$\tau_y = \frac{345}{\sqrt{3}} \approx 200\ MPa$$

Referring to Figure 3.27, it is evidently known that shear stress, for the face 2 in the direction 3, is

$$\sigma_{23} = \tau$$

While the compatible shear strain is

$$\varepsilon_{23} = \gamma$$

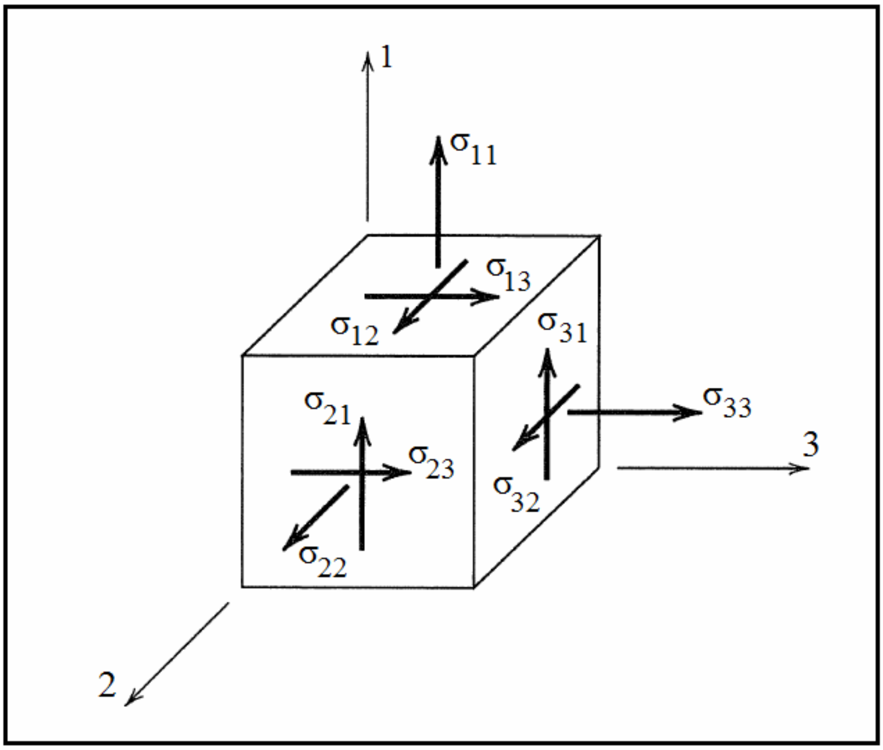


Figure 3.27: Principal stresses and principal directions

Figure 3.28 shows the shear stress strain curve (τ-ε) for shell element no. 21 which is located in the web of the short link of the middle coupling beam.

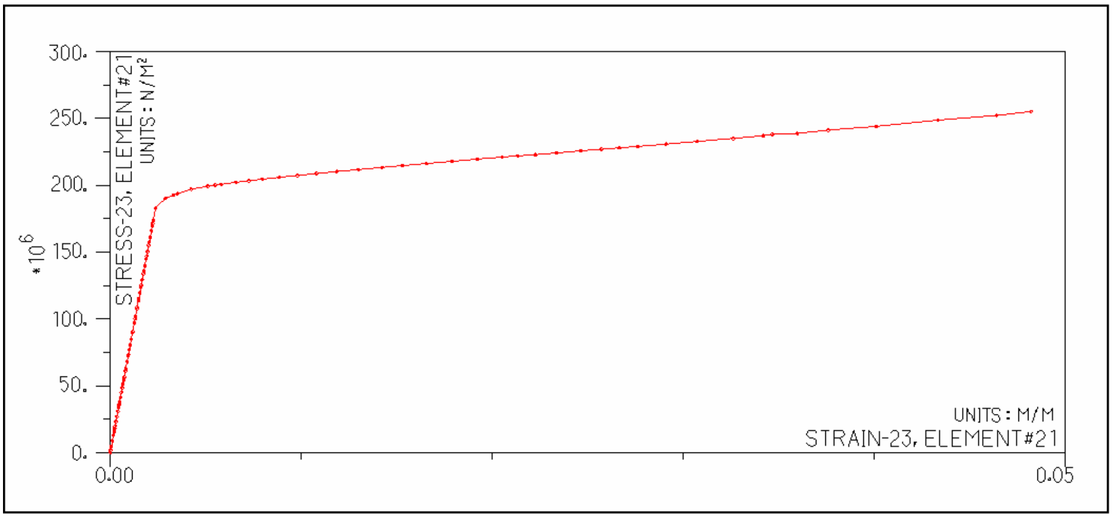


Figure 3.28: Shear stress strain curve for element no. 21 (ADINA output)

Figure 3.28 shows that ductility exhibited by the link zone can be calculated:

$$\mu_{c(21)} = \frac{\varepsilon_{23}}{\varepsilon_{23_y}} \approx \frac{48 \ x \ 10^{-3}}{2.5 \ x \ 10^{-3}} = 19.2$$

Another example for element no. 4 at the link zone of the lowermost coupling beam is shown in Figure 3.29.

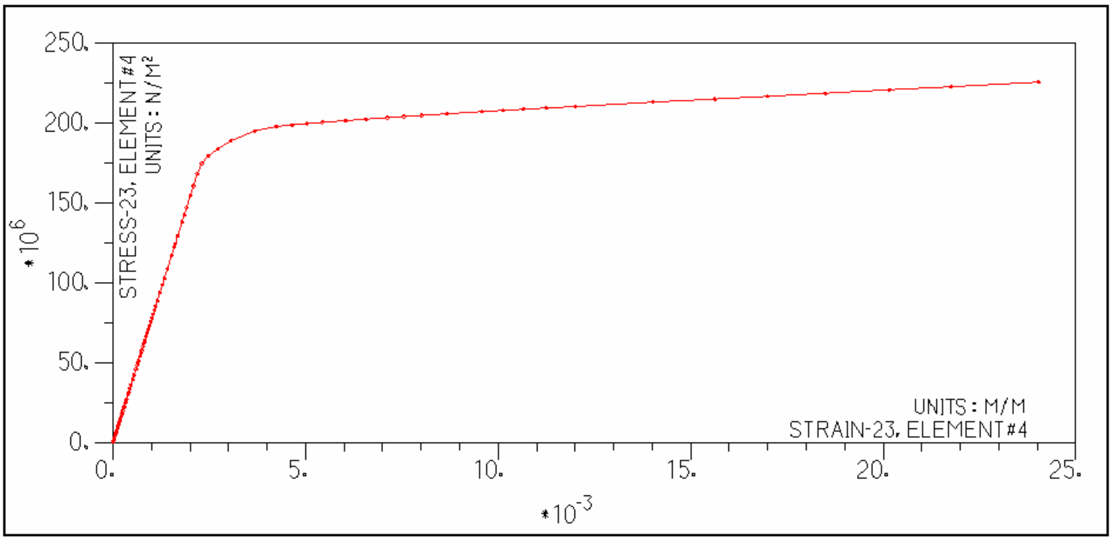


Figure 3.29: Shear stress strain curve for element no. 4 (ADINA output)

The ductility capacity can be calculated as following

$$\mu_{c(4)} = \frac{\varepsilon_{23}}{\varepsilon_{23_y}} \approx \frac{25 \ x \ 10^{-3}}{2.5 \ x \ 10^{-3}} = 10$$

Table 3.2 summarizes values of available ductility (ductility capacity) for each shear link at each story

Table 3.2: ductility capacities of link zone

Story no.	Element no. (Link zone)	ε_y	ε	μ_c
5	36	2.50E-03	41.0E-03	16.5
4	29	2.50E-03	46.0E-03	18.5
3	21	2.50E-03	48.0E-03	19.2
2	12	2.50E-03	48.0E-03	19.2
1	4	2.50E-03	25.0E-03	10

3.3.1.5.2 Global Ductility

Global ductility, which is presented by top displacement of the structure, is calculated:

Displacement in the yield range, $\Delta_y \approx 30$ mm

Maximum displacement attained, $\Delta_u \approx 165$ mm

So,

$$\mu_c = \frac{\Delta_u}{\Delta_y} = \frac{165}{30} \approx 5.5$$

3.3.1.6 Effect of Coupling Beam Size on Response

3.3.1.6.1 General

Coupling beam Size

Coupling beam size (i.e. geometric dimensions of the section) directly affects the degree of wall coupling. However, this coupling must be well controlled (i.e. neither heavily coupled nor lightly coupled).

Another issue to be taken into consideration is the shear behavior in the link; the coupling beam must not experience any flexural behavior in the link zone, any increase in the web size must be proportioned to flange sizes, since overstrengthening the web element without considering the flange parts can transform the link behavior from shear dominant to flexural dominant behavior.

Also, it is important to point out that in the various cases of increasing web and flanges sizes, the diagonal braces must remain in the elastic range, which can be represented by the overstrength factor.

3.3.1.6.2 Controlling Web Size

The hybrid brace-coupled shear walls system is modeled with variable web sizes. The system response is studied step by step, for a new web thickness of 30 mm. A description of the results is summarized next:

(1) First yield

The model with the new web thickness (i.e. 30 mm) shows a linear response until the first plastic formation in the link of the third story coupling beam (i.e. middle coupling beam), followed by another plastic hinge at the link located in the second story coupling beam (i.e. coupling beam beneath). These inelastic excursions during system response are, unfortunately, preceded by a large portion of steel reinforcement yield at the base of the wall due to increasing the coupling ratio.

At this stage it is seen that the flanges of the coupling beam show the tendency to receive plastic excursions as well as the link region, this abrupt behavior can be discussed in the following stage. See Figure 3.30.

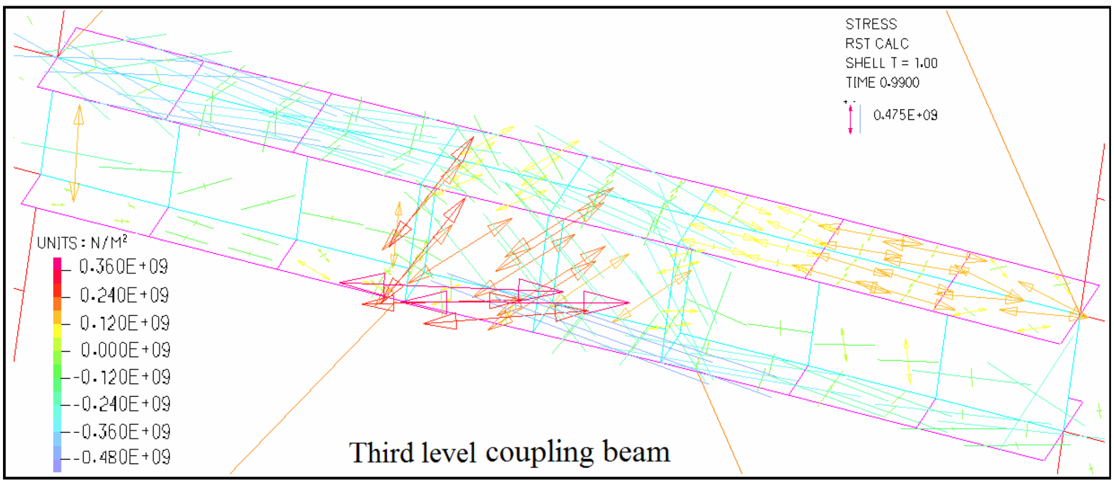


Figure 3.30: Vector Plot: stresses in link region (ADINA output)

(2) Yielding at the ends of the coupling beams

This type of yielding has been classified previously as a reservation capacity in the system. But in this case, the ends of the coupling beams experience plastic excursions before the predetermined locations in the system do (i.e. before the remaining links in the coupling beam), and this phenomenon of premature yielding must be well recognized. See Figure 3.31.

In this particular case, premature yielding at the ends of the coupling beams cannot be classified as a reservation in the capacity of the system since it will obstruct the adequate response of the system.

Then, one of the recommendations can be derived; Yielding of the ends of the coupling beams must be controlled to function after the yielding of the whole links zones (i.e. yielding in the second phase) to ensure the desired behavior of the system.

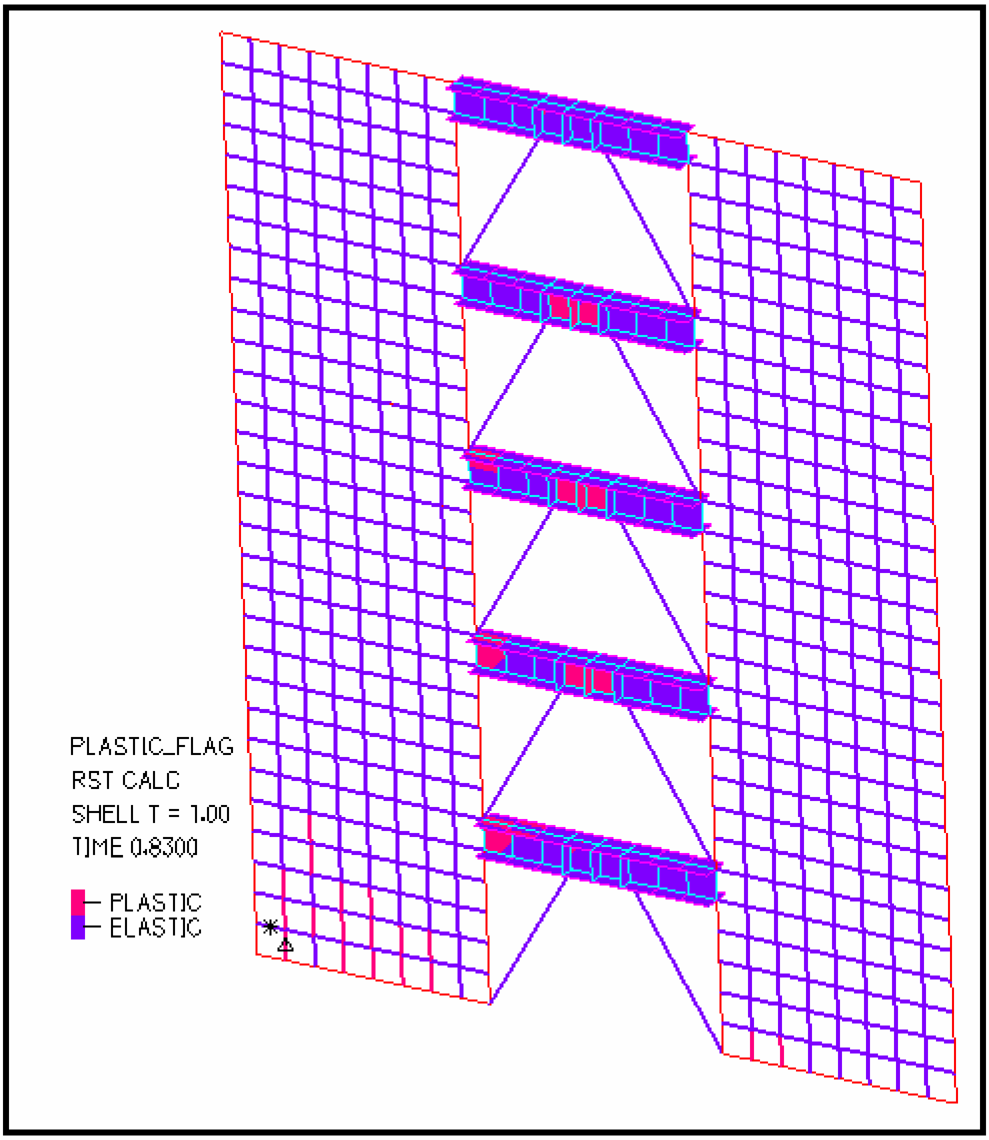


Figure 3.31: Early plastic excursions at the ends of the coupling beams (ADINA output)

(3) Final stage

The overall behavior of the system changes drastically due to this abrupt increment in the web thickness of the wide flange section. It is observed that at the final stage, the yielding in the reinforcement in the base of the wall could not grow uniformly, and the diagonal braces have employed an inelastic response due to the incremented thickness of the web. See Figure 3.32.

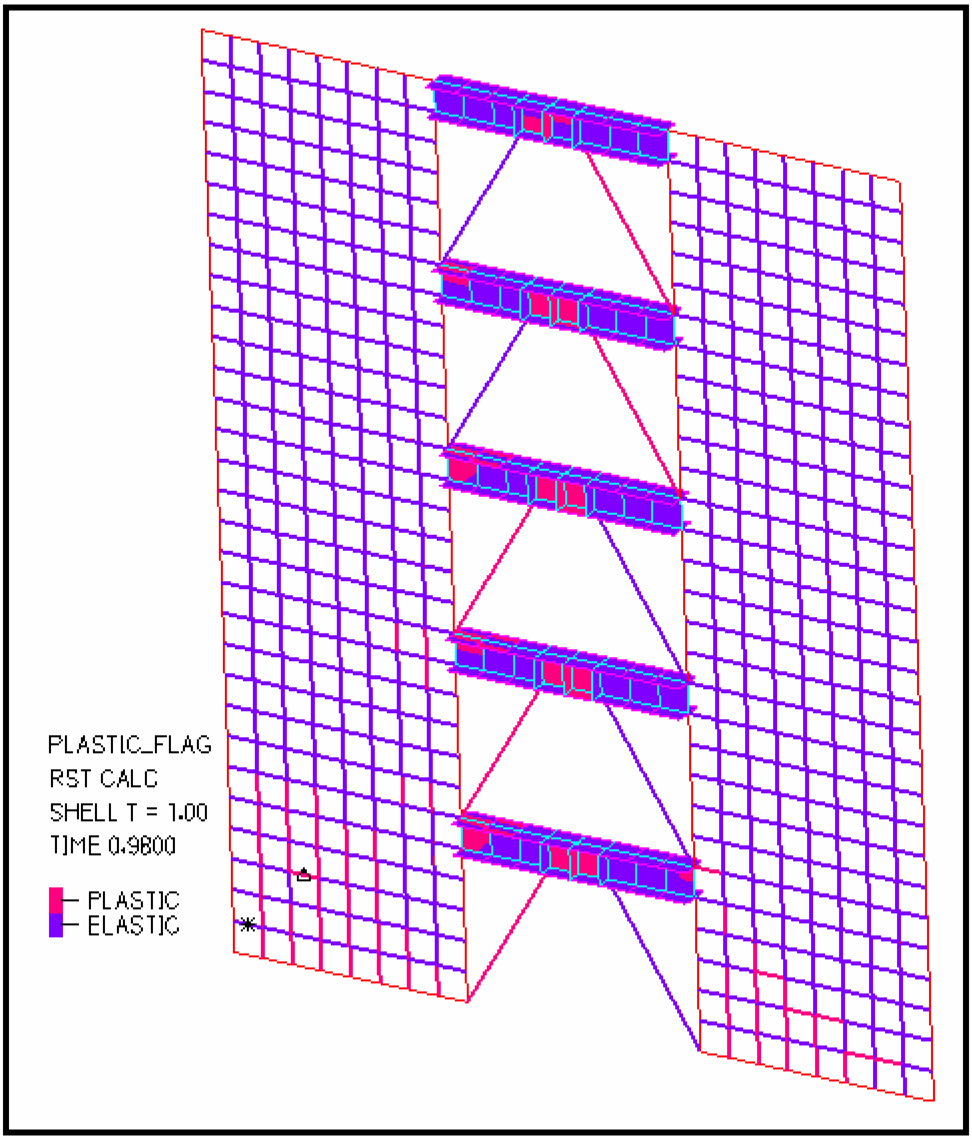


Figure 3.32: Final stage prior to collapse

Increasing the web size increases the strength of the system directly, but this type of arbitrarily increment without considering the flanges sizes and the diagonal braces sizes will elevate the possibility of experiencing plastic excursions in unfavorable places and therefore affecting the ductility of the system in an opposite manner.

This will result in a remarkable conclusion in this research; No arbitrary increment in the web size of the coupling beam is allowed. Any increasing in the size

of the web must be function of flanges and braces sizes to ensure the ductile behavior of the system.

Ductility evaluations of system capacity after such increment in the web size of the coupling beam can perfectly describe the system behavior under ductility demands. Stress strain curves for shear stresses, τ, and shear strains, γ, are shown in Figures 3.33 and Figure 3.34 for links at first and third stories, respectively.

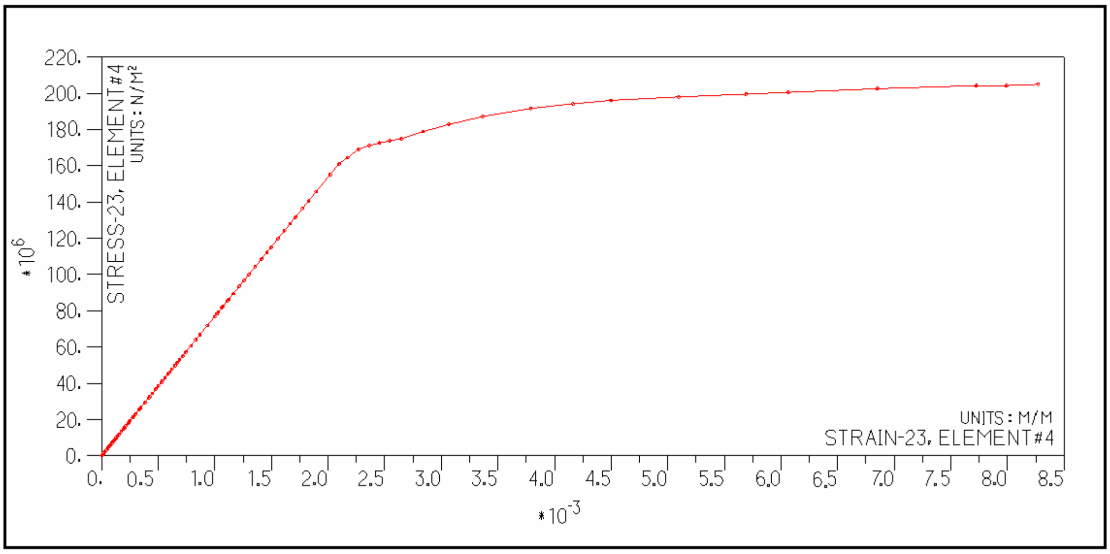


Figure 3.33: Shear stress strain curve for element no. 4 (ADINA output)

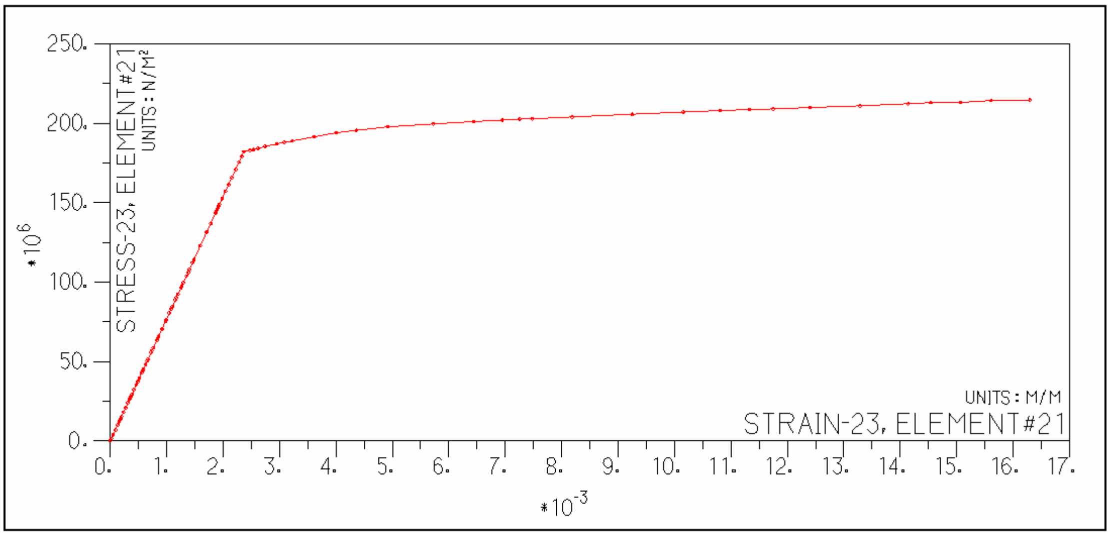


Figure 3.34: Shear stress strain curve for element no. 21 (ADINA output)

From Figure 3.35, the ductility capacity employed by the link zone at the first story can be calculated as follows

$$\mu_{available(4)} = \frac{\varepsilon_{23_u}}{\varepsilon_{23_y}} \approx \frac{8.2\ x\ 10^{-3}}{2.0\ x\ 10^{-3}} = 4.1$$

The ductility capacity exhibited by the link zone at the third story which is represented by element no. 21, can be calculated as following

$$\mu_{available(21)} = \frac{\varepsilon_{23_u}}{\varepsilon_{23_y}} \approx \frac{16.0\ x\ 10^{-3}}{2.0\ x\ 10^{-3}} = 8.0$$

Comparing to the system with the 20 mm web thickness (i.e. lowered web size) of the coupling beam, the local ductility of the system with the 30 mm web thickness (i.e. thicker web size) is subjected to a serious reduction in its ductility capacity.

The reduction in ductility, between the system with the thicker web thickness, μ_{30mm}, and the system with the thinner web thickness, μ_{20mm}, for the first story link (element 4) is

$$Ductility\ Reduction = \frac{\mu_{30mm}}{\mu_{20mm}} = \frac{4.1}{18.5} \approx 0.22\ (22\%)$$

$$\mu_{30mm} = 22\%\ of\ \mu_{20mm}$$

The ductility was reduced to 22% of the employed ductility by the thinner web system. While the ductility reduction for the third link story is as following

$$Ductility\ Reduction = \frac{\mu_{30mm}}{\mu_{20mm}} = \frac{8.0}{19.2} \approx 0.42\ (42\%)$$

$$\mu_{30mm} = 42\%\ of\ \mu_{20mm}$$

The global response of the system does not differ than the local response that much; the overall system has become stiffer than before (i.e. before increasing web size of the coupling beam), but the ductility was tragically reduced after web thickness increment.

The yield displacement of the system, Δ_y, was about ≈ 43 mm, while the maximum displacement of the system, Δ_u≈ 119 mm. thus the global ductility of the system

$$\mu_c = \frac{\Delta_u}{\Delta_y} = \frac{119}{43} \approx 2.75$$

The reduction factor in the global ductility, between the system with the thicker web coupling beam and the system with the thinner web thickness, is

$$Ductility\ Reduction = \frac{\mu_{30mm}}{\mu_{20mm}} = \frac{2.75}{5.5} \approx 0.50\ (50\%)$$

$$\mu_{30mm} = 50\%\ of\ \mu_{20mm}$$

Table 3.3 and Table 3.4 summarize the effect of the web size of the coupling beam on local and global ductilities, respectively. It is evidently noticed that despite the fact that increasing the web size, independently than other parameters, provides a stiffer system it harms the overall ductility capacity

Table 3.3: Local ductility*

Local Ductility in short links, μ_c					
Web Size (mm)	Floor Number				
	1st	2nd	3rd	4th	5th
20	10	19	19	19	17
25	3	7	8	7	5
30	4	7	8	6	3
35	-	2	2	2	-

* Values in tables are rounded.

It can be seen from Table 3.3 that the lesser the web thickness the better the ductility achieved. This proves that no incrimination in the web size can be provided independently than other parameters, such as flanges and diagonal bracing sizes.

Table 3.4: Global ductility*

Web Thick. (mm)	Top displacement (mm)		Global Ductility
	Δy	Δu	μc
20	30	165	5.5
25	36	96	2.67
30	43	119	2.75

* Values in tables are rounded.

Table 3.4 shows that a huge reduction on the global ductility occurs due to increasing the web size.

However, when the web of the coupling beam was increased to more than 35 mm thickness (40 mm thickness for example) the response of the system was very different, since the short links did not employ their plastic properties properly. Contrary to this, flanges and diagonal braces have experienced undesirable large amount of plastic excursions. The selected geometrical size of the web has forced the system to perform in an unfavorable response under seismic excitations, due to the reasons mentioned in advance.

On the other hand, if the web thickness of the coupling beam is lowered beneath the values suggested by AISC, or any other modern code, and due to slenderness ratios, the link can never attain neither its full strength capacity nor the required rotation, before local buckling occurrence.

3.3.1.6.3 Controlling Flange Size

Controlling the flange size (and the diagonal bracing size alike) is considered as a part of the overstrength factor implemented in the capacity design topic, refer to Section 2.2.1.3.

However, during this research it is detected that coupling beams are subjected, in their flanges, to inelastic response despite the fact that they are not employed to yield under various types of events since the behavior of the system must be a shear dominant in the shear link zone. This type of plastic excursion is termed, in this research, as the second phase of plasticization in the coupling beam and can be improved by increasing the section size to force coupling beam to yield well, in such phase.

The system was studied with variable flange sizes of the coupling beam. The response of the system with 60 mm thickness (instead of 50 mm) of the flanges of the coupling beam was recognized.

The stage prior to collapse is shown in Figure 3.35. One of the most important notes to be taken, in this model, is the disappearance of the flexural yielding from the inelastic response of the system (i.e. shear yielding and shear-flexural yielding only exist). This is one of the advantages of the increasing of the flanges sizes.

It is vital to mention that increasing the flange size is limited to two main controlling parameters; the first one is the economical parameter, in which the incremented flange size must improve the response of the system in a convenient manner compared to the elevated cost. The other parameter is the coupling ratio, since over coupling the system will introduce higher moments to the base of the wall in unpleasing manner.

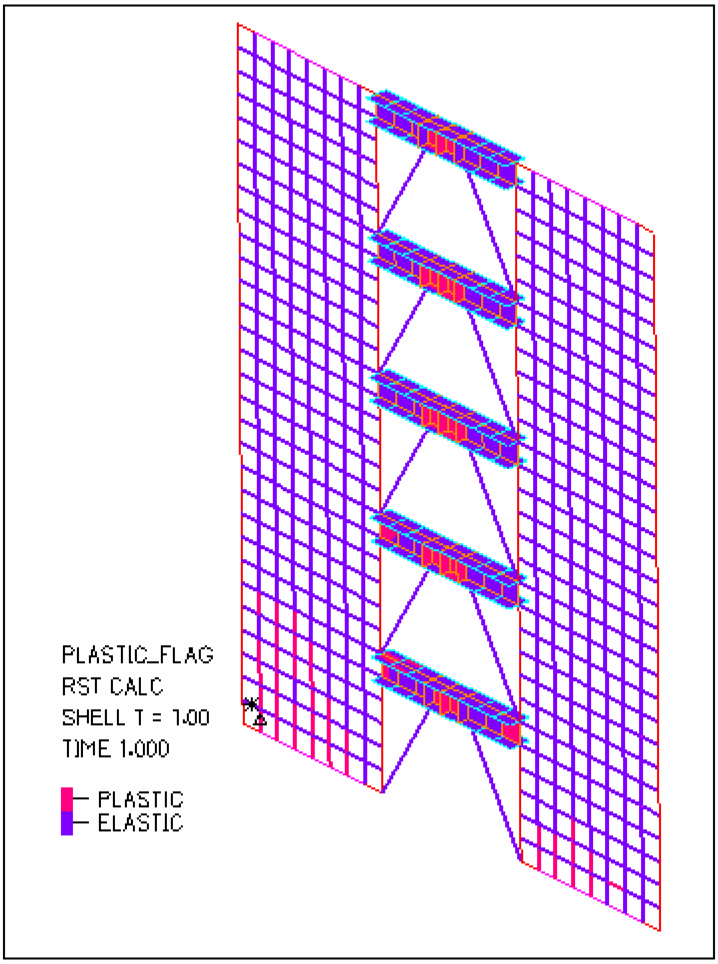


Figure 3.35: Final yielding stage (ADINA output)

3.3.1.6.4 Optimized Selection

It is shown in the preceding sections that the arbitrary selection of structural components sizes will produce an improper behavior of the system, especially during severe seismic events. Arbitrary selection of the web size of the coupling beam leads to unexpected plastic excursions in non-ductile regions, such as the premature yielding in flanges at the end of the coupling beams, or bracing elements plasticization. While the problem of overcoupling the system is expected in the case of heavier flanges selection.

From the previous discussion, the importance of the optimal selection of the various structural elements of the coupling system arises. A correlation must be formed and strictly followed while selecting these structural elements.

Brittle response of the system, which leads to improper results, can be described as one of the following types: flexural yielding in the flanges of the coupling beams, plastic excursions in diagonal braces and other brittle types of failure in wall, such as horizontal and vertical shear. Overcoupling of the system cannot be classified as a brittle response, but it is an unwise criterion to be followed, since the idea of coupling shear walls is to dissipate the energy over the entire height of the wall, while the overcoupling criterion goes against this structural concept.

3.3.2 Various Systems Comparison

The behavior of the new proposed system in this research was discussed, in details, in the previous section, and termed as the hybrid brace-coupled shear walls model in this study. This hybrid brace-coupled shear walls model, which is composed of two cantilever shear walls coupled with eccentric steel bracing system, is a combination of more than one system to form a hybrid system behavior. However, this section will compare between the behavior of the new proposed seismic resistant system and the traditional seismic resistant systems. Thus, the studied systems in this research are: (1) Cantilever shear wall, (2) Hybrid beam-coupled shear walls system, and (3) Hybrid brace-coupled shear walls system which is discussed previously.

3.3.2.1 Model 1: Cantilever Model

Despite the fact that this study is concentrating on the response of the coupling beams and shear links created between the diagonal braces, the cantilever shear wall is the main item in all of the proposed systems.

A bare cantilever uncoupled shear wall is selected for studying and for comparison. The dimensions of the wall are typically derived from one of the coupled two walls previously studied.

The cantilever model in this research failed before the monotonic loading increment reaches quarter the value reached in the hybrid brace-coupled shear walls model.

Figure 3.36 shows that top displacement during excitation has reached up to 275 mm.

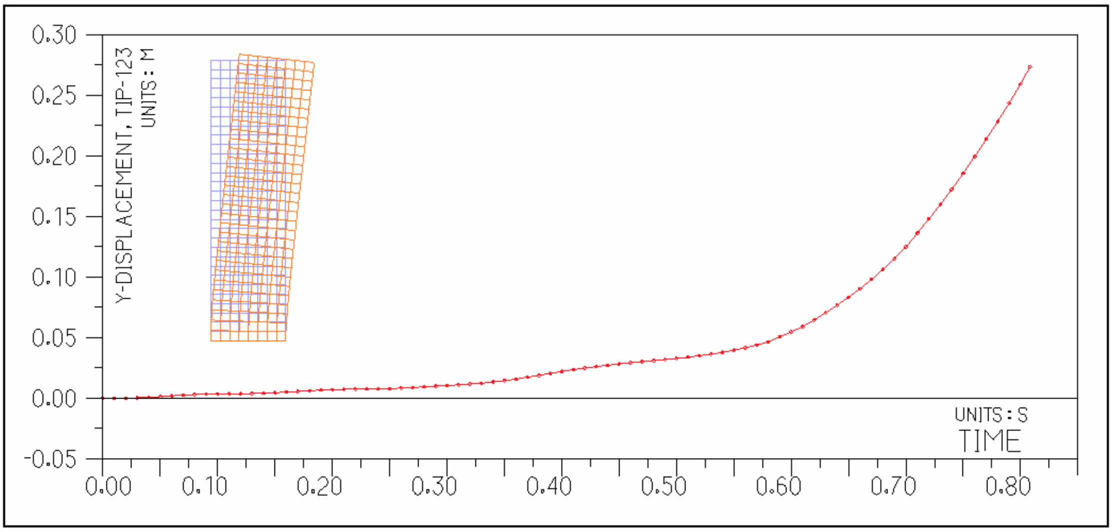


Figure 3.36: Increasing top displacement of the wall (ADINA output)

3.3.2.2 Model 2: Hybrid Beam-Coupling Model

The hybrid beam-coupling model is identical to the hybrid brace-coupled shear walls model but without diagonal braces, as shown in Figure 3.37.

This hybrid beam-coupled shear walls model is subjected to the same incremental, step by step, static loading that have been introduced to the previous models.

It must be mentioned that the model collapsed before reaching 60% of the maximum load value resisted by the hybrid brace-coupling model; this particular fact is a very important observation to be taken into account in this research to bring forward the advantages of introducing the proposed hybrid brace-coupled shear walls system.

First Yield

The earlier inelastic response in this model appears, unfortunately, at the base of the wall. This type of early yield in this particular region directly conflicts with the principal principle of coupling shear walls systems which is to dissipate potential energy along the entire height of the system and not to concentrate these plastic accumulation into the base region as in the case of cantilever wall, see Figure 3.38.

In response to seismic excitation, steel coupling beams are expected to dissipate energy in a manner that is similar to the response of shear links in eccentrically braced frames (ASCE, 2005). Shear links, and coupling beams in turn, fall into three categories: short, intermediate and long, depending on their structural and geometric properties (AISC seismic provisions, 2005). When architectural constraints permit, short coupling beams which dissipate energy primarily through inelastic shear distortion are preferred to longer coupling beams that dissipate energy through flexural hinge rotation. Mechanisms that involve inelastic shear deformation in steel coupling beams

are generally more ductile than those involving flexure-related plastic hinge deformations (ASCE, 2005).

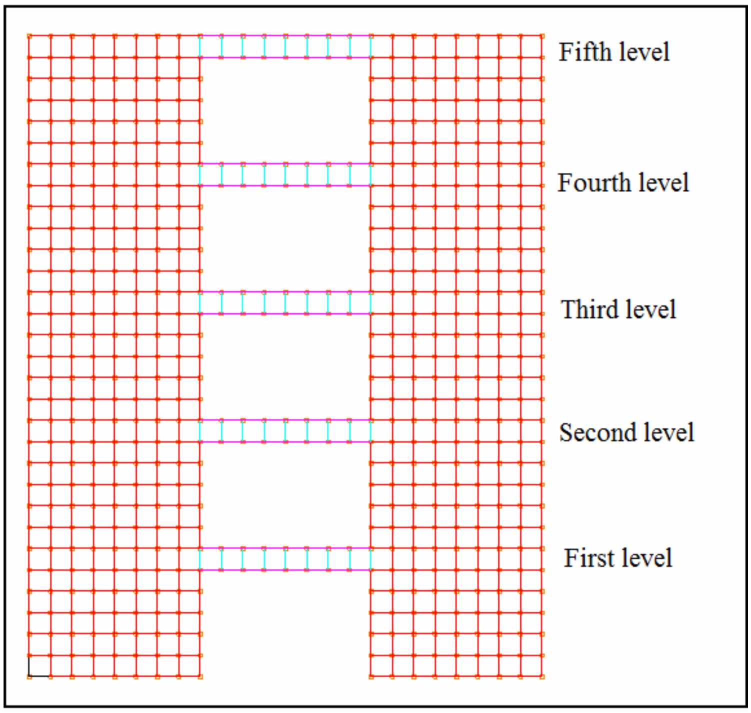


Figure 3.37: Beam-coupling model

Unfavorable behavior appeared in the coupling beam, due to the fact that the coupling is weak as a result for the large gap existed between the coupled walls. Accordingly, the yielding behavior in the coupling beams is flexural, not shear dominant, and as discussed previously, this type of yielding in this system is weak, brittle and unable to transform shear forces between the two shear walls.

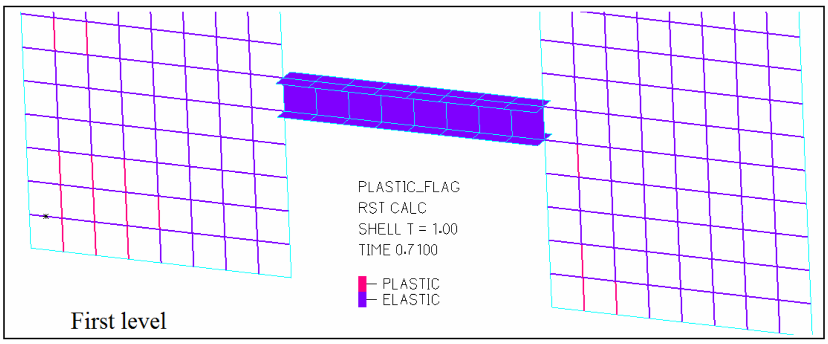


Figure 3.38: First yield in model (ADINA output)

Coupling beam Yielding

Coupling beam yielded after yielding of the reinforcement at the base of the wall, this type of yielding is a flexural type which cannot dissipate energy through potential plastic hinge. The top flange yielded in the leeward direction of the excitation, and the bottom flange in the outward direction.

This coupling beam yielding restricts, somehow, the yielding in the base of the wall, but with a limited scale, since the plastic hinge continued to grow along the base of the wall, but slower than before, see Figure 3.39.

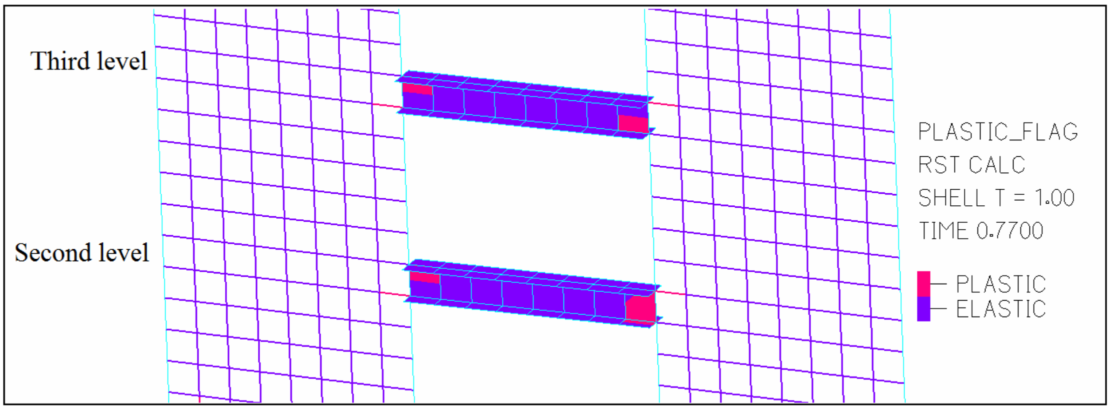


Figure 3.39: Flexural yielding in coupling beams (ADINA output)

Failure stage

At failure stage, the plastic strains continue to accumulate at the ends of the coupling beams as shown in Figure 3.40. Although the yielding type is flexural, the stresses were growing in the web part of the wide flange since they failed to propagate in flange part.

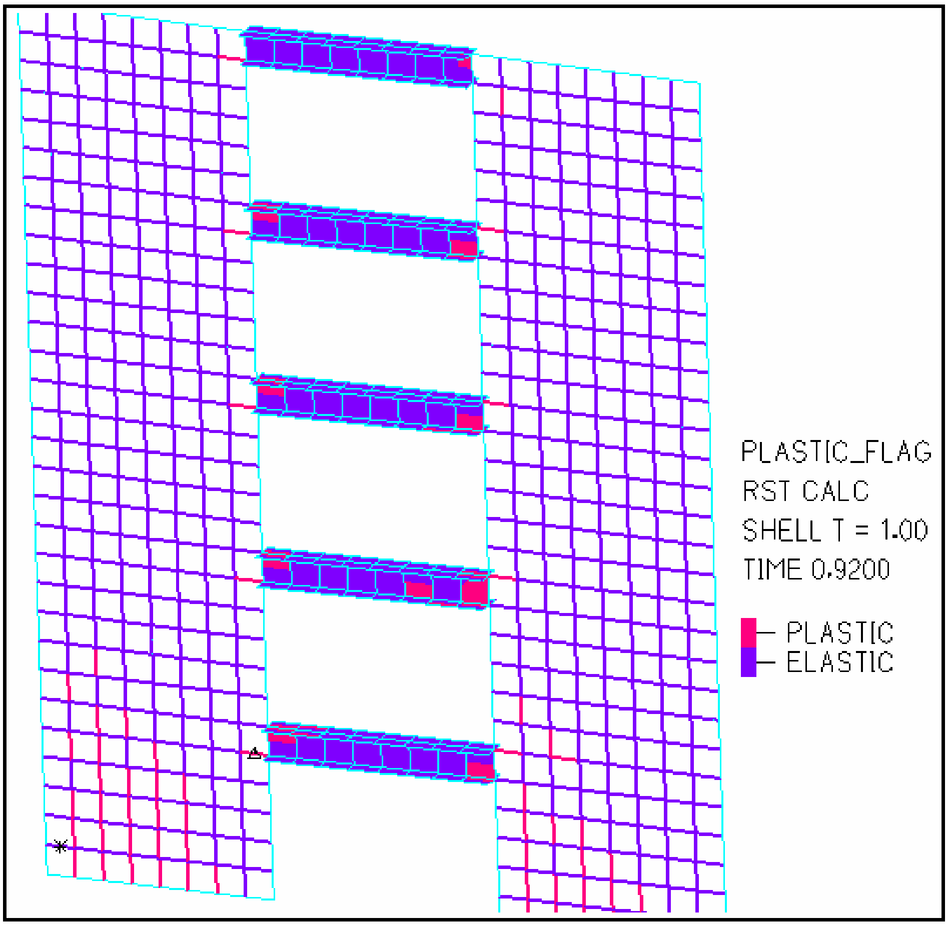


Figure 3.40: Plasticity in model prior to failure stage (ADINA output)

Stress strain curves for web element no. 24 at the end of the coupling beam of the second story are shown in Figure 3.41.

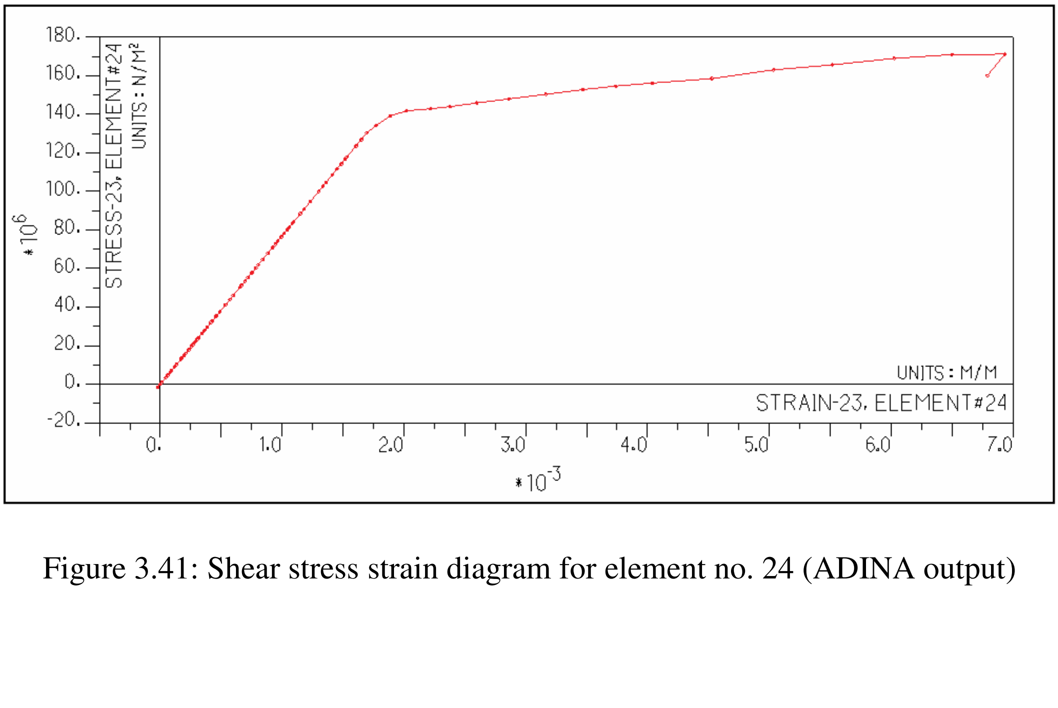


Figure 3.41: Shear stress strain diagram for element no. 24 (ADINA output)

Therefore, ductility can be calculated from Figure 3.42

$\varepsilon_y = 1.70x10^{-3}$

$\varepsilon = 6.80x10^{-3}$

$$\mu_{c\,(2nd)} = \frac{6.8x10^{-3}}{1.7x10^{-3}} \approx 4.0$$

Anyhow, it must be mentioned that shear stress has not reached yield in this element due to the domination of flexural yielding type, referring to Figure 3.42, $\tau_{max} \approx$ 160 MPa.

Other elements, such as element no. 9 at the web of end of the first story coupling beam, have dissipated energy through a potential plastic hinge. Refer to Figure 3.42.

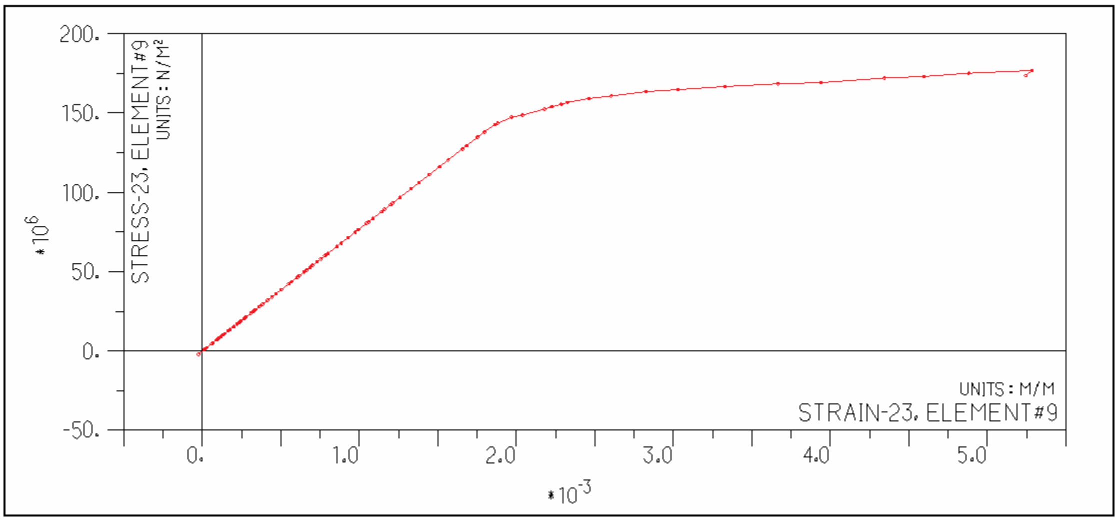


Figure 3.42: Shear stress strain curve for element no. 9 (ADINA output)

Ductility can be calculated through strains

$\varepsilon_y = 5.40x10^{-3}$

$\varepsilon = 1.80x10^{-3}$

$$\mu_{c\,(1st)} = \frac{5.4x10^{-3}}{1.8x10^{-3}} \approx 3.0$$

The ductility value derived from normal strains, ε_{22}, can be calculated also due to the reason of existence of flexural yielding type, refer to Figure 3.43

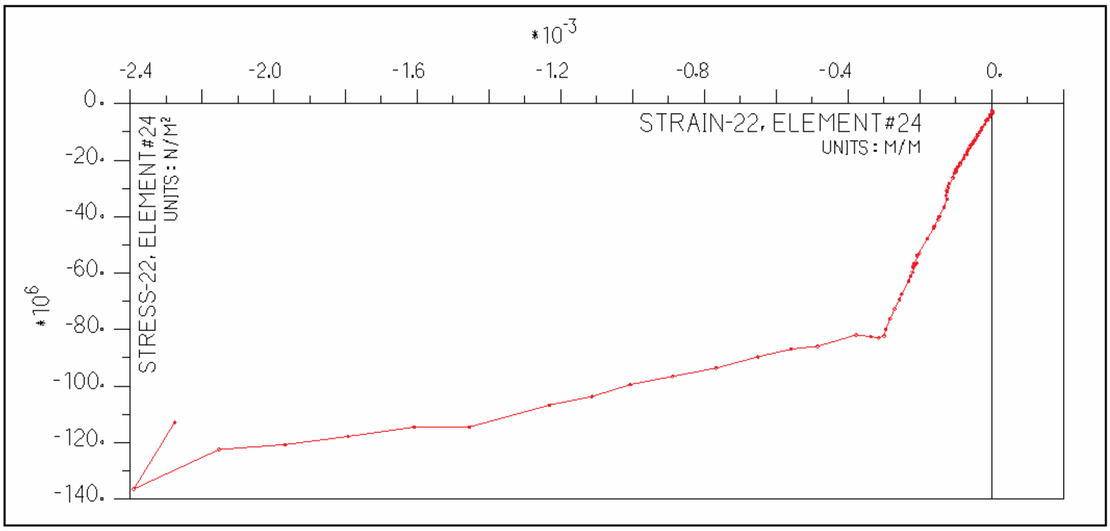


Figure 3.43: Normal stress strain curve for element no. 24 (ADINA output)

Ductility calculated through Figure 3.43

$\varepsilon_y \approx -0.3\text{x}10^{-3}$

$\varepsilon \approx -2.4\text{x}10^{-3}$

$$\mu_{c\,(1st)} = \frac{-2.40x10^{-3}}{-0.3x10^{-3}} \approx 8.0$$

The value of this type of ductility which is calculated using normal strains is higher than value obtained from shear strains; nevertheless the calculations are submitted through a web element. Anyhow, this type of ductility urges this study to calculate ductility in the flange element above the web where axial stresses, due to flexure, must expand in. Refer to Figure 3.44 for normal stress strain curve in flange element no. 72 at the first story coupling beam. It can be seen from the curve, shown in Figure 3.44, that the overstrength factor is minimized comparing to overstrength value obtained from the normal stress strain curve for web element, shown in Figure 3.43.

However, the maximum normal stresses are higher in the flange element, since it is near to extreme stress fiber.

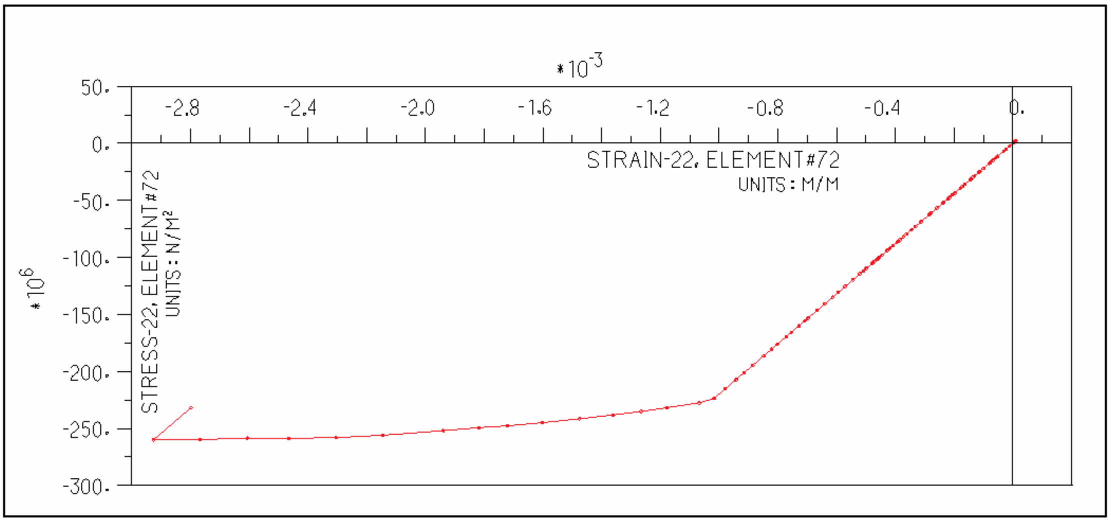


Figure 3.44: Shear stress strain curve in flange element no. 72 (ADINA output)

Ductility calculated through Figure 3.44

$\varepsilon_y \approx -1.00 \text{ x}10^{-3}$

$\varepsilon \approx -2.90\text{x}10^{-4}$

$$\mu_{c\,(1st)} = \frac{-2.90x10^{-3}}{-1.00x10^{-3}} \approx 2.9$$

The previously studied elements are shown in Figure 3.45 for more clarification; web elements are orange colored, while flange elements are turquoise.

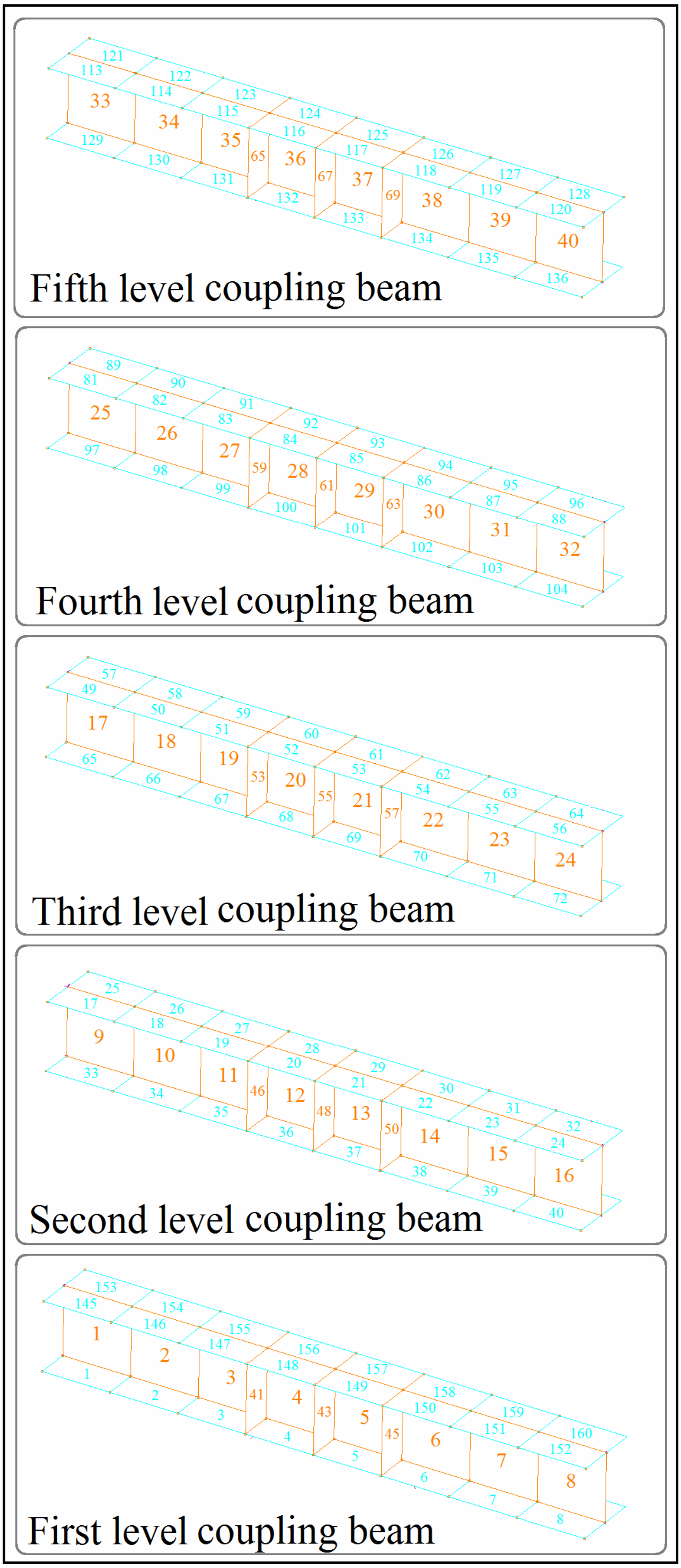


Figure 3.45: Flange and web elements

3.3.2.3 Response Comparison

3.3.2.3.1 Elastic Stiffness

Stiffness, for each of the three models, is calculated using the simplest form

$$P = k\,\Delta$$

(Eq. 3.1)

Thus;

$$k = \frac{P}{\Delta}$$

(Eq. 3.2)

where

P is the force prescribed to the system

k is the stiffness of the system

Δ is the elastic displacement

A value of P= 1,000 N is prescribed laterally at the top of each model, and the displacement values are calculated accordingly, and then the stiffness is calculated for each model according to Eq. 3.2.

Cantilever model provides the following stiffness value, refer to Figure 3.46

$$k = \frac{1{,}000\ N}{7.154x10^{-5}\ m} = 139.777\ x\ 10^{6}\ N/m$$

For comparison matters, and since two walls exist in the system, even if they are not coupled during analysis of the cantilever shear wall model, the stiffness value of the model is doubled

$$k_{cantilevers} = 2\,(139.777\ x\ 10^{6}) = 279.555\ 10^{6}\ N/m$$

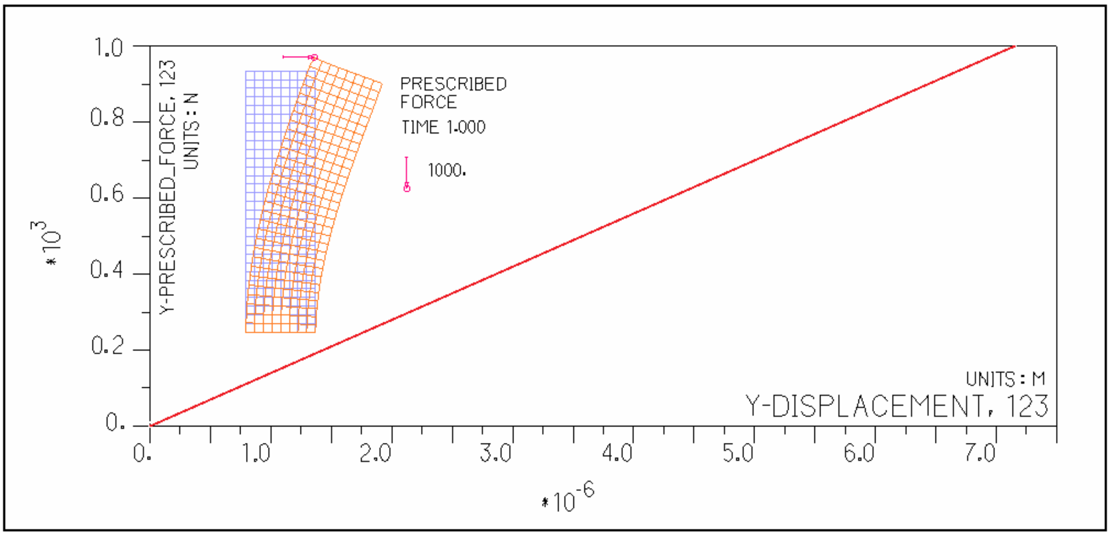


Figure 3.46: Stiffness calculations – cantilever shear wall model

On the other hand, the hybrid beam-coupling model provides the following stiffness value, refer to Figure 3.47

$$k_{beam-coupling} = \frac{1{,}000\ N}{2.950x10^{-6}\ m} = 339.010\ x\ 10^{6}\ N/m$$

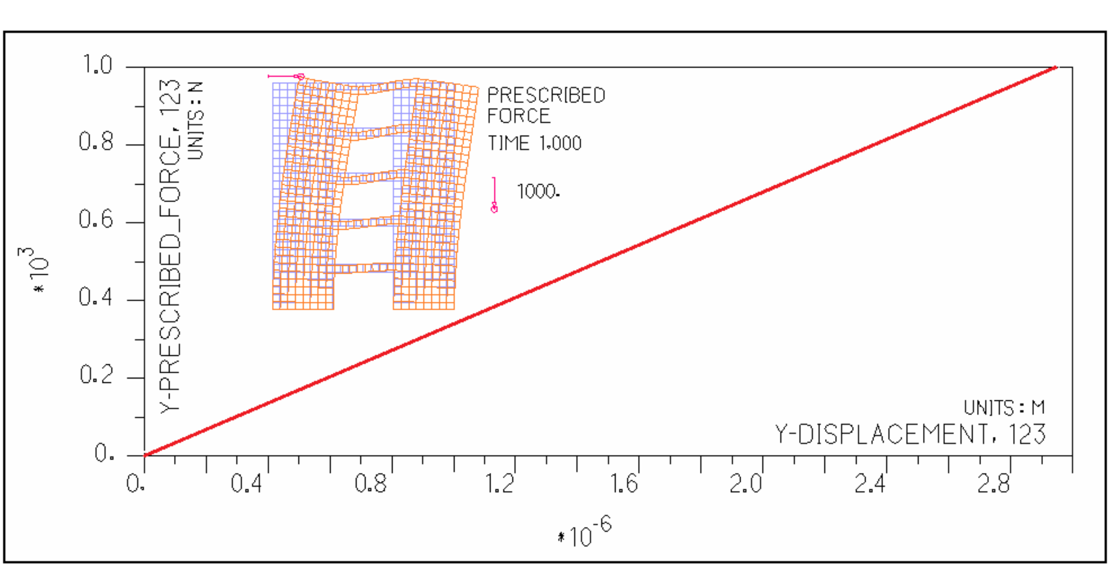


Figure 3.47: Stiffness calculations – hybrid beam-coupling model

As discussed previously, coupled shear walls are significantly stiffer than the sum of their component wall piers.

The hybrid brace-coupling model provides the following stiffness value, refer to Figure 3.48

$$k_{brace-coupling} = \frac{1{,}000\ N}{1.795x10^{-6}\ m} = 557.130\ x\ 10^{6}\ N/m$$

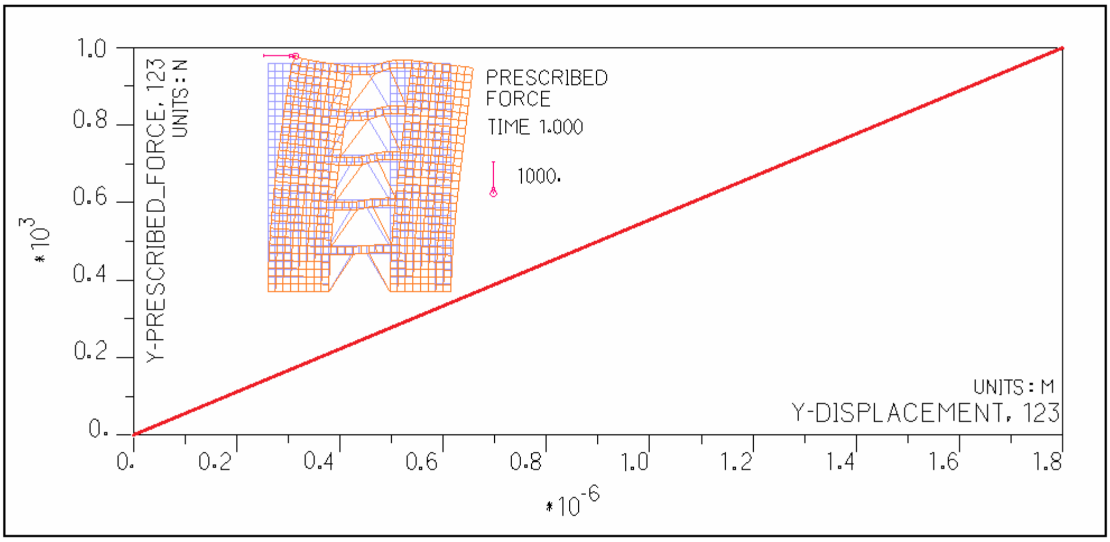


Figure 3.48: Stiffness calculations – hybrid brace-coupling model

Table 3.5 provides the values of stiffness for each system, and the increment percentage in stiffness values to compare between the three models.

Table 3.5: Stiffness values

Model Type	**k** (N/m)	Percentage Increment	
2 Cantilevers	279.0 E+06	-	
Beam-Coupling	339.0 E+06	**122 %**	x **k** (2 cantilevers)
Brace-Coupling	557.0 E+06	**200 %**	x **k** (2 cantilevers)
		164 %	x **k** beam-coupling

As shown in the table, the stiffness value of the hybrid beam-coupling model is increased by 22% over the uncoupled cantilever shear walls model stiffness, while the

hybrid brace-coupled shear walls system introduced an increment over the hybrid beam-coupling model by 64% and by 100% over the cantilever uncoupled system.

As a result, coupling shear walls using the proposed hybrid brace-coupling system has increased the overall stiffness of the system in a wise manner up to about double the uncoupled shear walls system.

3.3.2.3.2 Maximum Top Displacement

The value of the maximum top displacement was measured for each of the three models at a stage prior to failure, and the results are as shown in Table 3.6

Table 3.6: Displacement control

Model Type	Δ_u (mm)	Reduction Percentage	
Cantilever	273	-	
Beam-coupling	213	**22%**	**x** $\mathbf{\Delta_y}$ cantilever
Brace-coupling	165	**40%**	**x** $\mathbf{\Delta_y}$ cantilever
		23%	**x** $\mathbf{\Delta_y}$ beam-coupling

The hybrid beam-coupling model eliminates up 22% of the lateral displacement employed by the uncoupled cantilever model. On the other hand, the hybrid brace-coupling model has reduced up to 40% of the lateral displacement provided by the cantilever model.

Beside the 40% displacement control, the hybrid brace-coupling system proved the ability to sustain various large incremental steps without inelastic excursion in the concrete elements. Concrete model free of cracks and crushing with an easy replaceable fuse after earthquake events are introduced by the hybrid brace-coupled shear walls system proposed in this study.

3.3.2.3.3 Ductility Capacity

The maximum available local and global ductilities (i.e. ductility capacity) for the hybrid beam-coupling model and the hybrid brace-coupling model are tabulated in Table 3.7 as following

Table 3.7: Ductilities of various models

Model Type	Maximum Local Ductility, μ_l	Global Ductility, μ_g
Beam-coupling	8	3.3
Brace-coupling	19	5.5

It should be mentioned that the value of maximum local ductility is measured in the web element no. 24 for the hybrid beam-coupling model. While for the hybrid brace-coupling model, the maximum local ductility value is introduced by web element no. 21, for more information refer previous section discussion.

For more clarification about web and flange elements refer to Figure 3.45.

The hybrid brace-coupling model provides about 238% of the maximum local ductility provided by the system of hybrid beam-coupling model. On the other hand, the hybrid brace-coupling model has enhanced the global ductility of the system to about 167% compared to the hybrid beam-coupling system.

Through ductility calculations the new proposed system of hybrid brace-coupled shear walls proved efficient compared to other traditional systems.

3.3.3 Cyclic Loading

3.3.3.1 General

Cyclic loading tests are generally required to describe the true behavior of the systems under seismic events.

The main advantage of such type of loading is the ability to plot the hysteresis loops in stress-strain curves and force-deflection curves for example.

The area enclosed by these loops (which are formed by loading, unloading and reloading in the reversed direction) is the dissipated energy.

The hybrid brace-coupled shear walls model is subjected to an incremental cyclic static loading up to failure, where the magnitude of the load is functioning in a sinusoidal manner, which its amplitude correlates to yielding in links, and its response is characterized a step by step during excitation.

The top displacement in the system is characterized as shown in Figure 3.49.

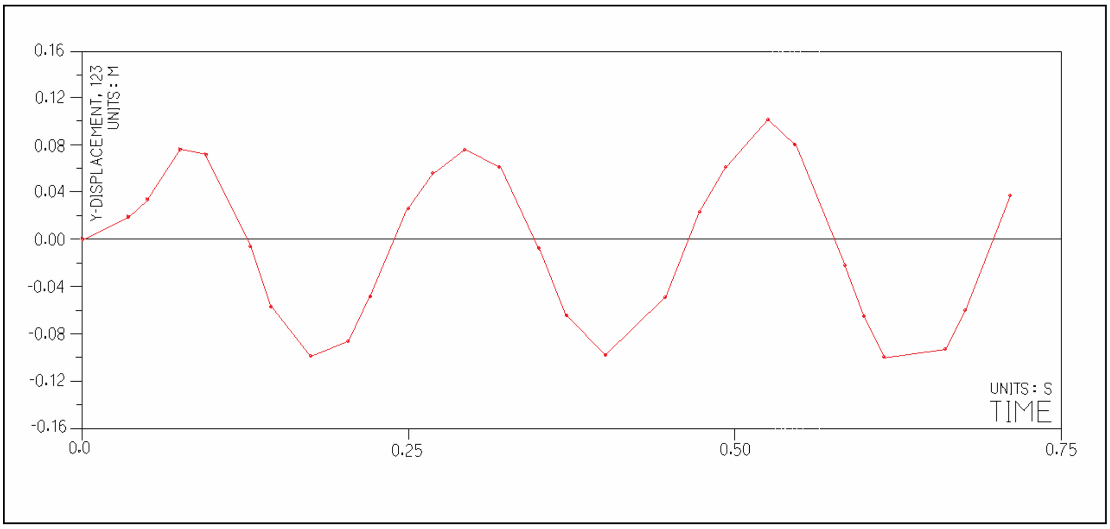


Figure 3.49: Top displacement time history (ADINA output)

It is also noted from Figure 3.49 that the top displacement increases at each subsequent cycle; this phenomenon takes place due to the fact that the system, under cyclic loading, loses its stiffness cycle by cycle. Refer to Section 2.3.1.1.7.

The response of the system under cyclic loading is similar to the response under pushover analysis in the first loading stage and the desired links have yielded under such excitation, after the loading stage is finished and during the process of unloading and reloading in the reversed direction, the plastic excursions disappear from the links for an instant, to be formed again in the other direction (i.e. yielding in compression then yielding in tension). See Figures 3.50 and 3.51.

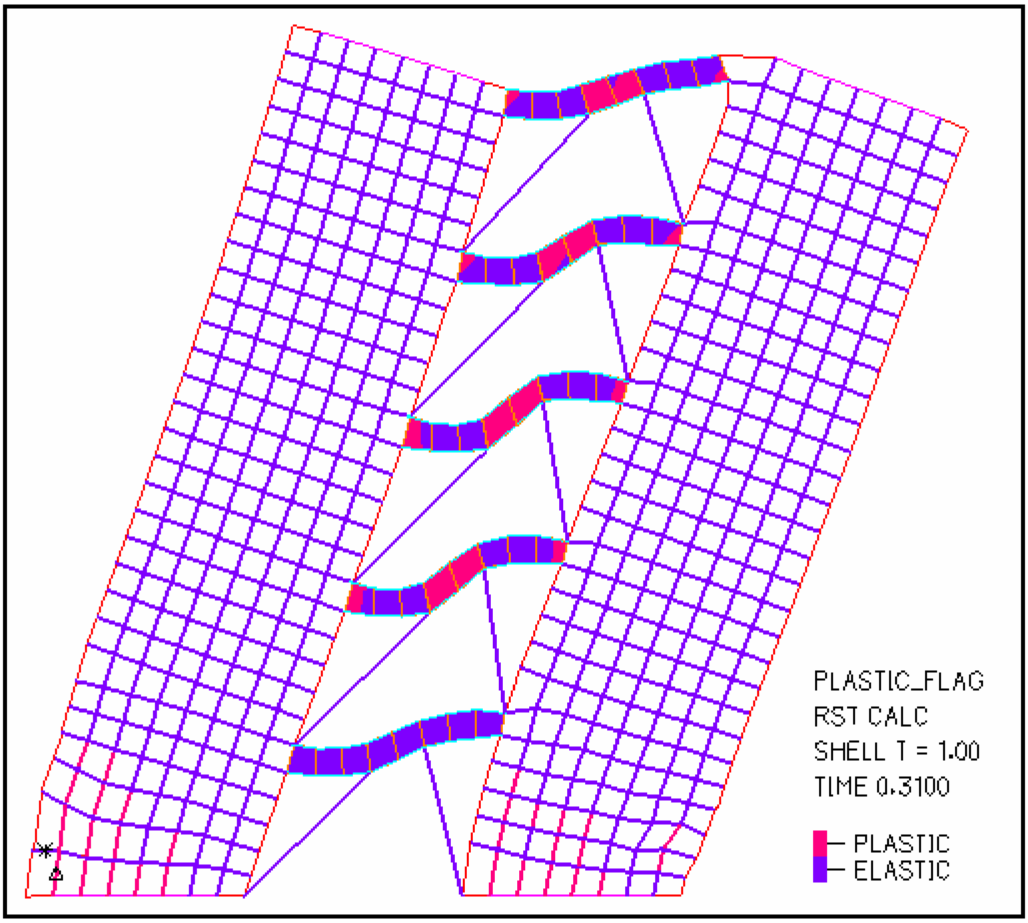


Figure 3.50: Exaggerated response +Y direction loading (ADINA output)

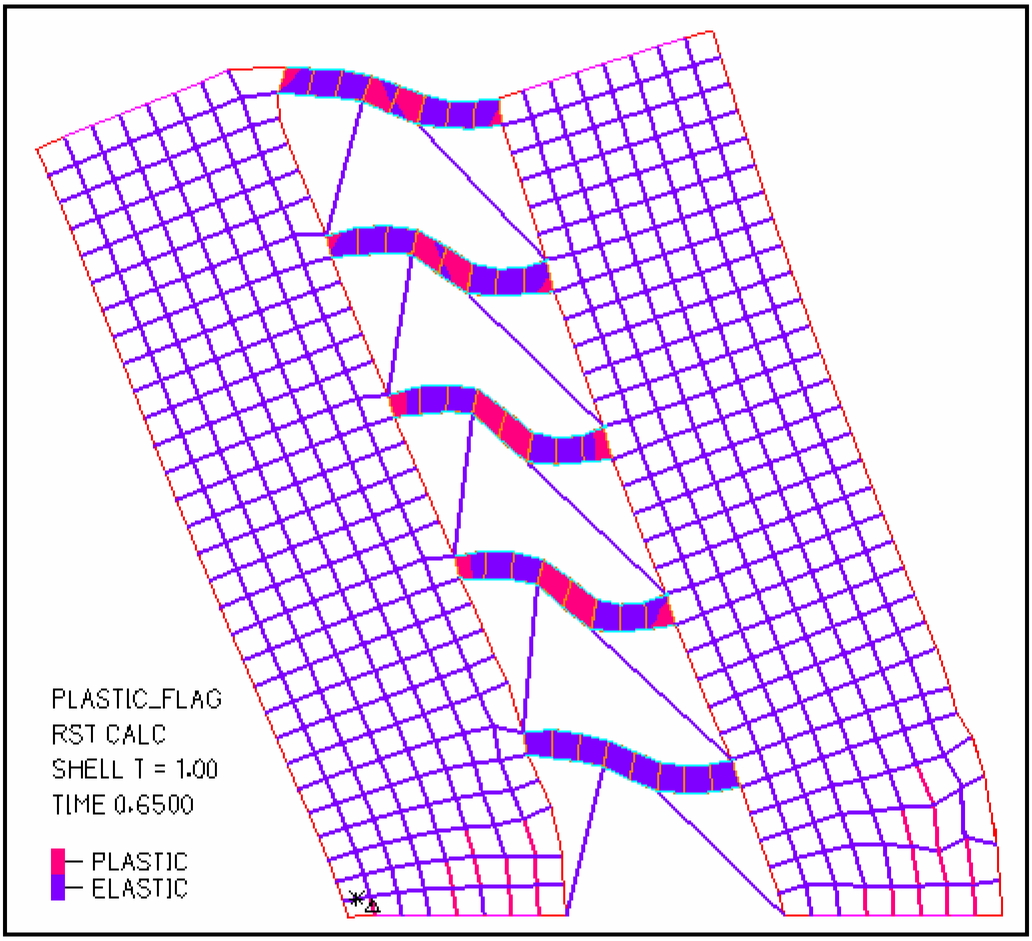


Figure 3.51: Exaggerated response -Y direction loading (ADINA output)

In the link zone of the coupling beam, the direction of stresses is reversed in each load cycle according to the direction of loading as shown in Figure 3.52 and Figure 3.53.

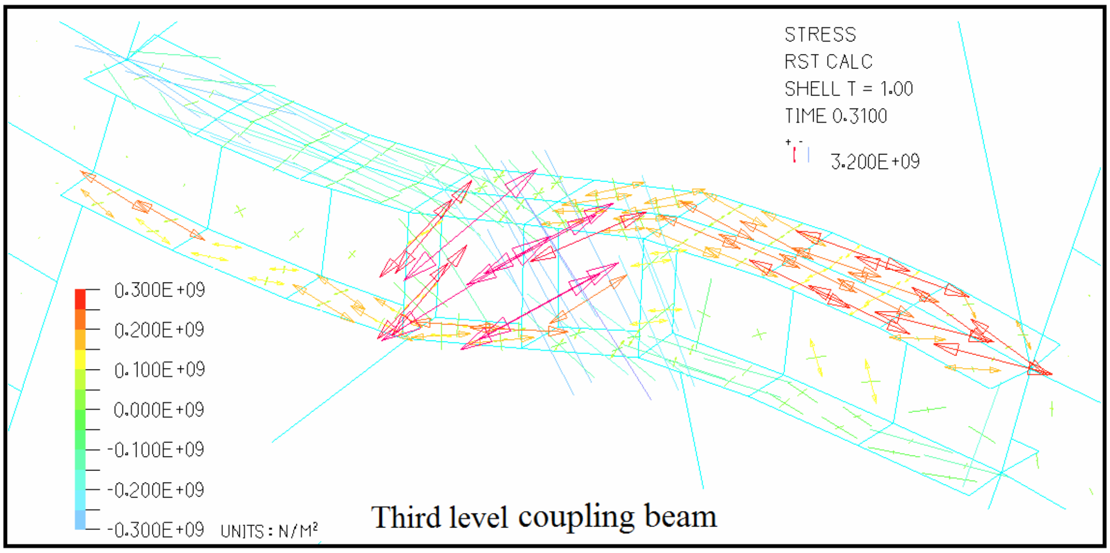


Figure 3.52: Vector plot: stresses in link zone +Y direction loading (ADINA output)

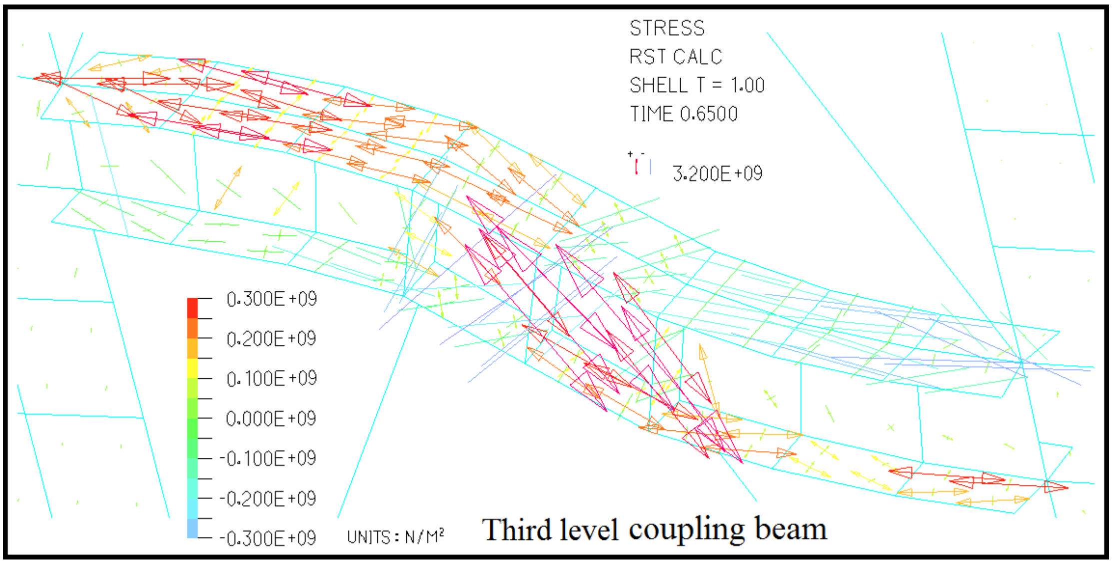


Figure 3.53: Vector plot: stresses in link zone -Y direction loading (ADINA output)

3.3.3.2 Hysteretic Response

The stress and strain curves of the elements that are intended to dissipate energy absorbed by the system (i.e. short links) are shown in Figures 3.54 to 3.57. The desired fat loops of the hysteretic response are obviously obtained.

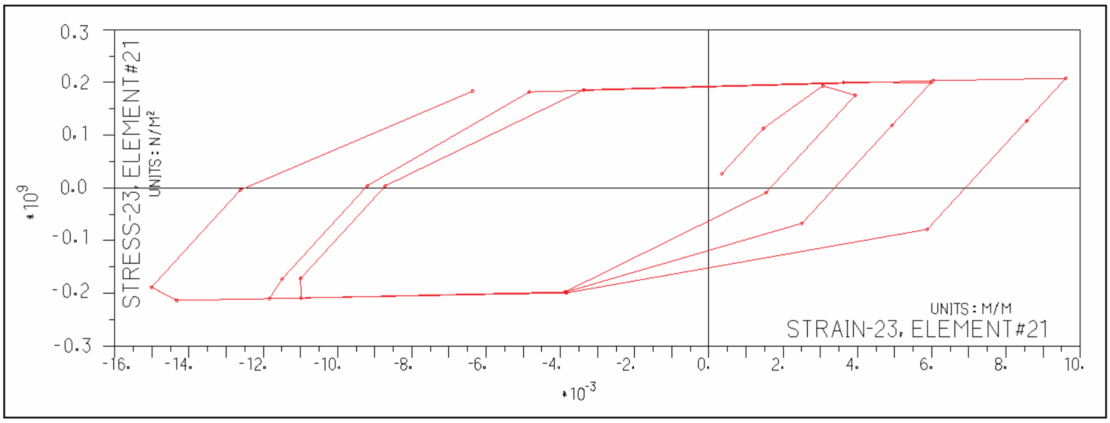


Figure 3.54: Hysteresis loops for third story link (ADINA output)

Ductility can be calculated for the third story

$\varepsilon_y = -3.8x10^{-3}$

$\varepsilon = -15.1x10^{-3}$

$$\mu_{c\,(3rd)} = \frac{-15.1x10^{-3}}{-3.8x10^{-3}} \approx 4.0$$

Other links have provided the desired ductility capacity as following:

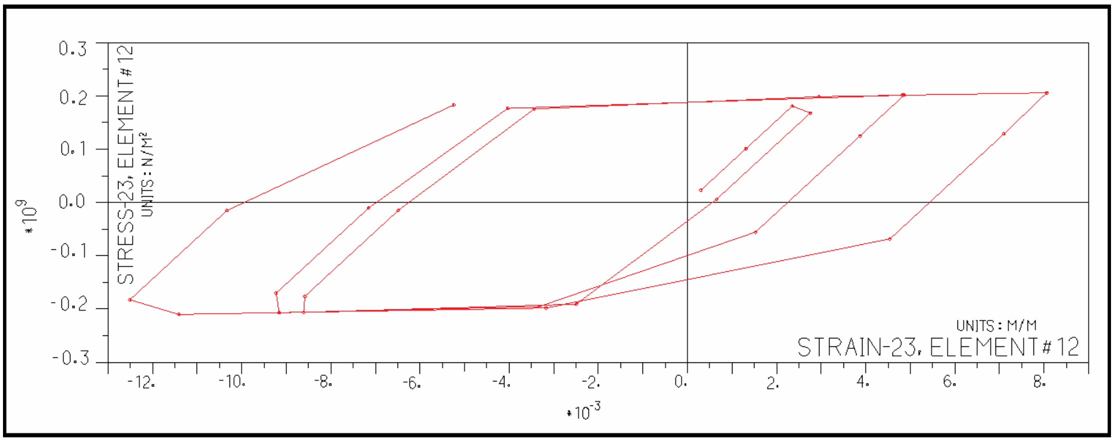


Figure 3.55: Hysteresis loops for second story link (ADINA output)

Ductility calculations for the second story

$\varepsilon_y = -2.5x10^{-3}$

ε = -12.5x10^{-3}

$$\mu_{c\,(2nd)} = \frac{-12.5x10^{-3}}{-2.5x10^{-3}} \approx 5.0$$

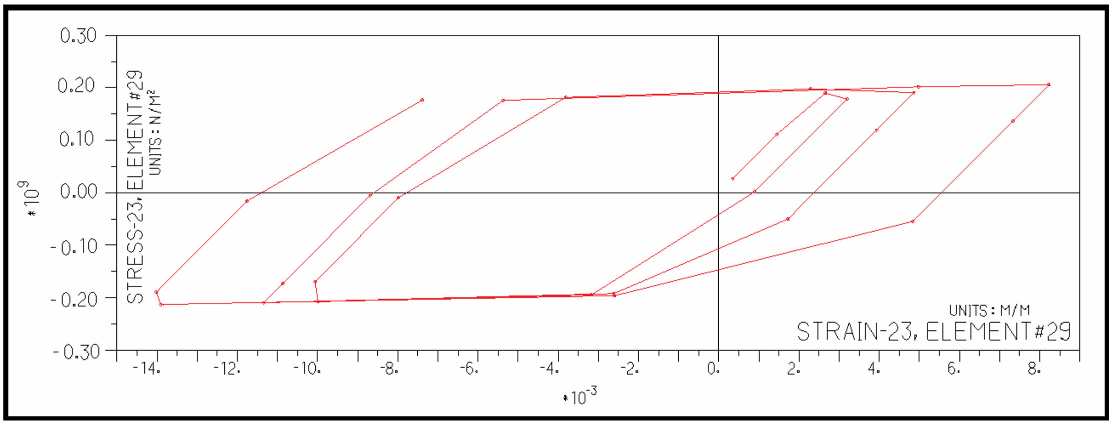


Figure 3.56: Hysteresis loops for fourth story link (ADINA output)

Ductility calculations for the fourth story

ε_y = -2.5x10^{-3}

ε = -14.0x10^{-3}

$$\mu_{c\,(4th)} = \frac{-14.0x10^{-3}}{-2.5x10^{-3}} \approx 5.6$$

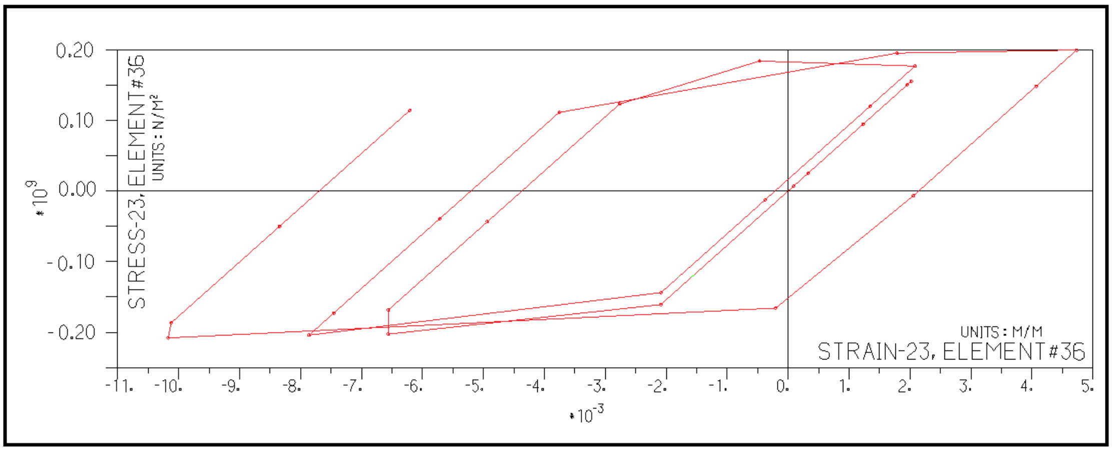


Figure 3.57: Hysteresis loops for fifth story link (ADINA output)

Ductility calculations for the fifth story

$\varepsilon_y = -2.0x10^{-3}$

$\varepsilon = -10.0x10^{-3}$

$$\mu_{c\,(5th)} = \frac{-10.0x10^{-3}}{-2.0x10^{-3}} \approx 5.0$$

The force-displacement curves for the top of the system provide the hysteretic loops as shown in Figure 3.58.

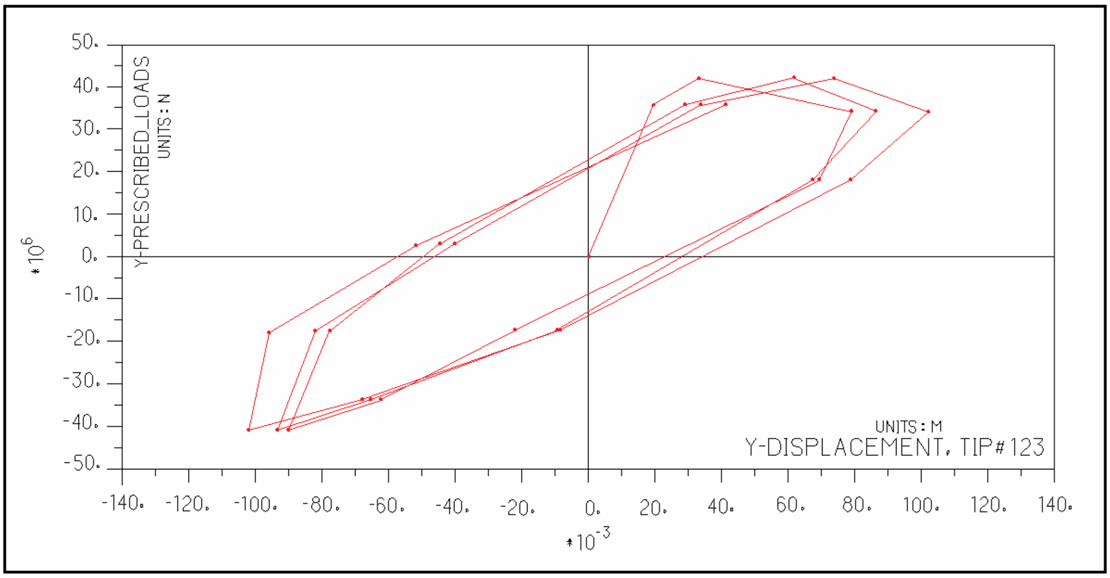


Figure 3.58: Force-displacement diagrams of the structure (ADINA output)

Global ductility calculations

$\Delta_y \approx 19.0x10^{-3}$

$\Delta_u \approx 102.0x10^{-3}$

$$\mu_{c\,(Global)} = \frac{102.0x10^{-3}}{19.0x10^{-3}} \approx 5.35$$

This ductility value gained from the cyclic response calculations (μ_c = 5.35) is very near to the value obtained from the monotonic response calculations (μ_c = 5.5).

The studied specimen of this new proposed hybrid brace-coupled shear walls system proved efficient all along this study and provided an outstanding response, under monotonic and cyclic loading, therefore it is recommended for the follower researchers to continue on this effort by performing a parametric study for this proposed system.

CHAPTER FOUR
SUMMARY AND CONCLUSIONS

4.1 Summary

This research focuses on the response of various seismic resistant systems under earthquake excitations. Chapter two shed some light on the general response of structural elements and systems under quake loadings and provided a common sense for the readers to fulfill the understanding of the traditional seismic resistant systems and finally to introduce a proposal for a new hybrid brace-coupling shear walls system.

Chapter three has solely focused on the behavior of the proposed seismic resistant systems, under finite element environment ADINA, and discussed how they respond to loading. A detailed comparison is provided in the same chapter to boost the understanding of the performance of each model and to produce comparison between them.

This current chapter summarizes the thesis works and provides conclusion on what has been previously discussed.

4.2 Conclusions

1. Coupling neighbor walls can dissipate seismic energy over the entire height of the wall, and can help the system to avoid the formation of solitaire plastic hinge at the base of such walls. This criterion can help in leading to ease of repairing. However, arbitrary coupling type will lead to a seismic behavior that is totally undependable.
2. Eccentrically braced frames are effective systems to consider in a structural design of buildings in seismic areas. Shear walls and coupled shear walls can also provide a recognized behavior under quake excitations. Combining these two systems in a hybrid brace-coupled shear walls system (i.e. hybrid coupled shear walls using eccentric steel bracing system) is the idea of this research and remarkable results are obtained through the study, such as higher ductility values and top displacement control.
3. Openings in shear walls can create an obstruction against producing the proper structural integrity under seismic excitations; the usage of diagonal braces to enhance coupling beams is an efficient available alternative.
4. No arbitrary increment in the web size of the coupling beam is allowed. Any increasing in the size of the web must be function of flanges and braces sizes to ensure the ductile behavior of the system.
5. In the hybrid brace-coupled walls system: if adequately detailed coupling beams, this study has noticed two phases of plastic hinge formation in these coupling beams; the first is in the short link zone and the later is at the end of the coupling beam, outer the link zone. Controlling such phenomenon positively can increase the ductility capacity of the system and can dissipate the seismic energy over the total height of the wall on two steps.

6. Yielding of the ends of the coupling beams must be controlled to yield after the yielding of the whole links to ensure the desired behavior of the system.
7. Coupling systems should be proportioned to avoid over coupling (i.e. system that acts as a single pierced wall) and light coupling (i.e. a system that performs as a number of isolated shear walls).
8. Lateral stiffness of the proposed specimen deteriorates rapidly after the plasticization of the whole links, and not after the first inelastic excursion in the system.
9. The hybrid brace-coupled shear walls model reduced the lateral displacement up to 40% of the lateral displacement provided by the cantilever shear wall model.
10. The hybrid brace-coupled shear walls model improved the ductility up to 238% of the maximum local ductility provided by the system of hybrid beam-coupling model. On the other hand, the hybrid brace-coupling model has enhanced the global ductility of the system to about 167% compared to the hybrid beam-coupling system.

REFERENCES

ADINA R & D, Inc. (2005), **ADINA: Theory and Modeling Guide.**

American Concrete Institute, ACI committee 318 (2008), **Building Requirement for Structural Concrete (ACI 318-08) and Commentary 318R-05**, Farmington Hills.

American Institute of Steel Construction (AISC) (2005), **Manual of Steel Construction**, Chicago.

American Institute of Steel Construction (AISC) (2005), **Seismic Provisions for Structural Steel Buildings**, Chicago.

American Society of Civil Engineers (ASCE) (2005), **Recommendations for Seismic Design of Hybrid Coupled Walls**, USA.

Armouti, Nazzal S. (2004), **Earthquake Engineering: Theory and Implementation**. First Edition, Jordan.

Boresi, A. and Schmidt R. (2003), **Advanced Mechanics of Materials**. Sixth Edition, USA: John Wiley & Sons

Chen, W. and Han, D. (1988), **Plasticity for Structural Engineers**. First Edition, USA: Springer Virlag.

Chen, W. and Sohal, I. (1994), **Plastic Design and Second-Order Analysis of Steel Frames**. First edition, USA: Springer Verlag.

Chen, W. and Lui, E. (2006), **Earthquake Engineering for Structural Design**. First Edition, USA: Taylor & Francis Group.

Construction Industry Research and Information Association (1984), **Design of Shear Wall Buildings** (CIRIA Report 102). London.

De Matteis, G. Landolfo, R. Mazzolani, F. (2003), Seismic Response of MR Steel Frames with Low-Yield Steel Shear Panels. **Engineering Structures**.

El-Tawil, S. Kuenzli, C. and Hassan, M. (2002a), Pushover of Hybrid Coupled Walls. I: Design and Modeling. **ASCE Journal**.

El-Tawil, S. and Kuenzli, C. (2002b), Pushover of Hybrid Coupled Walls. II: Analysis and Behavior. **ASCE Journal**.

Federal Emergency Management Agency (FEMA) (2002), **Prestandard and Commentary for The Seismic Rehabilitation of Buildings**, Washington D. C.

Fukumoto, Y. (2000), Reduction of Structural Ductility Factor Due to Variability of Steel Properties. **Engineering Structures**.

Gioncu, V. and Petcu, D. (1997), Available Rotation Capacity of Wide-Flange Beams and Beam-Columns – Part 1. Theoritical Approaches. **Journal of Constructional Steel Research**.

Gioncu, V. and Mazzolani, M. (2002), **Ductility of Seismic Resistant Steel Structures**. First Edition, Great Britain: Spon Press.

Gong, B. and Shahrooz, B. (2001), Steel-Concrete Composite Coupling Beams – Behavior and Design. **Engineering Structures**.

Hindi, R. and Hassan, M. (2004), Shear Capacity of Diagonally Reinforced Coupling Beams. **Engineering Structures**.

Khatri, D. and Anderson, J. (1995), Analysis of Reinforced Concrete Shear Wall Components Using the ADINA Nonlinear Concrete Model. **University of Southern California**, U.S.A.

Moghaddam, H. and Estekanchi, H. (1999), Seismic behaviour of offcentre Bracing Systems. **Journal of Constructional Steel Research**.

Naiem, F. (2001), **The Seismic Design Handbook**. Second Edition. USA: Kluwer Academic Publishers

Ozel, A. and Guneyisi, E. (2010), Effects of Eccentric Steel Bracing Systems on Seismic Fragilirt Curves of Mid-Rise R/C Buildings: A Case Study. **Gaziantep University**, Turkey. Accepted for publication.

Plumier, A. (2000), General Report on Local Ductility. **Journal of Constructional Steel Research**.

Pala, S. and Ozmen, G. (1994), Effective Stiffness of Coupling Beams in Structural Walls. **Computers and Structures**.

Park, W. and Yun, H. (2005), Seismic Behaviour of Coupling Beams in A Hybrid Coupled Shear Walls. **Journal of Constructional Steel Research**.

Park, W. Yun, H. Hwang, S. Han, B. and Yang, I. (2005), Shear Strength of the Conncetion Between A Steel Beam and a Reinforced Concrete Shear Wall in A Hybrid Wall System. **Journal of Constructional Steel Research**.

Paulay, T. and Taylor, R. (1981), Slab Coupling of Earthquake-Resisting Shearwalls. **ACI Journal**.

Paulay, T. (1982), Deterministic Seismic Design procedures for Reinforced Concrete Buildings. **Engineering Structures**.

Paulay, T. and Priestley, M. (1992), **Seismic Design of Reinforced Concrete and Masonry Buildings**. First Edition, USA: John Wiley & Sons.

Paulay, T. (2002), The Displacement Capacity of Reinforced Concrete Coupled Walls. **Engineering Structures**.

Portland Cement Association (1998), **Shear Wall-Frame Interaction: A Design Aid** (Engineering Bulletin). Illinois.

Shahrooz, M. Fortney, P. Rassati G. (2006), **Hybrid Coupled Core Wall Systems: An Innovative Approach to Post-Event Damage Mitigation**. Proc. Of the Eighth U.S. National Conference on Earthquake Engineering.

Smith, B. and Coull, A. (1991), **Tall Building Structures: Analysis and Design**. First Edition, USA: John Wiley and Sons.

Su, R. Lam, W. and Pam, H. (2007), Behaviour of Embedded Steel Plate in Composite Coupling Beams. **Journal of Constructional Steel Research**.

Taranath, B. (2010), **Reinforced Concrete Design of Tall Buildings**. First Edition, USA: CRC Group.

Vayas, I. (1997), Stability and Ductility of Steel Elements. **Journal of Constructional Steel Research**.

Wight, J. and MacGregor, J. (2009), **Reinforced Concrete: Mechanics and Design**. Fifth Edition. USA: Pearson Prentice Hall.

Wong, M. (2009), **Plastic Analysis and Design of Steel Structures**. First Edition. USA: Elsevier.

Zhao, Z. Kwanm, A. and He, X. (2004), Nonlinear Finite Element Analysis of Deep Reinforced Concrete Coupling Beams. **Engineering Structures**.

التصرف الزلزالي للجدران هجينة الربط باستخدام التكتيف المعدني اللامركزي

إعداد

يحيى وليد إستانبولي

المشرف

الدكتور نزّال العرموطي

ملخّص

يهدف هذا البحث إلى دراسة التصرُّف الزلزالي لجُدران القص العمودية المُرتبطة بأنظمة التكتيف المعدني اللامركزي.

خلال هذه الرسالة، تمّ دراسة هذا النظام الإنشائي باستخدام البرنامج (ADINA) الذي يقدم نتائجه باستخدام بيئة العنصر المحدود. العينة المقترحة تتكون من جِداريّ قص بارتفاع 15 متراً وعرض 4 أمتار، لكل منهما، وقد تم ربطهما باستخدام نظام تكتيف معدني لا مركزي. وقد تمت مقارنة النتائج لهذا النظام الإنشائي المطروح بنظامين تقليديين لمقاومة أفعال الزلازل، ألا وهما: جدران القص العموديّة، والجدران هجينة الربط باستخدام الجسور المعدنية. تمّت دراسة هذه النماذج الثلاثة باستخدام طريقة التحليل باستخدام الدفع الإطرادي لحين حصول الفشل اللدن في المُنشأ، ومن خلال هذه الطريقة تمت دراسة الخصائص الميكانيكية للأنظمة، والمتمثلة في مراحل الاستجابة الثلاثة؛ الجساءة، والممانعة، والممطوليّة.

لقد ظهرت كفاءة العيّنة المطروحة للدراسة؛ أي العينة المكونة من نظام الجدران هجينة الربط باستخدام التكتيف المعدني اللامركزي، مقارنةً بالأنظمة التقليدية المقدمة خلال هذه

الدراسة، وذلك من خلال جساءة النظام المطروح، والتحكم بالإزاحة الأفقية للطوابق، وقيمة الترخيم في أعلى المنشأ، والخصائص المتعلقة بالممطولية.

خلال عملية التحليل، استطاع النظام المقدم للدراسة أن يقوم بتشكيل مفاصل لدنة على مرحلتين، وذلك مع ارتفاع المنشأ. أول ظهور للمفاصل اللدنة كان في مرابط التكتيف المعدني اللامركزي، في حين أن الظهور الثاني للمفاصل اللدنة كان في نهايات الجسور الرابطة.

لفحص قدرة النظام المذكورة آنفاً على تبديد الطاقة الممتصة خلال أفعال الزلازل، تم تحميله جانبياً باستخدام إقتران دوري في بيئة البرنامج (ADINA). لقد استطاع النظام المطروح أن يقدم استجابة زمنية متميزة، والتي أثبتت بدورها قدرته على تشكيل مفاصل لدنة في مناطق مسبقة التخمين في النظام المطروح، وإمكانية تبديد الطاقة مع ارتفاع المنشأ.